1974

A new electrochemical technique for the study of photochemical reactions in liquid media

Paul Robert Gaines
Iowa State University

A new electrochemical technique for the study of photochemical reactions in liquid media

by

Paul Robert Gaines

A Dissertation Submitted to the
Graduate Faculty in Partial Fulfillment of
The Requirements for the Degree of
DOCTOR OF PHILOSOPHY

Department: Chemistry
Major: Analytical Chemistry

Approved:

Signature was redacted for privacy.

In Charge of Major Work

Signature was redacted for privacy.

For the Major Department

Signature was redacted for privacy.

For the Graduate College

Iowa State University
Ames, Iowa

1974

TABLE OF CONTENTS

I. INTRODUCTION

Methods have been developed for the application of an electrochemical detector for the study of the photochemical behavior of chemical species in liquid media. Photochemically generated intermediates are swept to the detector immediately after production by means of convective diffusional mass transport. When they reach the electrode they may undergo electrochemical oxidation or reduction. The resultant electrochemical current is referred to as photocurrent.

The transient behavior of photolytically generated species is frequently studied with ultraviolet-visible detector systems. Ultraviolet-visible detection is frequently used in photochemical studies because of simplicity of instrument design and high sensitivity for species with large molar absorptivities. When the transmittance spectrum for the transient species is not significantly different from the spectrum of the parent compound, then another detection system must be used. Ultraviolet-visible detection is also undesirable when the transient species have low molar absorptivities.

The purpose of this research was the investigation of the use of electrochemical detectors in photochemical studies. Electrochemical detectors used previously were

hanging or dropping mercury electrodes. Mercury drop detectors have limited usefulness in photochemical studies for the following reasons:

1) electrons are photoemitted from the Hg°;

2) the drop causes a shadow which results in a nonhomogeneous production of the transient species;

3) the absorptive pathlength is difficult to determine due to the curvature of the drop.

Due to the above problems, a mathematical interpretation of the data is difficult.

This thesis describes applications of the rotating photoelectrode introduced by Johnson and Resnick (77). The experimental results of photochemical investigations of several model systems are given to illustrate the usefulness and bring to light the limitations of the rotating photoelectrode.

II. LITERATURE REVIEW

A. Photoelectrochemistry

Photoelectrochemistry involves the electrochemical monitoring of intermediates and products of photochemical reactions in liquid media. A review of the literature of photoelectrochemistry was presented by Kuwana (86) in 1966 and later by Honda (75) in 1969. The general theory of photoelectrochemistry was reviewed by Weller (152, 151). The following review of photoelectrochemistry will be limited to studies using immersed Hg electrodes. The use of other electrode materials has been very limited. Although photoelectrochemistry is generally thought to involve the oxidation or reduction of the products of an excited state, Stutter (142) published a theoretical paper on the determination of the $E_{1/2}$ of the excited-state molecules. The following electrode reactions were considered:

$$A + ze \underset{k_+}{\overset{k_-}{\rightleftharpoons}} A^{z-} \qquad \text{(II.1)}$$

$$A^* + ze \underset{k_+^*}{\overset{k_-^*}{\rightleftharpoons}} A^{z-} \qquad \text{(II.2)}$$

Stutter suggested that intense short light flashes be used to excite the molecules (A) immediately before the growth of the Hg drop. He stressed that although the existence of redox potentials of excited molecules and the respective

processes according to Equation II.2 are very probable, direct evidence is not available.

Photopolarography is the electrochemical monitoring of photochemically generated species with a dropping mercury electrode. Berg (17, 20-29) examined the effects of continuous and intermittent irradiation upon current and potential characteristics using photopolarography. On the basis of the results of his studies, he has described three types of photopolarographic currents: photoresidual current, photochemically altered diffusion current, and photokinetic current.

Photoresidual currents are observed when the surface is directly irradiated with high-energy ultraviolet radiation. Photoemission of electrons occurs and the emitted electrons are solvated and may diffuse from the electrode surface. In order for a photoresidual current to be detected, the emitted electron must undergo an irreversible process, such as formation of hydrogen gas, or else it can return to the electrode surface and result in zero net electronic current.

The mechanism for the production of photoresidual currents has recently been investigated by Heyrovsky (74), Baker and coworkers (12), Marinus and coworkers (96), Delevie and Kreuser (62), Yamashita and Imai (154), Levin and Delahay (92), and Bomehil and coworkers (33).

A photochemically altered diffusion current is a diffusion current which is modified by the formation or consumption of an electrochemically active substance in a concurrent, fast photochemical reaction in the bulk of the solution or at the electrode surface:

$$\begin{array}{l} A + ne \longrightarrow A^{-n} \\ \quad\downarrow h\nu \\ \quad B \end{array} \qquad \text{(II.3)}$$

Photokinetic currents are anodic or cathodic currents limited by the rate of a photochemical reaction near or at the electrode surface. Due to the design of the photoelectrode, the choice of electrode potential, and the chemical systems studied, the photocurrents discussed in this thesis are all photokinetic currents.

Schweiss (134) and Perone and coworkers (113, 114, 115) have demonstrated the use of time-delayed potentiostatic measurements following flash photolysis at stationary mercury-drop electrodes. Individual current-time curves following the flash are utilized to obtain kinetic data. The time delay, following the flash, allows the photoresidual current to decay before potentiostatic monitoring of the photolytically generated intermediates is begun. Although this technique is an improvement over conventional photopolarography, quantitative application of the hanging

mercury drop, like the dropping mercury electrode, is subject to some serious difficulties. There is always a shadow cast by the drop on the solution away from the lamp. Also, the intensity profile of the light beam is difficult to describe since the absorption pathlength varies with the curvature of the drop. Therefore, there is a nonhomogeneous formation of the photolytically generated intermediate, and accurate mathematical treatment of the data is very difficult or impossible. Physical factors influencing the accuracy of results obtained with the dropping-Hg electrode in measurements of photochemical reactions rates is reviewed by Manning (95).

Kemula and coworkers (80), and Kalinowski and coworkers (78) have used the method of cyclic voltammetry at the stationary mercury-drop electrode in the study of the photochemical reduction of aromatic ketones.

Johnson and Resnick (77) have described a rotating photoelectrode (RPE) to be used in photochemical studies. The photoelectrode has a quartz disk which is optically transparent and a platinum ring electrode surrounding the quartz disk. The photoelectrode is rotated in a solution about an axis which is perpendicular to and which passes through the center of the quartz disk. An intense beam of light is directed through the optically transparent disk. A fraction of the products of photolytic reactions occurring

in the vicinity of the quartz disk of the rotating photoelectrode is transported radially, by convective-diffusional processes, to the surface of the ring electrode where they may undergo electrochemical reaction. If desired, the platinum ring can be coated with a thin film of Hg° to obtain a larger negative potential range. Since the beam of light does not impinge on the surface of the ring electrode, there is no photoemission of electrons and steady-state currents are measured in the ring electrode during continuous photolysis. The electroanalytical techniques associated with the application of the RPE to the investigation of photochemical reactions are described in this thesis.

B. Photochemistry of Benzophenone

The mechanism for the photochemical reduction of benzophenone in alkaline, alcohol-water solutions has been established to proceed as follows:

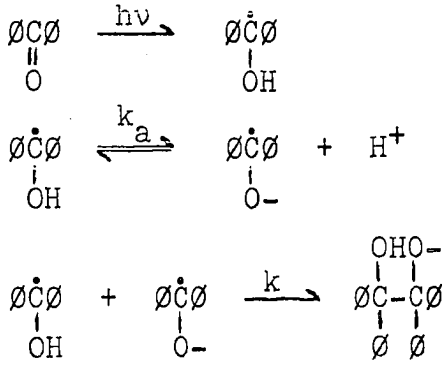

(II.4)

(II.5)

(II.6)

The literature values of the pK_a and k are 9.2 and 1.1×10^9 $\underline{M}^{-1}$ sec^{-1} respectively (15). Similar mechanisms were given for the photoreduction of benzophenone in amines (42, 43, 47, 48, 51, 53-56, 89, 126), ethers (2, 14), alcohols (1, 6, 9-11, 43-46, 49, 50, 65, 66, 73, 81, 82, 91, 97, 98, 101-103, 112, 116, 118, 119, 127, 130, 132, 136, 41, 144-146, 155), benzene (36, 60, 128, 133), water (87, 90), and hydrocarbons (7, 35, 43) as solvents.

C. Electrochemistry of Benzophenone

The electrochemical behavior of benzophenone in alcoholic-water media of various values of pH has been studied with the dropping mercury electrode (58, 13, 52, 57, 69, 70, 79, 84, 85, 94, 100, 108, 110, 125, 129, 141, 143, 148, 149, 153, 156), the stationary mercury drop (63), and the amalgamated rotating ring-disk electrode (104, 105). The electrochemical behavior of benzophenone has been well characterized over the entire pH range. The following mechanism and values of $E_{1/2}$ are generally accepted in alkaline media.

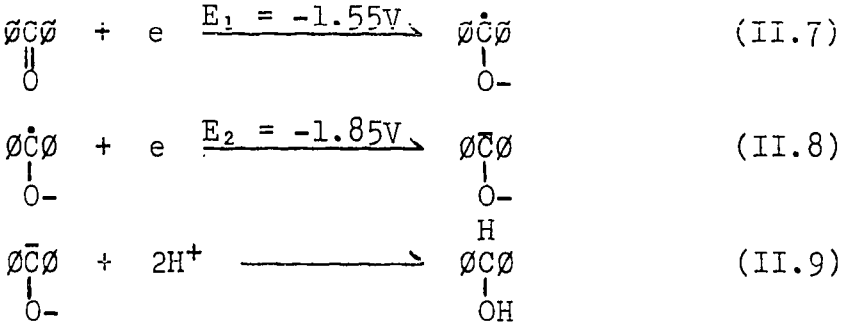

(II.7)

(II.8)

(II.9)

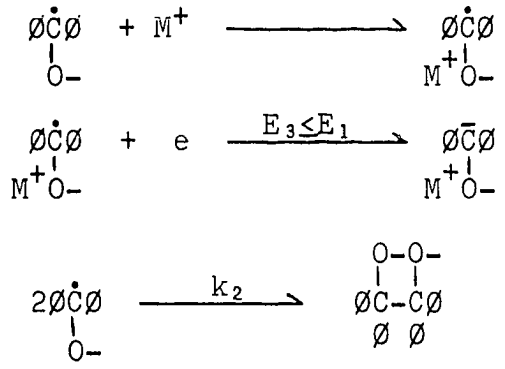

(II.10)

(II.11)

(II.12)

The ion pair formation between the ketyl free radical anion and the cation of the electrolyte (M^+) shown in Equation II.10 predominates when the ionic strength is high and the dielectric constant of the solvent is low. When the electrolyte concentration is sufficiently large so that all of the ketyl radical anion reacts to form the ion pair, one reduction wave is observed which is equal in height to the sum of the reduction waves for reactions II.7 and II.8 observed at low ionic strength. It should be noted that the main difference in the electrochemical and photochemical behavior of benzophenone is the method of generation of the ketyl radical anion. The homogeneous kinetics of the ketyl radical and radical anion are not affected by the method of their generation.

D. Electrochemistry of Benzil

Several studies have been reported of the electrochemical reduction of benzil in alcohol-water solutions (32, 34, 39, 59, 109, 110, 117, 138). They are adequately

reviewed by Stapelfeldt and Perone (138, 139). These workers concluded that in acidic and neutral solutions, benzil is electrochemically reduced by an irreversible, two-electron process to stilbendiol which has two geometric forms. Two anodic peaks were obtained using cyclic voltammetry at a stationary mercury electrode, and they were concluded to result from the oxidation of the cis- and trans-stilbendiol; the anodic peak for the cis-isomer was about 90 mV more positive than the peak for the trans-isomer (39, 138). Stilbendiol undergoes a rearrangement, called ketolization, to benzoin. The rate of ketolization in 50% methanol solution at a pH of 7.5 was determined to be $(7.9 \pm 0.6) \times 10^{-3}$ sec^{-1} for trans-stilbendiol and $(2.4 \pm 0.3) \times 10^{-3}$ sec^{-1} for cis-stilbendiol (138). The rates of ketolization increase with increasing pH for $6 < pH < 11$ (139). The overall process in acidic and neutral solution is described in Equation II.13.

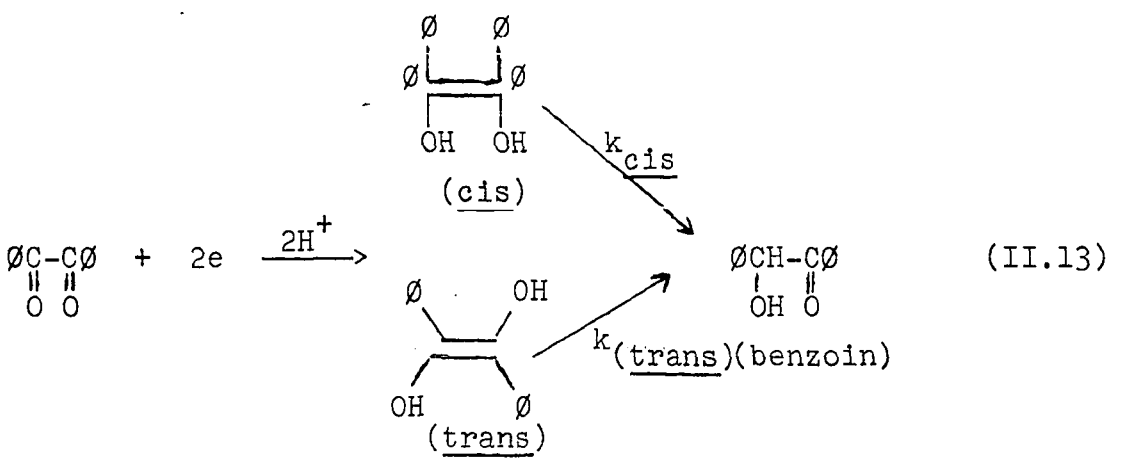

(II.13)

In strongly alkaline solution, pH > 11, the reduction of benzil occurs by a reversible, two-electron process. Using cyclic voltammetry at a stationary mercury electrode, Stapelfeldt and Perone (139) observed only one peak for the oxidation of the product of the reduction reaction. They concluded the product was stilbendiolate but reported that no experimental evidence was found to suggest a specific structural formula for the stilbendiolate. The overall reaction was given as described by Equation II.14 (139).

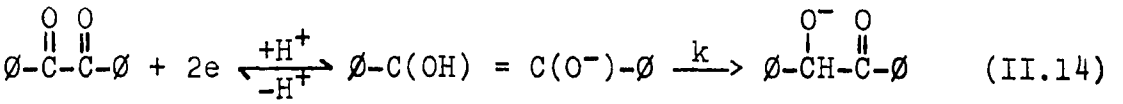

(II.14)

The rate constant of ketolization by the intermediate was determined to be 2 sec^{-1}.

Chodkowska and Grabowski (39) observed that alkaline solutions of benzil turned purple-violet when electrolyzed at constant potential, and they determined the reaction products to be benzoin and a ketyl radical anion. The radical anion was not produced directly at the electrode but by a homogeneous reaction between benzil and benzoin or stilbendiolate according to Equations II.15 or II.16

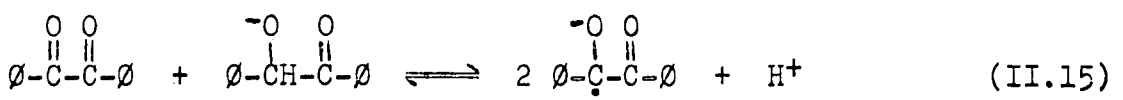

(II.15)

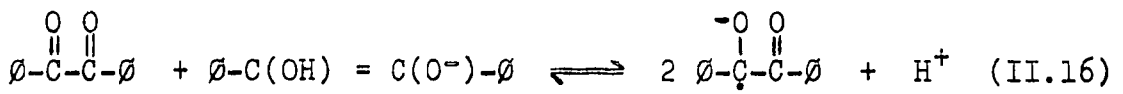

(II.16)

(39, 139). The pK_a for the free radical is approximately 5.9 (16). The equilibrium constant for Reaction II.15 was determined to be 4×10^{-3} in strongly alkaline media (68).

E. Photochemistry of Benzil

The photochemical reactions of benzil in liquid solutions have been studied by several workers (16, 19, 22, 37, 106, 140). Stapelfeldt and Perone (140) suggested the following mechanism based on results of photoelectrochemical studies with a hanging mercury-drop electrode in alkaline alcohol-water media:

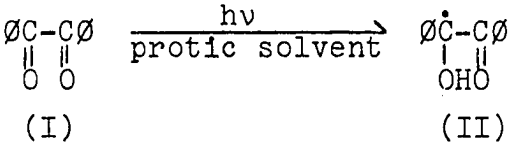

(I) (II) (II.17)

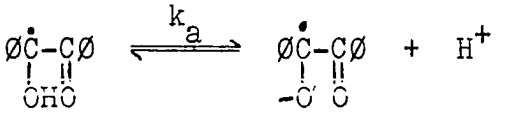

(II) (III) (II.18)

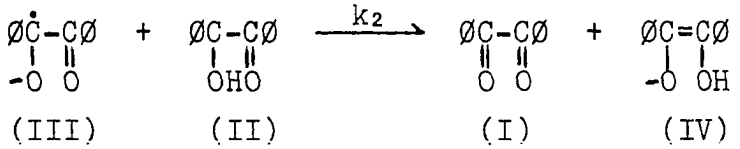

(III) (II) (I) (IV) (II.19)

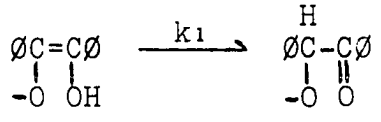

(IV) (V) (II.20)

In the above reactions, I is benzil, II is the ketyl radical, III is the ketyl radical anion, IV is monoprotonated stilbendiolate, V is the benzoin anion, k_2 is a second-order rate constant, and k_1 is a first-order rate constant. Beckett and coworkers (16) determined the pK_a for the ketyl radical to be approximately 5.9. Although Perone strongly indicated that no dimerization of the ketyl radical to form benzil pinacol occurs, Ogata and coworkers (106) reported that when 10^{-2} M solutions of benzil were irradiated in 2-propanol, considerably more benzil pinacol than benzoin is produced. Bunburg and Chuang (37) determined that benzil pinacol is produced when benzil is photolyzed in 2-propanol. However, they concluded that the benzil pinacol is not produced by the dimerization of two ketyl radicals. Bunburg and Chuang observed that reduction of the benzil concentration causes a marked decrease in the production of benzil pinacol. They postulated that a complex is formed between the ketyl radical and an unexcited benzil molecule, and that this complex can abstract a hydrogen atom from the solvent to form the benzil pinacol.

F. Photochemistry of 9-Hydroxyfluorene

DeGroot (61) studied the photochemical behavior of 9-hydroxyfluorene but failed to give a mechanism or to determine the identity of the intermediates or products of

the photolysis. No other reports were found in the chemical literature of studies of the photochemical behavior of the 9-hydroxyfluorene.

III. INSTRUMENTATION

A. Potentiostatic Circuitry

The three-electrode potentiostat was constructed from operational amplifiers according to the conventional design (147). Photocurrents were calculated from the value of the output potential of the current follower amplifier and the value of the feedback resistor. Normally, a 100 KΩ ± 1% resistor was used. Electrical potentials were measured on a Systron Donner Model 7050 digital voltmeter. All electrode potentials were measured and are given versus a saturated calomel reference electrode.

The four-electrode potentiostat used in the study of the electrochemical behavior of benzil and benzophenone, is equivalent to that described in Reference (76).

A Hewlett-Packard x-y recorder (Model 7035B) was used to record current-potential data.

B. Electrodes

1. Photoelectrode

The photoelectrode was constructed by Pine Instrument Co. of Grove City, Pennsylvania, and its design is shown in Figure III.1.

2. Ring-Disk electrodes

The construction and typical applications of a rotating ring-disk electrode are described by Albery and

Figure III.1. The model DP photoelectrode

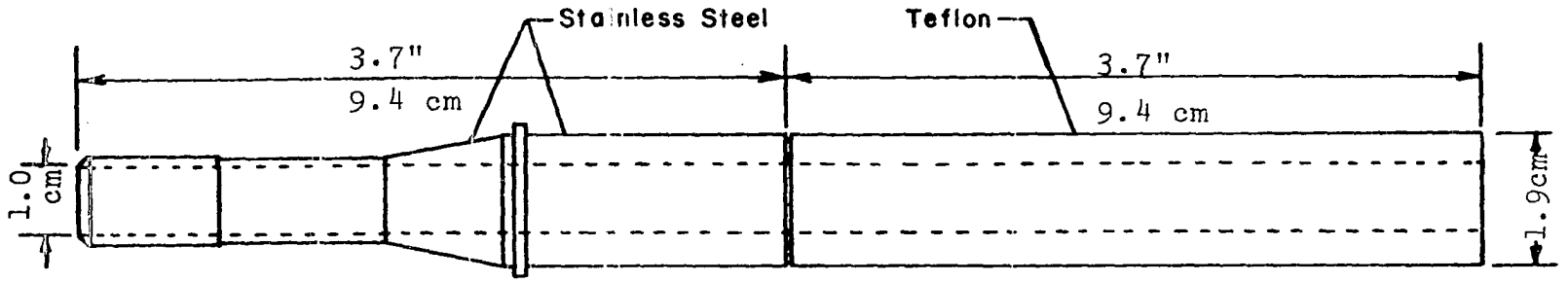

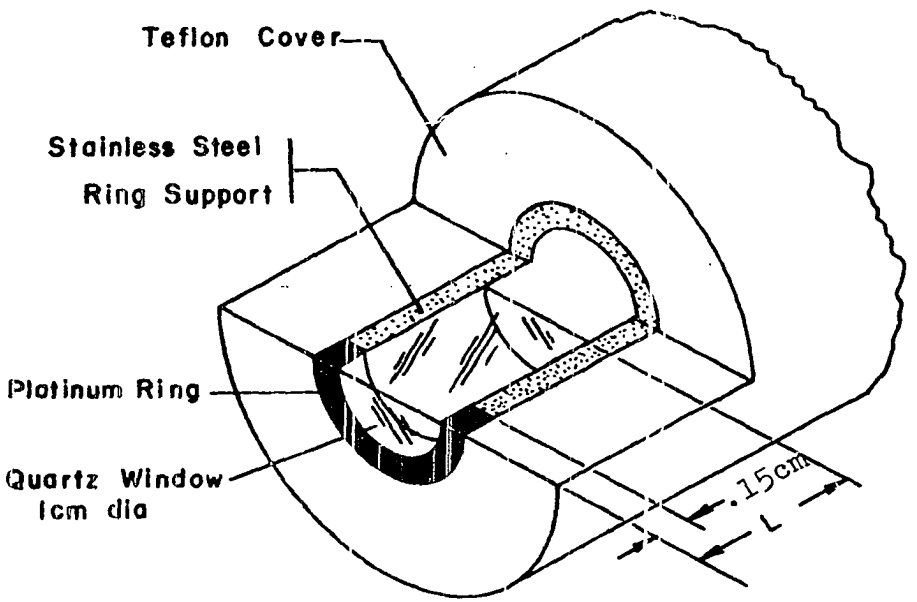

CUT AWAY VIEW OF DP PHOTO ELECTRODE

Hitchman in Reference 4. The pertinent geometric parameters of the platinum ring-disk electrode used in this research are as follows:

R_1 = radius of disk electrode

= 0.382 cm

R_2 = inner radius of ring electrode

= 0.397 cm

R_3 = outer radius of ring electrode

= 0.422 cm

N_0 = collection efficiency

= 0.189

$\beta^{2/3} = ((R_3/R_1)^3 - (R_2/R_1)^3)^{2/3}$

= 0.370

3. Mercury-coated electrodes

The ring and disk of the platinum ring-disk electrode and the platinum ring of the rotating photoelectrodes were coated with mercury at the start of each experimental day by one of two procedures. Kinetic data obtained using the electrode prepared by either method were identical within limits of experimental precision. The first procedure was essentially that of Brubaker (35a) according to which the electrode, having been previously reduced electrochemically, was dipped into a pool of mercury and any excess mercury loosely adhering to the electrode surfaces was removed by gentle wiping with a clean sheet of Scott's Micro-Wipe.

According to the second procedure, mercury was electrodeposited at the ring and disk electrodes from an acidic solution of Hg_2^{+2} (35b).

4. Rotator

The photoelectrode was rotated by a model PIR Photorotator (serial no. 38) from Pine Instrument Company. It was equipped with a variable speed motor and model ASR speed controller. The rotational velocity was continuously variable in the range 0-4000 rpm.

The ring-disk electrode was rotated with a model PIR rotator (serial no. 83) from Pine Instrument Company. Nine rotational velocities were available in the range 400-10,000 rpm.

C. Photochemical Instrumentation

1. Light-source and optical system

The light source was a 500-watt high pressure, Xenon arc (Model 959C-98) from Hanovia, Incorporated, of Newark, New Jersey. The lamp arc length was 0.6 mm. The lamp power supply was Model LPS-255 from Schoeffel Instrument Corporation of Westwood, New Jersey. The lamp housing and lens system are described in Reference (77). Isolation of the desired portion of the emission spectrum was achieved using a high-energy grating monochromator (Model GM250) from Schoeffel Instrument Corporation. The monochromator

had an aperture ratio of f/3.9 with a linear dispersion of 3.2 nm/mm. Slits of 12 mm width were used for an estimated spectral band-width of 38 nm. No colored glass filters were used for wavelength isolation. A schematic diagram of the optical system is shown in Figure III.2. Three neutral-density filters from Oriel Optics Corporation of Stamford, Connecticut, were used for variation of light intensity. Values of transmittance were 0.500, 0.316, and 0.100. The neutral density filters were placed in the filter holder described in Reference (77) mounted between the lamp housing and the monochromator.

2. Optical alignment procedure

The procedure for optical alignment was as follows: the positions of the lamp and spherical mirror in the lamp housing were adjusted so that the image of the lamp electrodes on the mirror was occluded by the electrodes themselves when viewed along the optical axis of the focusing lens. The monochromator was attached to the lens holder of the lamp housing and its position varied relative to the lamp housing until the light image viewed along the optical axis of the exit lens was symmetric about the axis. The 90° - light tube was attached to the exit port of the monochromator and the plane mirror adjusted so the collimated beam of light from the monochromator passed through the quartz disk parallel to the electrode axis. This adjustment was made by

Figure III.2. Optical diagram of instrument for use with the rotating photoelectrode

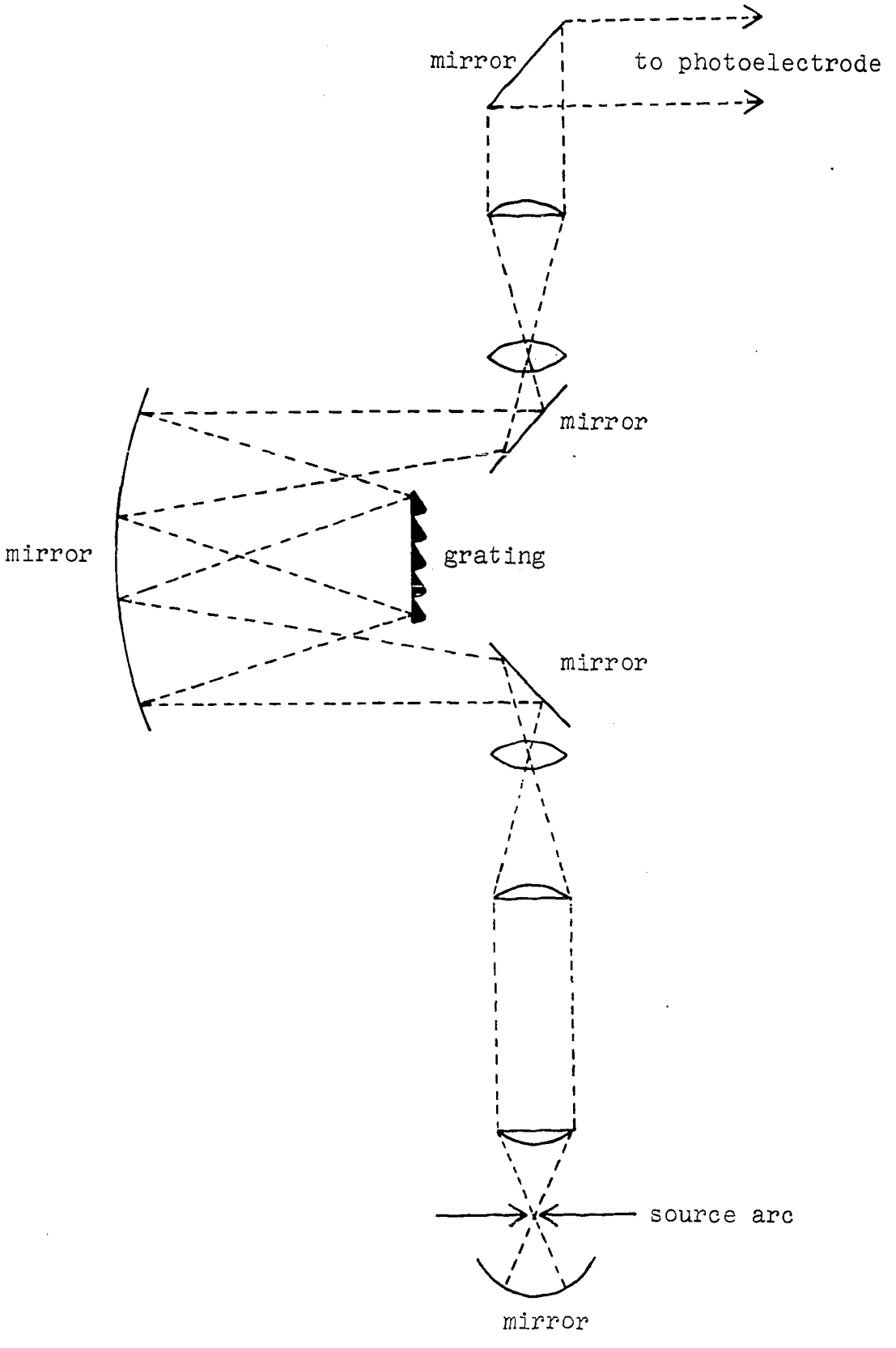
mirror
to photoelectrode
mirror
mirror
grating
mirror
source arc
mirror

taking intensity profiles along perpendicular diameters across the quartz disk. The position of the plane mirror was adjusted until the intensity profiles were as nearly symmetric as possible. Finally, the focusing lens on the lamp housing was adjusted until the light beam observed at the quartz disk was at maximum intensity.

3. Measurement of light intensity

Actinometric measurements were made using the ferri-oxalate procedure described in References (77) and (38) with a two-hour photolysis time. Interruption of the photolysis as described in Reference (77) was not necessary because no colored filters were used for spectral isolation.

4. Measurement of molar absorptivity

The molar absorptivities of the compounds under investigation were measured using a 1.00 - cm cell and a spectrophotometer fashioned from the light source, grating monochromator, and a Beckman Instruments "blue-sensitive" photodetector. Consequently, the spectral bandpass for the determination of molar absorptivity was identical to that for photolytic studies and actinometry.

5. Measurement of the light intensity profile

Measurement of the light intensity profile at the quartz disk was made by synchronously scanning the photo-detector across the face of the RPE during irradiation with

the Xenon lamp. The photodetector was mounted in a housing with a pinhole light entrance having a 0.1 - mm aperture. A voltage proportional to the detector current was recorded as a function of the position of the pinhole along the diameter of the quartz disk.

D. Ultraviolet Spectra

Transmittance spectra in the ultraviolet region of the electromagnetic spectrum between 200 nm and 350 nm were obtained using a Bausch and Lomb Spectronic 600 dual beam spectrophotometer and a Sargent Model SRLG recorder.

E. Electron Spin Resonance Spectra

Measurements of electron spin resonance were made using a Varian Model V-4500 spectrometer.

F. pH Measurements

pH measurements were made with a Corning Model 112 Digital pH meter equipped with a Corning (No. 476002) low Na^+ error pH glass electrode.

G. Liquid Chromatograph

All chromatographic separations were made using a Chromatronix Model 500 high pressure liquid chromatograph and a Chromatronix-type LC-6m, 6.3 mm, chromatography column.

H. Mass Spectra

Low resolution mass spectra were obtained on an Atlas model CH4 mass spectrometer. High resolution mass spectra were obtained on an AEI MS902 mass spectrometer.

IV. QUALITATIVE APPLICATIONS OF THE ROTATING PHOTOELECTRODE TO SELECTED PHOTOCHEMICAL RESEARCH

A. Benzophenone

1. Introduction

The literature of the photochemical behavior of benzophenone in alkaline, alcohol-water solutions was reviewed in Section II.B. The purpose of selecting such a well-known system for study with the RPE was to determine if the data obtained with the RPE was in agreement with the results obtained by other methods.

2. Experimental

a. Solutions and reagents Baker grade benzophenone from the J. T. Baker Chemical Company of Phillipsburg, New Jersey, was recrystallized three times from ethanol-water solution and dried under vacuum using Anhydrone, from the G. F. Smith Chemical Company of Columbus, Ohio, as a desiccant. Absolute ethanol from Commercial Solvents of Chicago, Illinois, was redistilled before using. Water was triply distilled with a demineralization following the first distillation and the second being from alkaline permanganate solution. Analyzed reagent grade sodium hydroxide from the J. T. Baker Chemical Company was used without further purification. Purified $NaClO_4 \cdot H_2O$ from the Fisher Chemical

Company of Fair Lawn, New Jersey, was used as a supporting electrolyte. All solutions were 1:1 (v:v) ethanol-water and were 0.1 M, 0.05 M, 0.02 M, or 0.01 M in NaOH. The ionic strength was adjusted to 0.1 by addition of $NaClO_4$. Solutions were deareated before use with dispersed nitrogen from Air Products and Chemicals of Allentown, Pennsylvania. A nitrogen atmosphere was maintained over the solution during photochemical measurements. Dissolved oxygen is reduced electrochemically at the potential used, and the presence of trace oxygen was signalled by observation of a large dark current.

All solutions, described in this manuscript, were thermostated at 25.0 ± 0.1C° with a Model 2095-2 Forma Temp Jr. Bath & Circulator.

b. Rotational velocity studies The dependence of the photocurrent upon the rotational velocity of the photoelectrode is an important diagnostic tool for mechanistic studies. Plots of photocurrent versus rotational velocity are always obtained at constant ring potential and fixed wavelength of the light beam used to generate the electrochemically active intermediates.

c. Photocurrent spectrum The photocurrent spectrum of a given photoproduct is the plot of the photocurrent at the ring electrode, due to the oxidation or reduction of photochemically produced compounds, versus the wavelength

of the photolysis radiation. The photocurrent spectrum is obtained at a constant rotational velocity and constant ring-potential.

d. Photocurrent-potential curves Plots of photocurrent versus ring-potential for the photolytically generated intermediates can be used to gain thermodynamic information pertaining to the intermediates. The photocurrent-potential curves are obtained at a constant rotational velocity and wavelength of the photolysis beam.

3. Results and discussion

The accepted mechanism for the photoreduction of benzophenone is given in Section II.B. At a ring potential of -0.80V, the only electrochemically active species in the solution at the surface of the ring electrode is the ketyl radical or radical anion. As the rotational velocity of the photoelectrode is increased, the photocurrents are expected to increase, since higher rotational velocities increase the rate of mass transport of reactive intermediates. Plots of photocurrent versus rotational velocity for a ring potential of -0.80V is shown in Figure IV.1 for several concentrations of NaOH. The fact that the photocurrent decreases with decreasing basicity can be explained after a consideration of the results obtained by Beckett and Porter (15). Beckett and Porter found that the observed

Figure IV.1. $I_{h\nu}$ *vs.* rotational velocity

0.01 *M* benzophenone, 50% EtOH,

50% H_2O (v/v), ⊖⊖⊖ 0.1 *M* NaOH,

△△△ 0.05 *M* NaOH, ⊟⊟⊟ 0.02 *M* NaOH,

⊖⊖⊖ 0.01 *M* NaOH, λ = 270 nm,

E_r = -0.80 volts

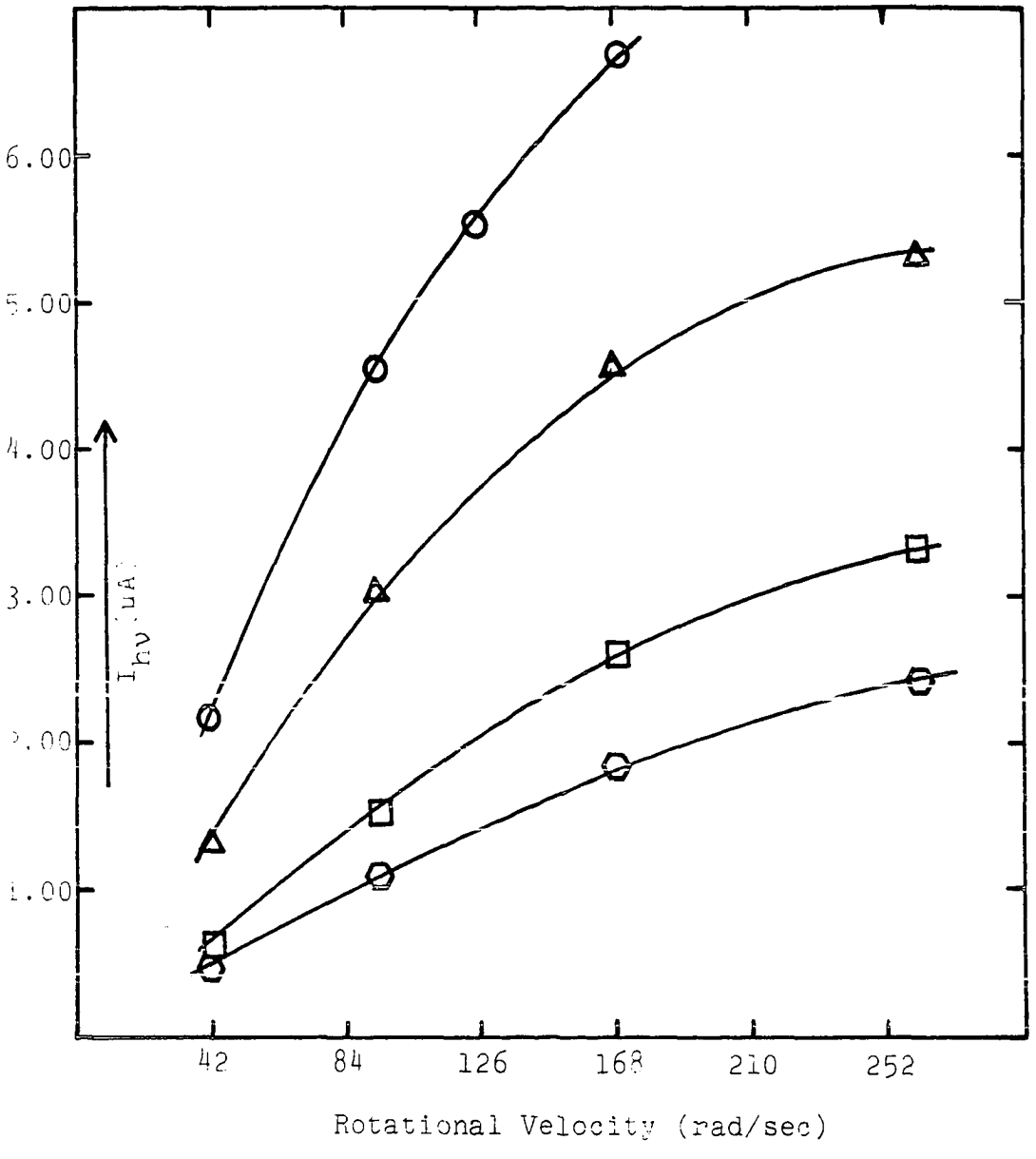
6.00
5.00
4.00
3.00
2.00
1.00
I_{hv}, uA
42
84
126
168
210
252
Rotational Velocity (rad/sec)

rate constant for the pinacolization of the ketyl radical (Equation II.6) increased with decreasing basicity. Thus, at a constant rotational velocity more of the ketyl radical is consumed by the pinacolization reaction resulting in a smaller photocurrent.

The photocurrent-ring potential profile shown in Figure IV.2 indicates the presence of at least three different electrode processes: an oxidation process at $E > -1.30V$, and an additional oxidation process at $E > -0.70V$, and a reduction process at $E < -1.3V$. These electrode processes correspond, respectively, to the oxidation of the ketyl radical or its anion, the oxidation of the pinacol, and the reduction of the ketyl radicals. The protonated and unprotonated forms of the ketyl radical have the same $E_{1/2}$. These studies are consistent with electrochemical studies of Kemula and coworkers (80) and photochemical studies of Pitts and coworkers (119), Schenck and coworkers (131), Porter and Wilkinson (120), and Perone and Birk (113).

In Figure IV.3 is shown both the photocurrent and transmittance spectra of benzophenone. From an inspection of Figure IV.3, it can be seen that the maximum photocurrent occurs at the same wavelength as the minimum in transmittance.

Figure IV.2. $I_{h\nu}$ *vs.* E_r

50% EtOH, 50% H_2O (v/v), 0.01 *M* benzophenone, 0.1 *M* NaOH, λ = 270 nm, rotational velocity = 94 rad/sec

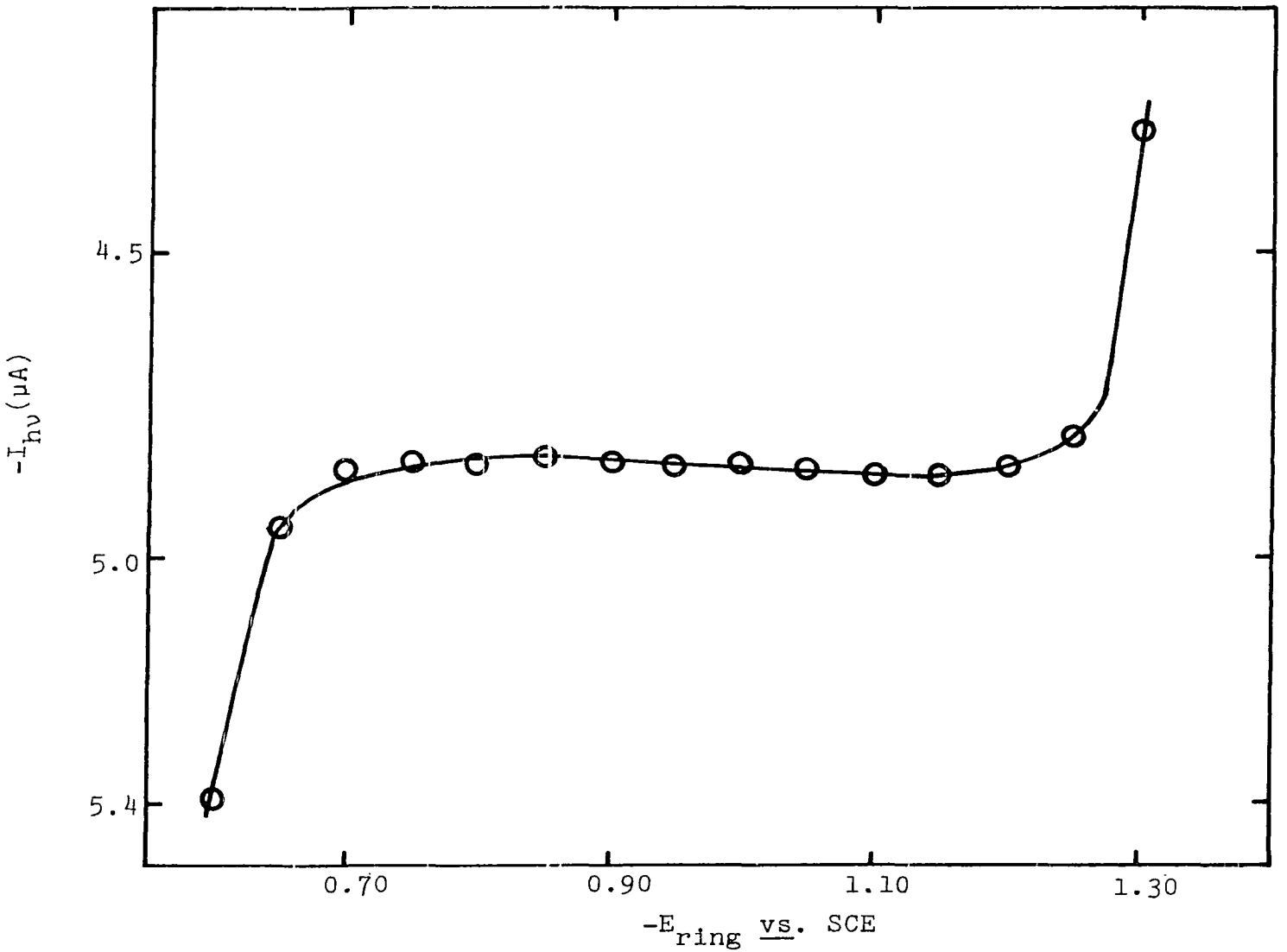
4.5
5.0
5.4
$-I_{h\nu}$ (μA)
0.70
0.90
1.10
1.30
$-E_{ring}$ vs. SCE

Figure IV.3. Spectra for benzophenone

——— % T *vs.* λ, 1.00 - cm cell,

CBULKA = 5.0×10^{-5} *M*, [NaOH] = 0.10 *M*;

~~o o o~~ $I_{h\nu}$ *vs.* λ, E_r = -0.80 *V* *vs.* SCE,

ω = 94.3 rad/sec, XII = 6.0×10^{14} quanta/sec,

CBULKA = 0.01 *M*, [NaOH) = 0.10 *M*

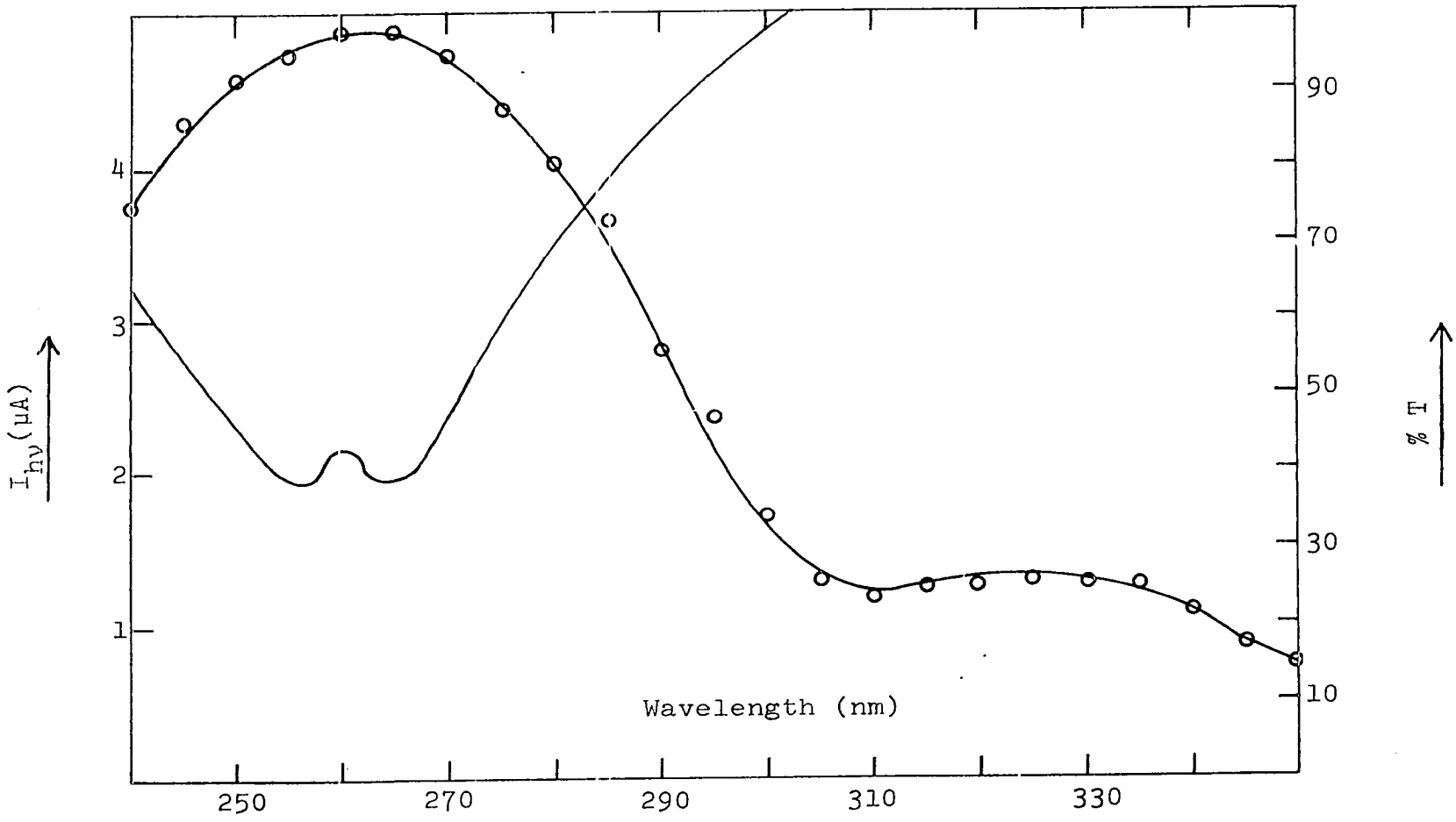
$I_{h\nu}$(μA)
4
3
2
1
90
70
50
30
10
% T
Wavelength (nm)
250
270
290
310
330

B. The Photoelectrochemical Behavior of Benzil

1. Introduction

The photochemical behavior of benzil was reviewed in Section II.E of this thesis. The mechanism proposed by Stapelfeldt and Perone (140) is seemingly not in agreement with the fact that Ogata and coworkers (106) and Bunburg and Chuang (37) found that more benzil pinacol than benzoin is formed when benzil is irradiated in 2-propanol. According to Perone's mechanism only benzoin should be observed as the photoproduct. However, for solutions of benzil below 10^{-3} M no benzil pinacol was found by Bunburg and Chuang (37) and their studies suggested that Perone's mechanism is correct at low benzil concentrations. The photoelectrode was used to investigate the photochemical behavior of benzil.

2. Experimental

Baker grade benzil was recrystallized three times from ethanol-water solution and dried under vacuum using Anhydrone, from the G. F. Smith Chemical Company of Columbus, Ohio, as a desiccant. The ethanol, water and sodium hydroxide used are described in Section IV.A.2 along with the treatment of the solution before and during photolysis. Baker Analyzed Reagent methanol was used without further purification.

3. Results and Discussion

Figure IV.4 is a plot of photocurrent versus ring potential at different concentrations of benzil. No data was obtained at potential values more negative than -0.80V due to a current limit of the amplifiers. The cathodic current obtained at potentials negative of -0.80V is due to the two electron reduction of benzil to benzoin.

Stapelfeldt and Perone (140) obtained a current-potential profile of the photolytically generated intermediates that was similar to that shown in Figure IV.4, but differed in the following respect: they obtained constant anodic currents from -0.80V to -0.30V and attributed this current to the oxidation of the ketyl radical or radical anion and stilbendiolate. All three species have identical half-wave potentials in basic media and it is, consequently, impossible to distinguish between the three. In addition to the above anodic process, an inspection of Figure IV.4 reveals another anodic process, which Stapelfeldt and Perone did not observe, beginning at approximately -0.55V. This additional wave is probably due to the oxidation of the benzil pinacol. The reason that Stapelfeldt and Perone did not observe this additional anodic process can be explained from the results obtained by Bunburg and Chuang (37). As was explained in Section II.3, Bunburg and Chuang observed no pinacol formation when the concentration of benzil was lowered to values used by Stapelfeldt and Perone.

Figure IV.4. $\underline{I}_{h\nu}$ *vs.* E_{ring}

The solvent is 70% MeOH, 30% H_2O (v/v) and the concentration of NaOH = 0.1 M.

~~A A A~~ 0.01 M Benzil

~~O O O~~ 0.005 M Benzil

~~□ □ □~~ 0.001 M Benzil

rotational velocity (ω) = 42 rad/sec

λ = 270 nm

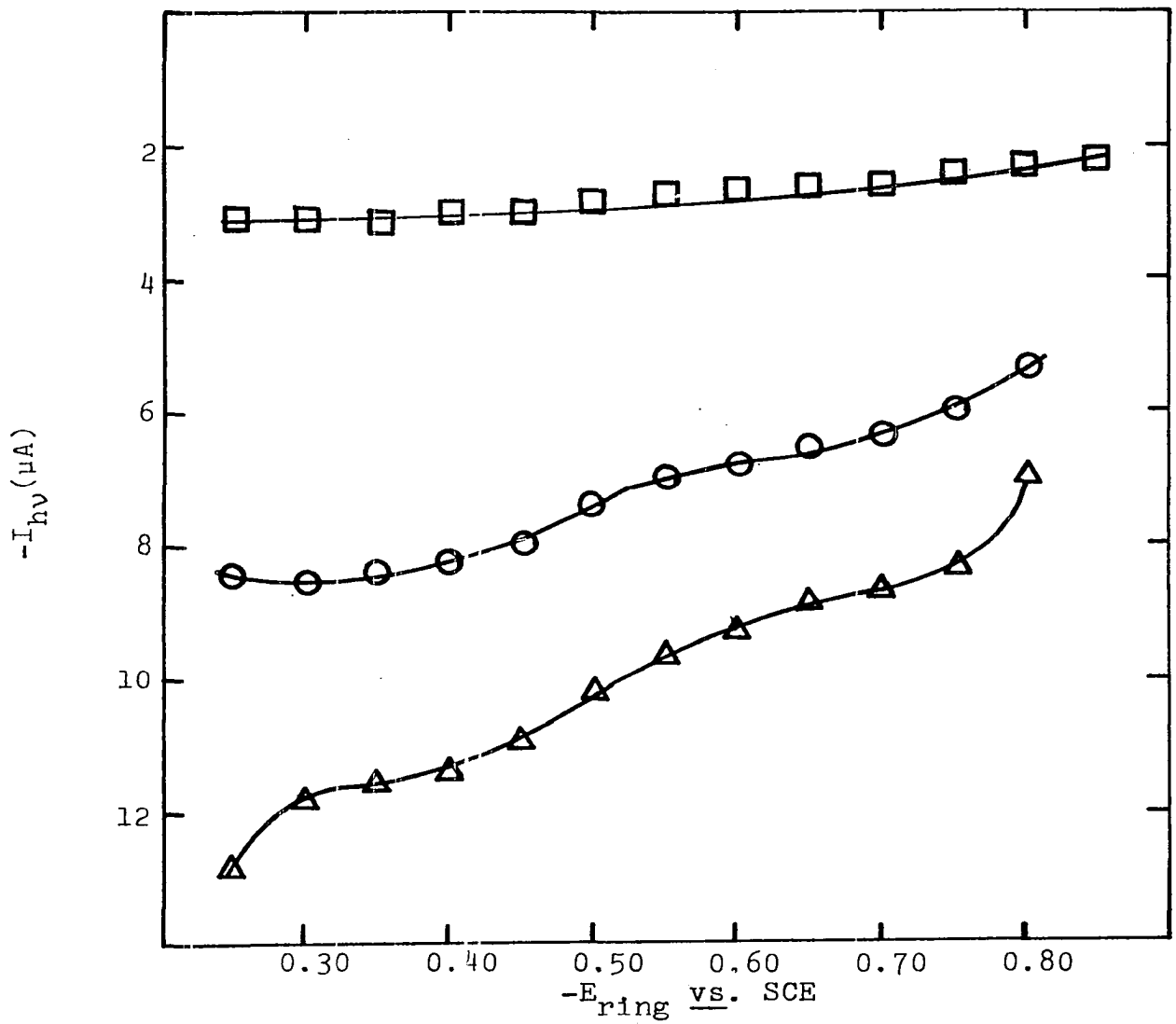
2
4
6
8
10
12
$-I_{h\nu}$ (μA)
0.30
0.40
0.50
0.60
0.70
0.80
$-E_{ring}$ vs. SCE

From an inspection of Figure IV.5, it can be seen that the photocurrent reaches a limiting value at relatively low rotational velocities. This behavior indicates that the photolytically generated intermediates undergo slow homogeneous kinetics thus explaining the relatively small amount of benzil pinacol observed in Figure IV.4.

The maximum in the photoelectrochemical spectrum shown in Figure IV.6 roughly corresponds to a minimum in the transmittance spectrum.

C. The Photoelectrochemical Behavior of 9-Hydroxyfluorene

1. Introduction

Described here is a qualitative application of a RPE in a study of the photochemistry of 9-hydroxyfluorene in methanol and isopropanol.

A single report of research on the photochemistry of 9-hydroxyfluorene was found in the chemical literature. DeGroot (61) investigated several aromatic alcohols and their derivatives by flash photolysis and ultraviolet-visible spectrophotometry. The absorption spectra of the primary photoproducts for such systems show triplet-triplet transitions and singlet-radical absorption (61). In attempting to resolve the spectra, DeGroot dissolved the compounds in monomethylmethacrylate and polymerized the

Figure IV.5. $I_{h\nu}$ *vs.* rotational velocity

0.01 *M* Benzil in 70% MeOH/30% H_2O (v/v),

~~o o o~~ 0.1 *M* NaOH, ~~Δ Δ Δ~~ 0.2 *M* NaOH

——— E_r = -0.650 V, – – – E_r = -0.250 V,

λ = 270 nm

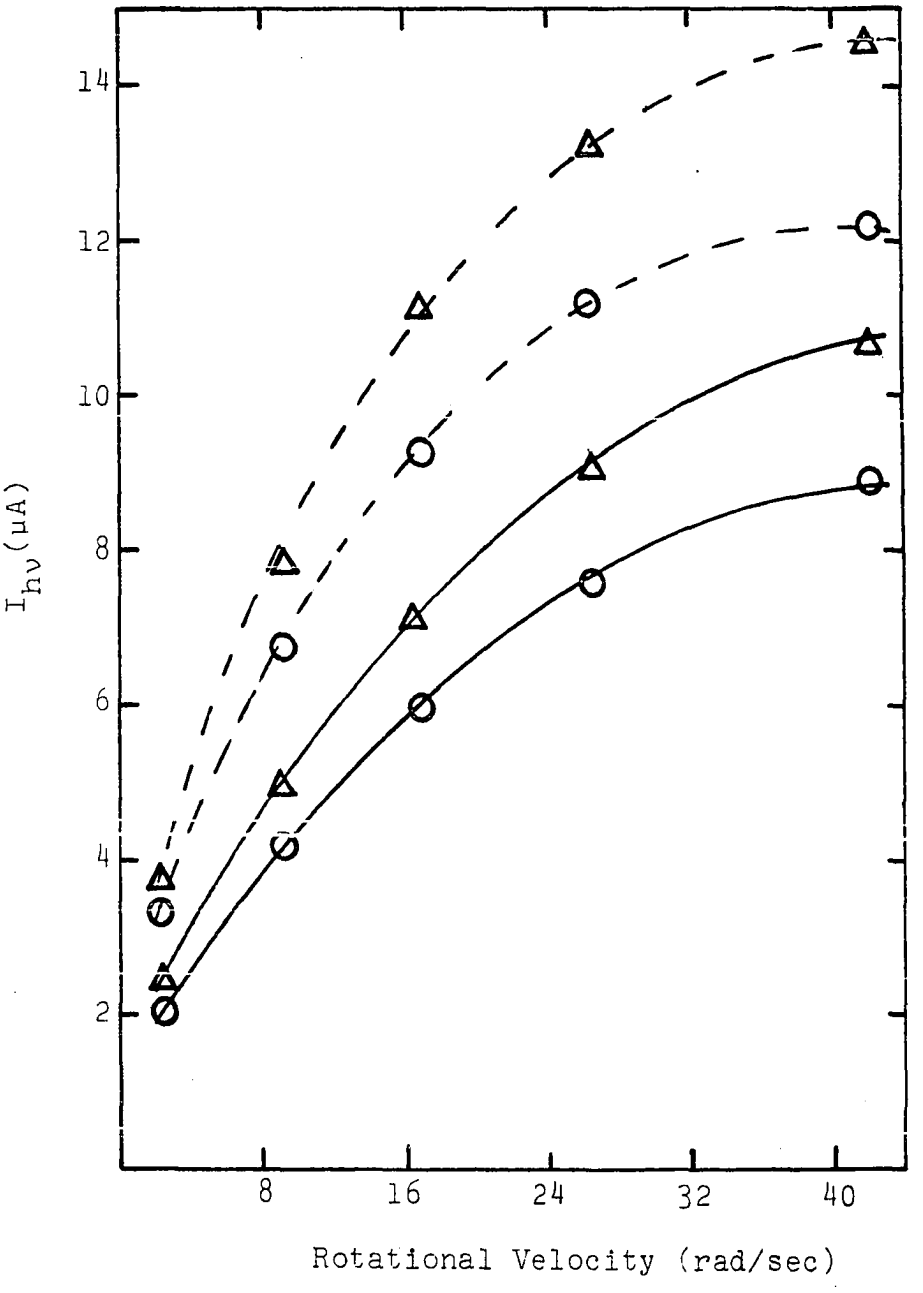
14
12
10
8
6
4
2
$I_{h\nu}$(μA)
8
16
24
32
40
Rotational Velocity (rad/sec)

Figure IV.6. ~~000~~ $I_{h\nu}$ *vs.* λ (nm)

0.01 M Benzil, 70% MeOH, 30% H_2O, (v/v)

0.1 M NaOH, rotational velocity = 42

rad/sec, E_r = -0.50 volts

——— % T *vs.* λ

1.23 x 10^{-4} M benzil in same solvent

system indicated above

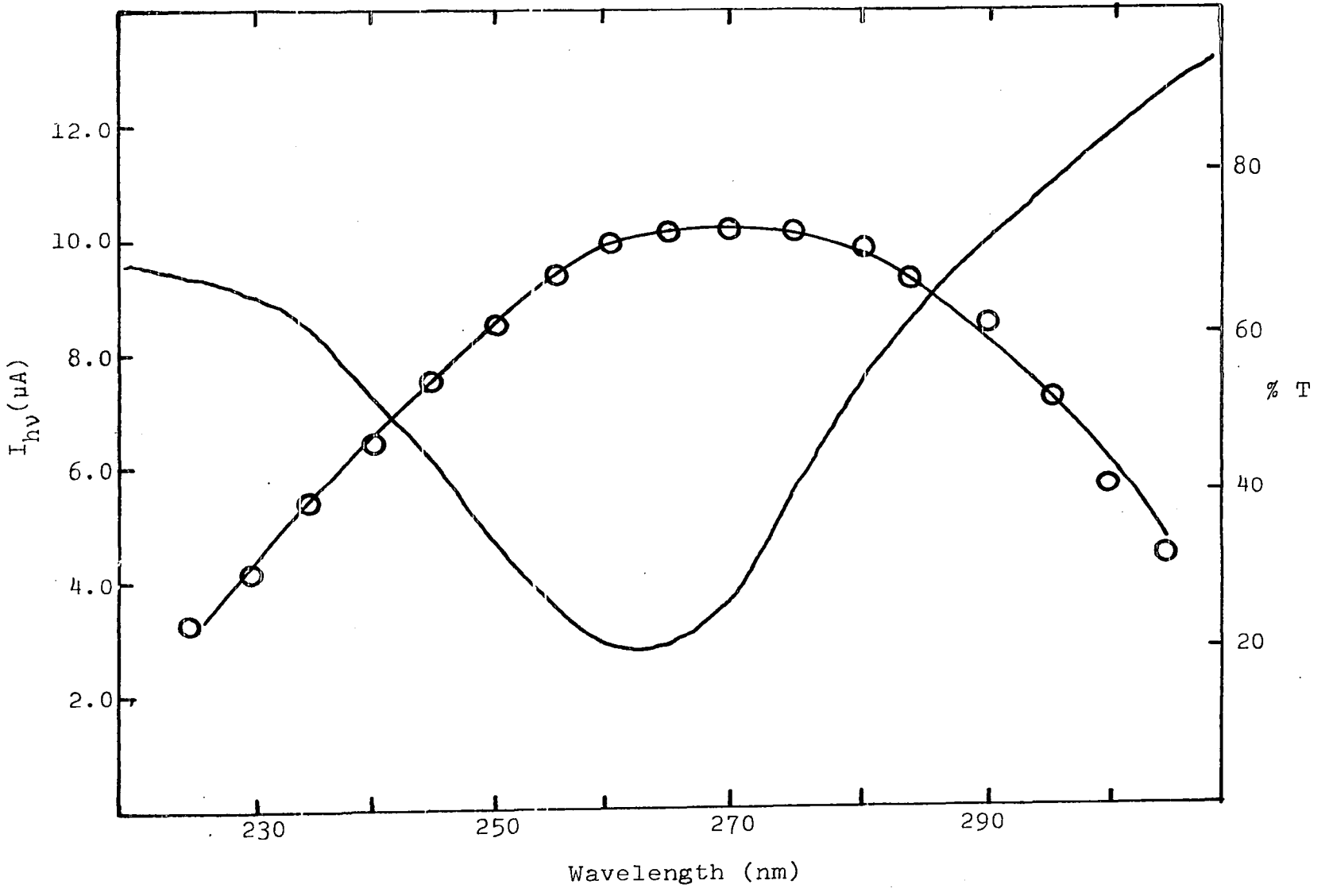
12.0
10.0
8.0
6.0
4.0
2.0
$I_{h\nu}$ (μA)
80
60
40
20
% T
230
250
270
290
Wavelength (nm)

samples. The lifetime of the radicals in solid polymethylmethacrylate is greatly increased over that in the liquid state and the radical spectra were obtained after decay of the triplet electronic states. DeGroot observed, however, that 9-hydroxyfluorene is quantitatively oxidized to 9-fluorenone during the polymerization and could not be studied in this media. He photolyzed 9-hydroxyfluorene in isooctane and detected a relatively stable photoproduct with a lifetime of approximately 15 minutes. The photoproduct gave absorption maxima at 384 nm, 365 nm, and 350 nm and was proposed by DeGroot to be the oxyradical of 9-hydroxyfluorene. DeGroot also studied the compound in triisopropylborate (TIPB). The flashed solutions produced absorption spectra with maxima at 350 nm. No electron spin resonance signal was detected for the photoproduct and DeGroot suggested it was a stable dimer of the oxyradical. Aromatic alcohols were found by Orloff (107) to react with TIPB to produce the corresponding di-isopropylborate ether derivatives of the alcohols. Hence, the photochemical behavior observed by DeGroot was that of the ether and not pure 9-hydroxyfluorene.

It is concluded from these results reported here that both the fluorenyl and 9-oxyfluorenyl radicals are produced by photolysis in the presence of methanol and isopropanol. All final products identified can be explained on the basis of reactions of these primary photoproducts.

2. Experimental

a. Instrumentation The photoelectrode, mercury-coating procedure, and rotator are described respectively in Sections III.B.1, III.B.3, and III.B.4. The light-source and optical system are described in Section III.C.1. The actinometric measurement of light intensity is described in Section III.C.3. The values of light intensity determined at several wavelengths is shown in Table IV.1.

Table IV.1. Light intensity at various wavelengths

λ(nm)	I_0 (quanta/sec)
240	3.6×10^{14}
270	6.0×10^{14}
290	1.0×10^{15}
310	1.3×10^{15}

Chromatographic separations were made on a Chromatronix Model 500 liquid chromatograph with a Model LC-6M column. The column was packed with 80-100 mesh Rohm and Haas Amberlite XAD-2 macroreticular resin with bed dimensions of 6.3 mm x 15 cm. The eluent was 90% methanol-10% chloroform at a flow rate of 24 ml/hr. The column temperature was 25 ± 3°C. The detector was a Model 200 UV from Chromatronix

and the chromatograms were recorded on a Sargent Model SRG stripchart recorder.

b. Solutions and reagents Unless designated to the contrary, all reagents were Baker Analyzed Reagents.

Methanol was made 2M in NaOH and distilled from $NaBH_4$. Isopropanol was also distilled from $NaBH_4$. Baker Analyzed chloroform and absolute ethanol from Commercial Solvents of Chicago, Illinois, were both distilled once before use. All water was triply distilled with demineralization after the first distillation and the second being from alkaline permanganate solution.

Purified $NaClO_4 \cdot H_2O$ was obtained from Fisher Scientific Company of Fairlawn, New Jersey. Sodium hydroxide was Baker Analyzed Reagent. Solutions were deaerated with dispersed prepurified N_2 from Air Products of Allentown, Pennsylvania. A N_2 atmosphere was maintained over solutions during photolytic studies with a RPE. Dissolved O_2 is reduced electrochemically at the electrode potentials used in this study and the presence of traces of O_2 was signaled by observation of a large dark current.

Analyzed fluorene, 9,9'-bifluorene, and 9-fluorenone were obtained from Aldrich Chemical Company of Milwaukee, Wisconsin. The 9-fluorenone was recrystallized three times from ethanol and fluorene and bifluorene were each recrystallized three times from 50% ethanol-50% benzene solutions.

The 9-hydroxyfluorene was synthesized from fluorenone by reduction with $LiAlH_4$ followed by three recrystallizations from petroleum ether. The melting point of the product was 158.9 ± 0.1°C. Fluorenyl ether was prepared and purified according to a procedure given by Klagel (83). The melting point of the product was 238.0 - 238.5°C. All solid organic compounds were stored in a vacuum over Anhydrone from G. F. Smith Chemical Co. of Columbus, Ohio.

c. Five-hour photolysis A sample of 9-hydroxyfluorene weighing 0.910 g was placed in a 500 ml volumetric flask and dissolved and diluted to volume with absolute isopropanol or absolute methanol. The solution was thoroughly mixed and half placed in each of two cells of the type used with the RPE. The solutions were deaerated for 20 min. with N_2. One solution was irradiated for 5 hr. at a specified wavelength with the beam transmitted by the quartz disk of the RPE. The second solution was kept in a dark place. A N_2 atmosphere was maintained over both solutions during the photolysis period to exclude O_2. Following irradiation, 50-µl aliquots of each solution were chromatographed.

d. Extended photolysis Elimination of dissolved O_2 was essential during all photolytic studies. A special cell was used for extended photolysis periods greater than 5 hr. which could be tightly sealed following deaeration.

Use of this cell resulted in conservation of N_2. The cell, shown schematically in Figure IV.7, was constructed from a 1.0-cm x 7.5-cm Pyrex tube which contained the solution to be photolyzed. Following deaeration, the tube was connected by Tygon tubing to a 2-cm length of Pyrex tubing sealed at the upper end with a quartz disk. The test tube was then immersed in a 1.75-cm x 15-cm test tube containing Hg. The tube with the quartz disk was inserted into the rotator port where the RPE is normally attached. Hence, the photolysis beam was identical to that used for all studies with the RPE. A water bath was placed around the cell and thermostated at 25.0 ± 0.1°C. The Hg surrounding the inner vessel served (i) as a mirror to reflect back into the solution transmitted radiation and (ii) as a thermal conductor between the solution and the bath.

A sample of 9-hydroxyfluorene weighing 19 mg was dissolved in 3 ml of absolute methanol and irradiated at 290 nm for 48 hr. At the conclusion of the photolysis period, 0.1-ml aliquots of the irradiated solution were chromatographed. Each chromatographic fraction for several injections was collected in separate flasks. The solvent in each flask was evaporated by passing dry N_2 through the solution. The residue on the walls was washed down with a few drops of alcohol before completion of the evaporation. Mass spectra were obtained for each residue.

Figure IV.7. Apparatus for extended photolysis

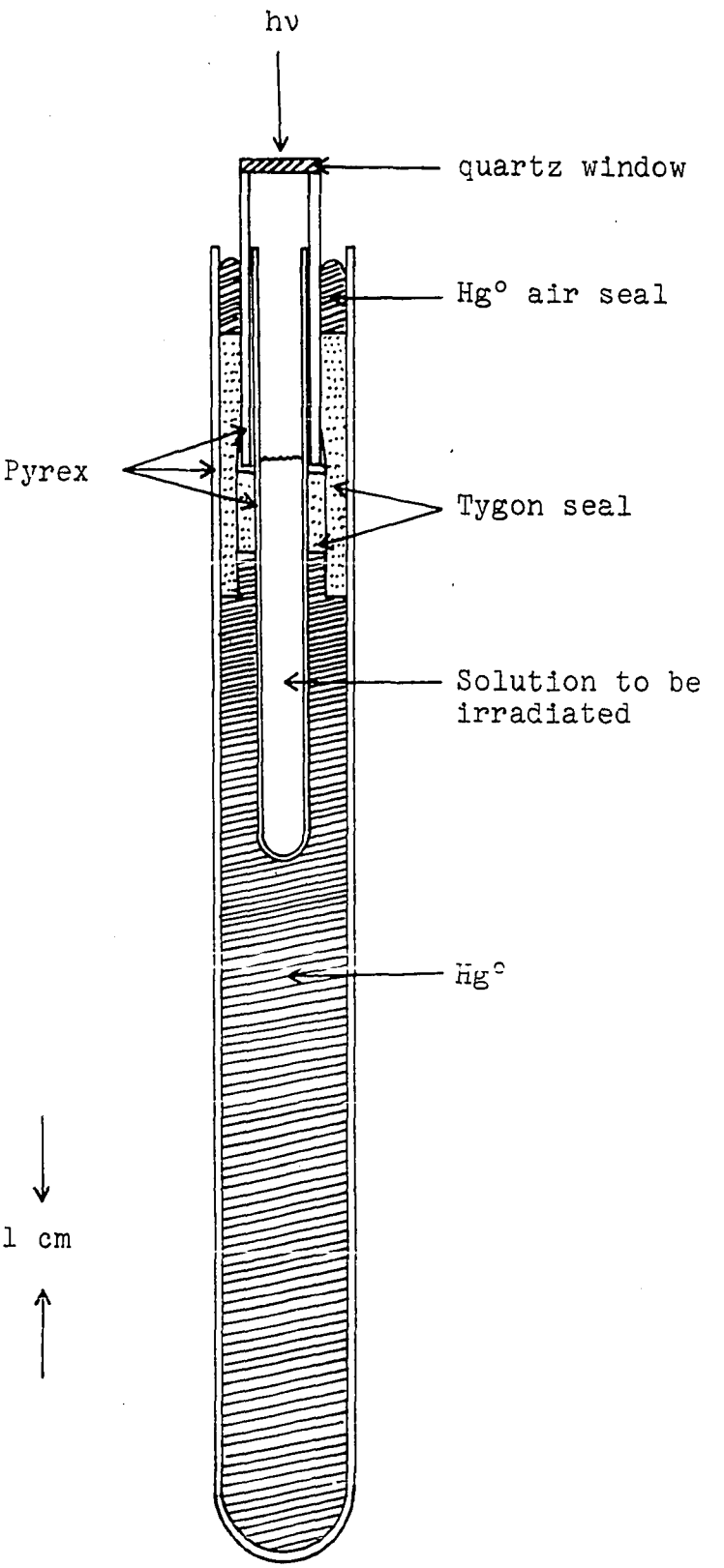
hν
quartz window
Hg° air seal
Pyrex
Tygon seal
Solution to be irradiated
Hg°
1 cm

3. Results and discussion

a. Photocurrent spectra Plots of photocurrent as a function of wavelength ($I_{h\nu}$-λ), hereafter referred to as photocurrent spectra, were obtained at E_{ring} = -0.80V and -1.40V and are shown in Figures IV.8 and IV.9 for 90% methanol-10% water and 90% isopropanol-10% water solutions which were 0.10 M in NaOH. Transmission spectra for the solutions are also given. Anodic maxima at 240 nm and 310 nm are observed in the photocurrent spectrum at E_{ring} = -0.80V for the isopropanol solution and very small photocurrents were obtained at E_{ring} = -0.80V for the methanol solution. This comparison of solvent effects is useful in recognizing products formed by hydrogen-abstraction reactions between a primary photoproduct and the organic solvent. The anodic photocurrents at E_{ring} = -0.80V are concluded to result from oxidation at the ring electrode of 2-hydroxy-2-propyl and hydroxymethyl radicals produced by these homogeneous reactions. Isopropanol is a more effective hydrogen donor than methanol and the larger anodic photocurrents in isopropanol is supporting evidence for the conclusion that the abstraction reaction in isopropanol is much faster than the reaction in methanol and fast relative to the rate of mass transport from the zone of the optical disk to the vicinity of the ring electrode of the RPE. Nekrasov and Korsun (104, 105) studied the electrochemistry of the radicals shown below:

Figure IV.8. $I_{h\nu}$ *vs.* wavelength and % T *vs.* wavelength

OO - 90% MeOH, 10% H_2O, 0.01 *M* NaOH

0.1 *M* 9-Hydroxyfluorene

ΔΔ - 90% i-PrOH, 10% H_2O, 0.1 *M* NaOH

0.1 *M* 9-Hydroxyfluorene

—— - Transmission spectrum for a

5×10^{-5} *M* solution of 9-Hydroxyfluorene

in 90% EtOH, 10% H_2O

E_r = -0.800 volts,

rotational velocity (ω) = 95 rad/sec

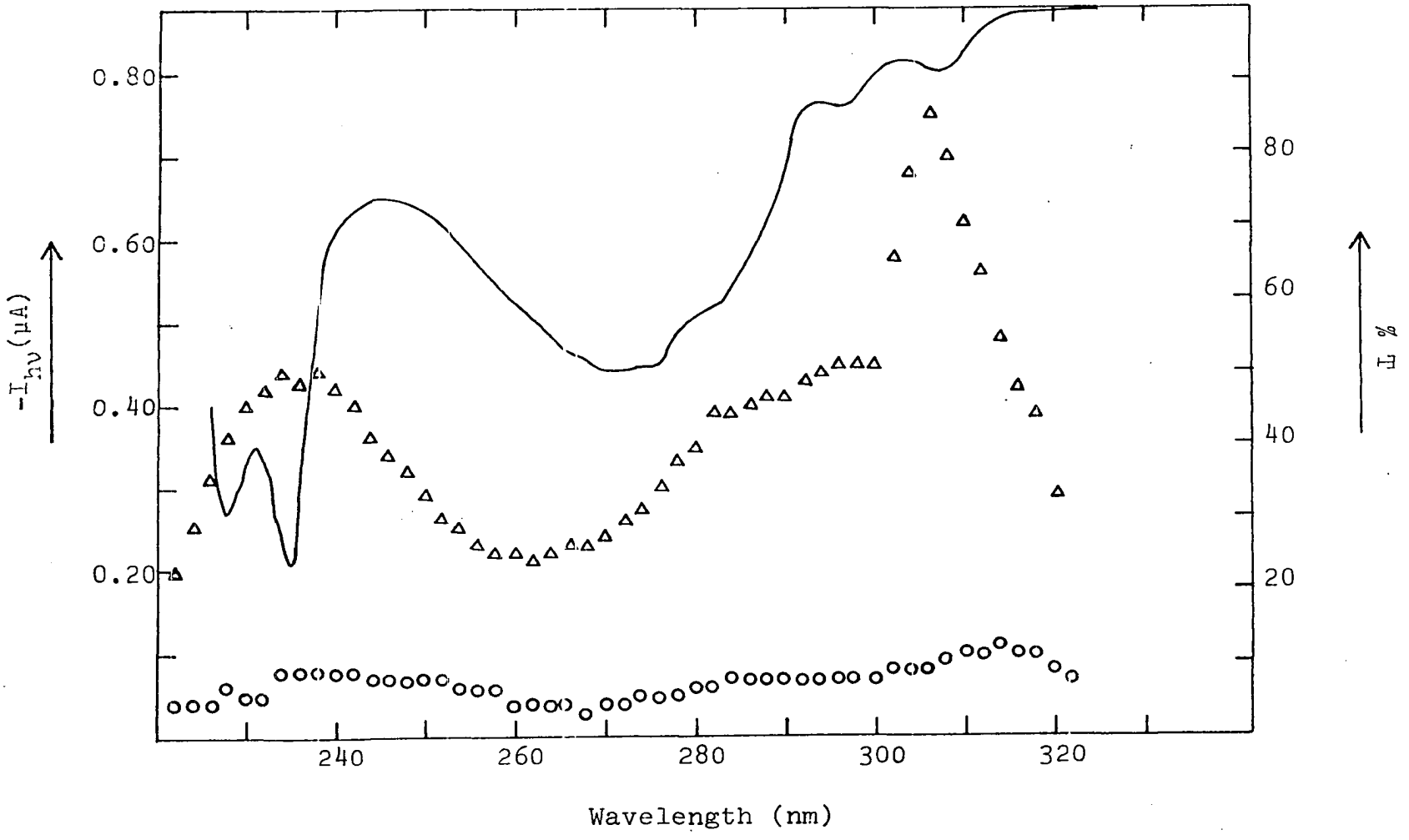
0.80
0.60
0.40
0.20
$-I_{h\nu}$ (μA)
80
60
40
20
% T
240
260
280
300
320
Wavelength (nm)

Figure IV.9. $I_{h\nu}$ *vs.* wavelength and % T *vs.* wavelength

OO - 90% MeOH, 10% H_2O, 0.1 *M* NaOH
0.1 *M* 9-Hydroxyfluorene

ΔΔ - 90% i-PrOH, 10% H_2O, 0.1 *M* NaOH
0.1 *M* 9-Hydroxyfluorene

—— - Transmission spectrum for a
5×10^{-5} *M* solution of 9-Hydroxyfluorene
in 90% EtOH, 10% H_2O

E_r = -1.40 volts,

rotational velocity (ω) = 95 rad/sec

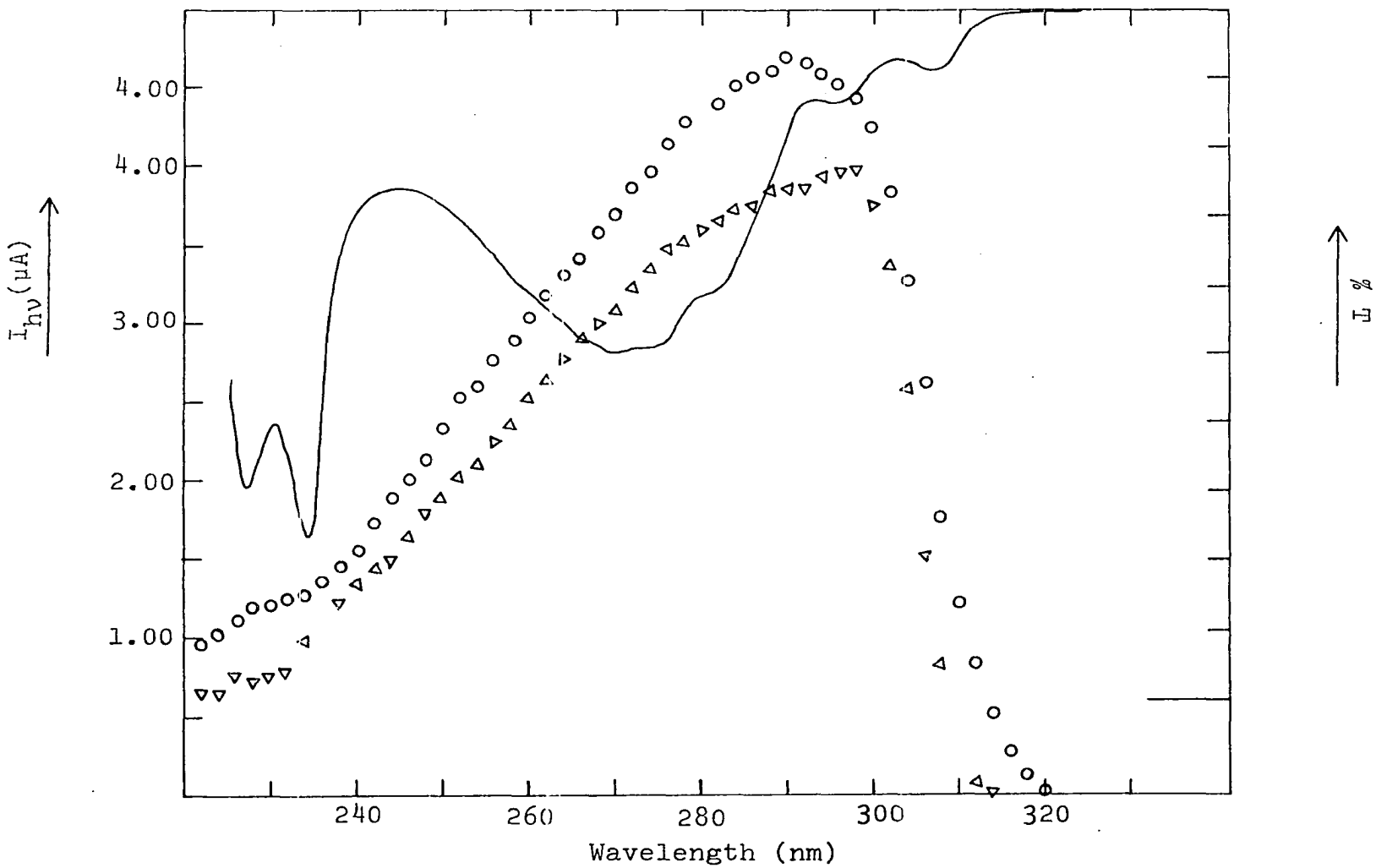
4.00
4.00
3.00
2.00
1.00
$I_{h\nu}$ (μA)
240
260
280
300
320
Wavelength (nm)
I %

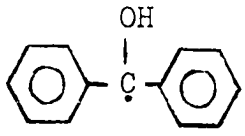

(A)

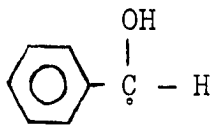

(B)

Radical (A) is oxidized at mercury electrodes in alkaline media for E > -1.20V. Substitution of a proton for the phenyl group (B) produced a negative shift of the oxidation potential to -1.50V. Hence, it is probable that the 2-hydroxy-2-propyl and hydroxymethyl radicals in these studies are oxidized at all values of E_{ring} used.

Large cathodic maxima at 290 nm are observed in Figure IV.9 at E_{ring} = -1.40V for both the methanol and isopropanol solutions and the magnitude of the photocurrents is nearly independent of the solvent. The maximum for isopropanol is slightly less than that for methanol but it must be kept in mind that the 2-hydroxy-2-propyl radical produced at 290 nm is probably simultaneously oxidized at this potential. The cathodic photocurrents decreased markedly with increasing wavelength through the region 305-320 nm where a sharp anodic maximum was obtained at E_{ring} = -0.80V in isopropanol. Apparently, the primary photoprocess changes upon changing the wavelength from 290 to 320 nm.

Photocurrent-potential ($I_{\pm h\nu}$-E_{ring}) curves for the photoproducts at 240 nm and 310 nm are shown in Figure IV.10 for methanol. Very small anodic photocurrents are

Figure IV.10. $I_{h\nu}$ *vs.* E_{ring}

o o o - 90% MeOH, 10% H_2O, 0.1 M NaOH,
0.1 M 9-Hydroxyfluorene, λ = 240 nm

o o o - 90% MeOH, 10% H_2O, 0.1 M NaOH,
0.1 M 9-Hydroxyfluorene, λ = 310 nm

rotational velocity (ω) = 95 rad/sec

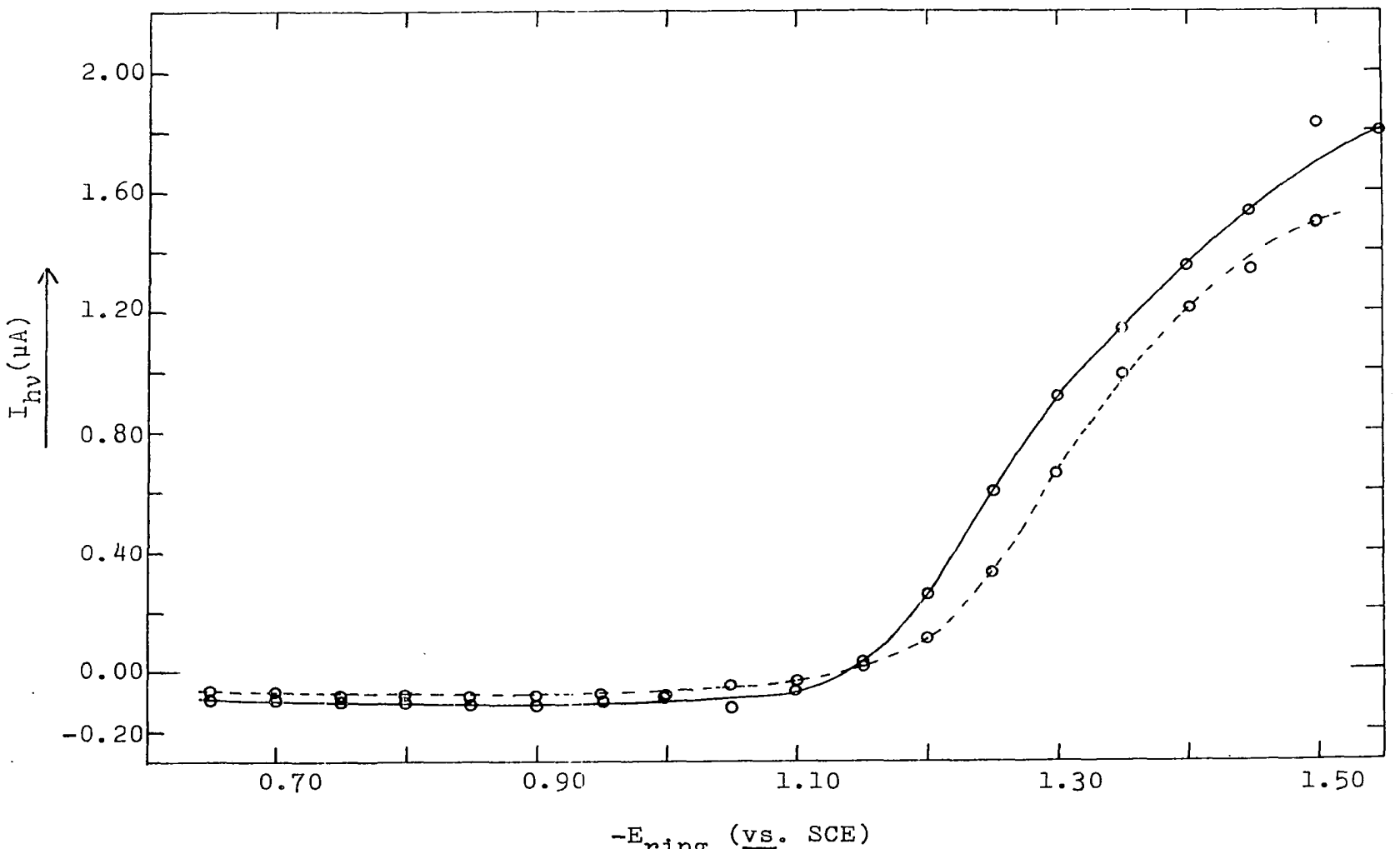
2.00
1.60
1.20
0.80
0.40
0.00
-0.20
$I_{h\nu}$ (μA)
0.70
0.90
1.10
1.30
1.50
$-E_{ring}$ (vs. SCE)

observed for $E_{ring} > -1.10V$ and relatively large cathodic currents are observed for $E_{ring} < -1.10V$. This large disparity between current magnitudes is consistent with the conclusion that the species reduced is not the same species oxidized at the ring electrode.

Photocurrent-potential curves for the photoproducts in isopropanol are shown in Figure IV.11. Large anodic currents were obtained for $E_{ring} > -1.10V$ relative to those in Figure IV.10 which is consistent with data shown in Figures IV.8 and IV.9. The ratio of cathodic current at $E_{ring} = -1.40V$ to anodic current at $E_{ring} = -0.80V$ is strongly dependent on wavelength and this is concluded to result because the primary photoproducts at the two wavelengths are not the same.

b. Variation of rotational velocity It will be demonstrated in Section VI that the digital simulation of the RPE (93) predicts that $I_{-h\nu}$-ω plots do exhibit maxima and the position of the maxima is a function of the rate of homogeneous reaction of the electroactive species produced photolytically. The maxima shift toward smaller values of ω as the rate of the homogeneous reaction decreases. The dependence of the photocurrent on the angular velocity of electrode rotation is shown in Figure IV.12. The position of the maxima for the two plots in Figure IV.12 are at different values of ω in agreement with an earlier conclusion that at least two photoproducts are formed in the wavelength

Figure IV.11. $\underline{I}_{h\nu}$ $\underline{vs}$. electrode potential

~~A A A~~ - 90% i-PrOH, 10% H_2O, 0.1 M NaOH,
0.1 M 9-Hydroxyfluorene, λ = 240 nm

~~A A A~~ - 90% i-PrOH, 10% H_2O, 0.1 M NaOH,
0.1 M 9-Hydroxyfluorene, λ = 310 nm

rotational velocity (ω) = 95 rad/sec

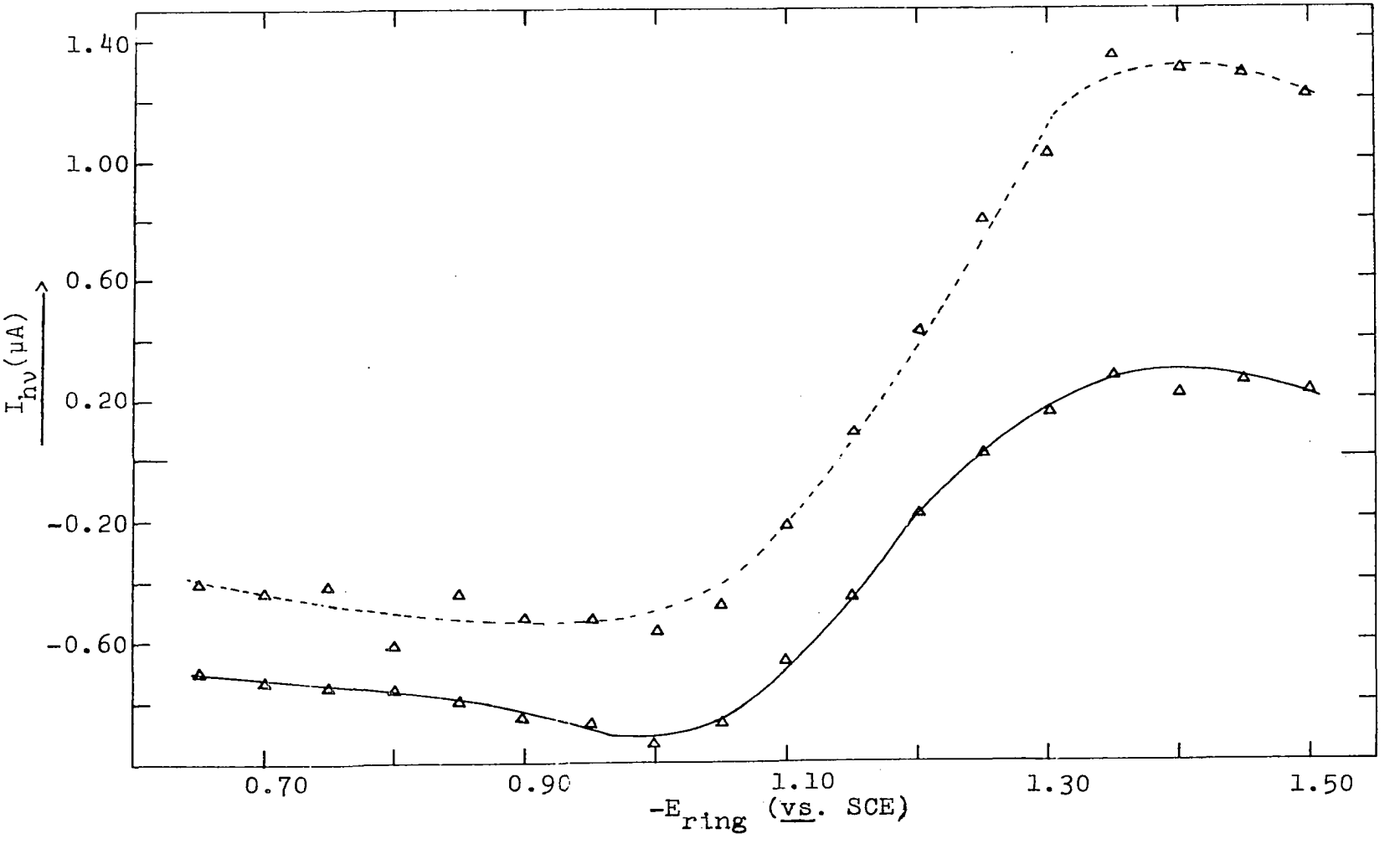
1.40
1.00
0.60
0.20
-0.20
-0.60
$I_{h\nu}$ (μA)
0.70
0.90
1.10
1.30
1.50
$-E_{ring}$ (vs. SCE)

Figure IV.12. $I_{h\nu}$ *vs.* rotational velocity

90% MeOH, 10% H_2O, 0.1 *M* NaOH,

0.1 *M* 9-Hydroxyfluorene

O - E_r = -1.40 volts

□ - E_r = -0.80 volts

---- λ = 240 nm

—— λ = 310 nm

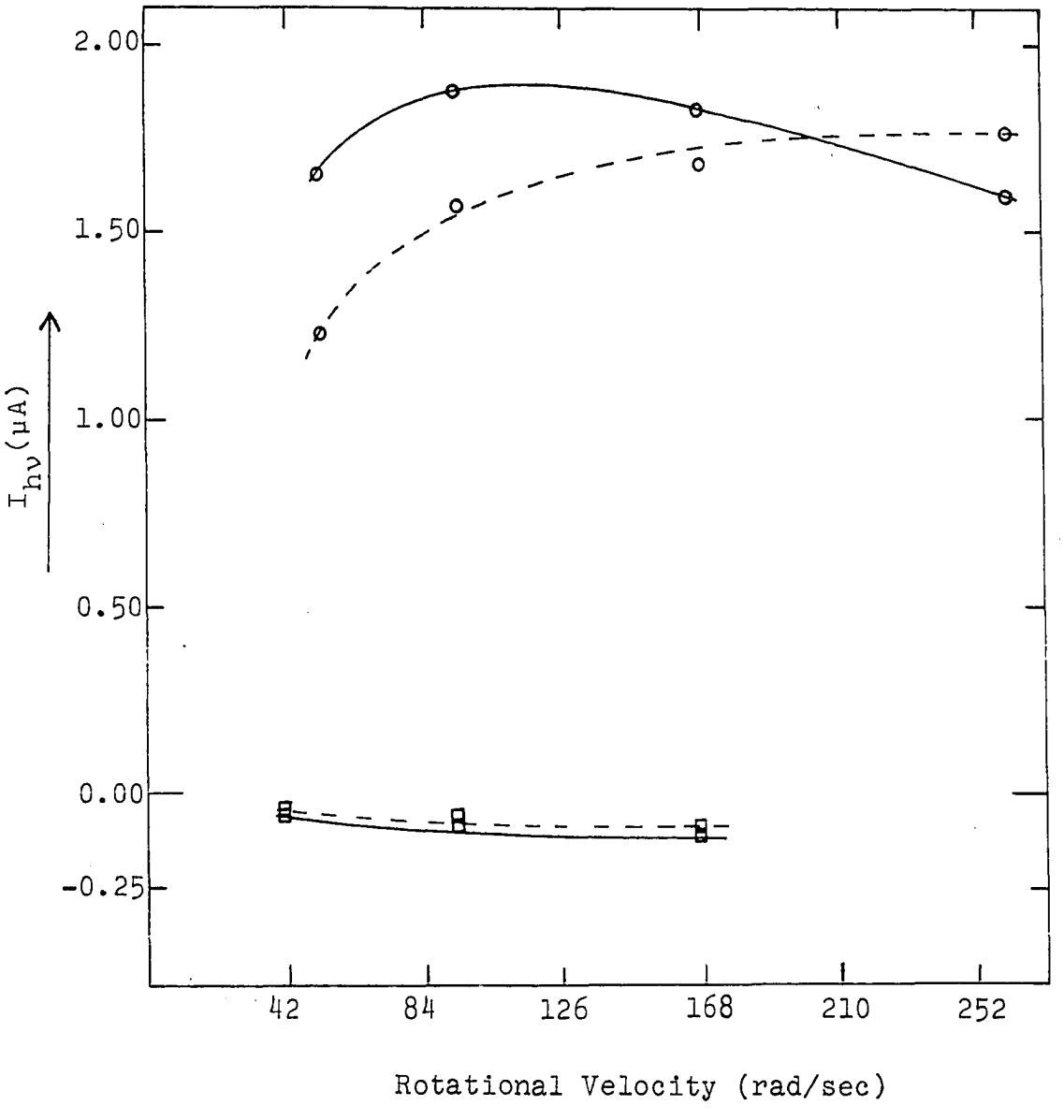
2.00
1.50
1.00
0.50
0.00
-0.25
$I_{h\nu}$ (μA)
42
84
126
168
210
252
Rotational Velocity (rad/sec)

range of Figure IV.10. The anodic photocurrents are very small in agreement with data shown in Figure IV.8. The plots of photocurrent versus rotational velocity for the isopropanol solution are shown in Figure IV.13. The data at E_{ring} = -1.40V is in agreement with the above conclusion of at least two primary photoproducts. The shape of the plots at E_{ring} = -0.80V are virtually the same in agreement with the conclusion that a single species is responsible for the anodic current at both wavelengths. This species is concluded to be the solvent radical produced by hydrogen abstraction from isopropanol.

c. Chromatographic separation Liquid chromatography was used to separate the photoproducts from a 5-hour photolysis. The chromatogram obtained for the methanol solution irradiated at 290 nm is shown in Figure IV.14. The solution kept in the dark produced a single chromatographic peak with a retention time identical to Peak 1 of Figure IV.14. The values of retention times for the peaks in Figure IV.14 are given in Table IV.2 together with retention times for various reference compounds suspected to be photoproducts. On the basis of data in Table IV.2, Peak 2 is tentatively identified as resulting predominantly from 9-fluorenone. A mechanism for the production of 9-fluorenone is given following Table IV.2.

Figure IV.13. $I_{h\nu}$ *vs.* rotational velocity

90% i-PrOH, 10% H_2O, 0.1 *M* NaOH,

0.1 *M* 9-hydroxyfluorene

O - E_r = -1.40 volts

□ - E_r = -0.80 volts

---- λ = 240 nm

—— λ = 310 nm

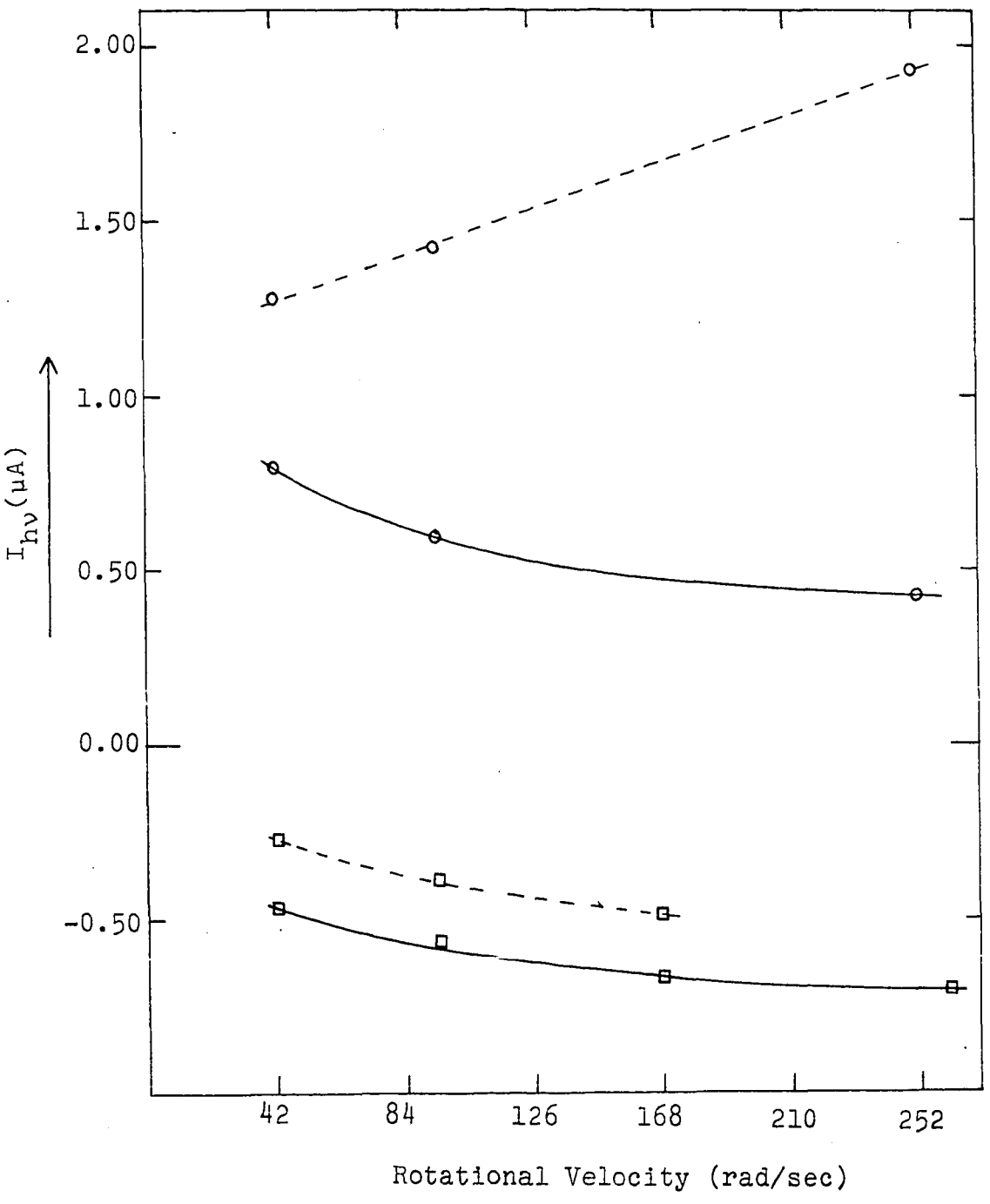
2.00
1.50
1.00
0.50
0.00
-0.50
$I_{h\nu}$ (μA)
42
84
126
168
210
252
Rotational Velocity (rad/sec)

Figure IV.14. High pressure liquid chromatogram for a 50 µl injection of a 0.01 M solution of 9-hydroxyfluorene irradiated at 290 nm for 5 hours. Resin = XAD-2, 80-100 mesh, eluent = 90% MeOH, 10% $CHCl_3$, flow rate = 24 ml hr^{-1}, temperature = 25±3°C

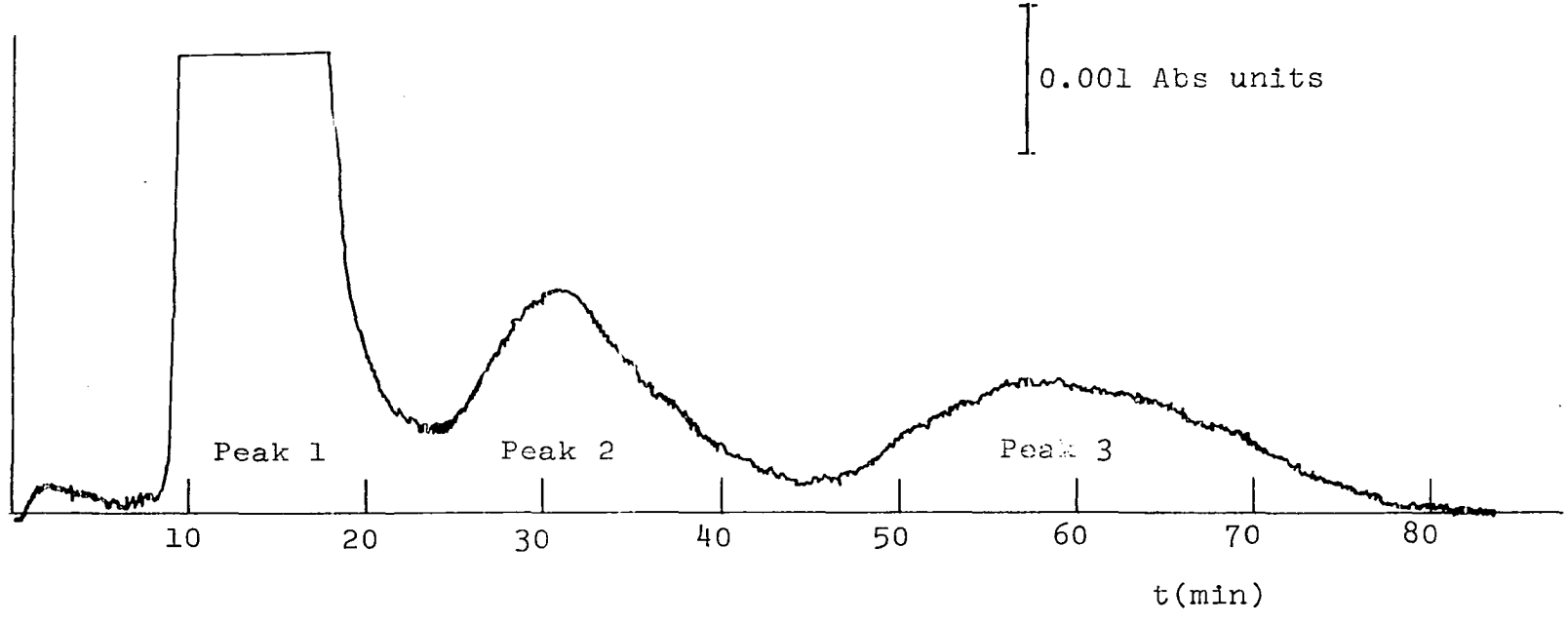
0.001 Abs units
Peak 1
Peak 2
Peak 3
10
20
30
40
50
60
70
80
t(min)

Table IV.2. Retention data

Compound	Retention Time (min)
Peak 1	11
Peak 2	31
Peak 3	57
9-Hydroxyfluorene	11
9-Fluorenone	30
Fluorene	50
9,9'-Bifluorene	60

Primary photochemical reaction (290-310 nm):

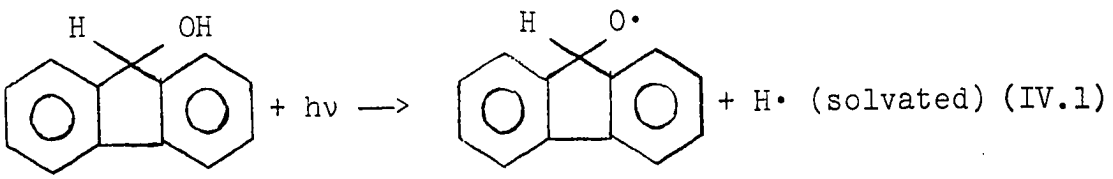

(IV.1)

Homogeneous chemical reaction:

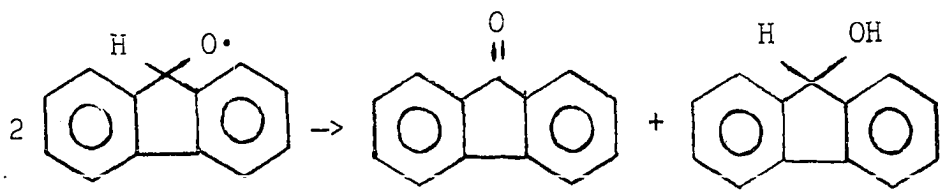

(IV.2)

The residue obtained following evaporation of the fraction corresponding to Peak 2 was milky yellow in color whereas pure 9-fluorenone is bright yellow. This fact is indicative of the presence of a contaminating species.

The retention time of Peak 3 is intermediate in that for fluorene and 9,9'-bifluorene. This is concluded to result because the fraction for Peak 3 contains both compounds.

The areas under the chromatographic peaks for the photoproducts (Peaks 2 and 3) are given in Table IV.3. Fluorene

Table IV.3. Chromatographic peak areas

Solvent	Wavelength	Peak 2 (sec)	Peak 3 (sec)
Methanol	240 nm	n.d.	0.281
Methanol	290 nm	1.37	1.96
Methanol	310 nm	1.41	0.169
Isopropanol	290 nm	n.d.	0.968

and 9,9'-bifluorene can both result from the fluorenyl radical; fluorene by hydrogen abstraction and bifluorene by radical dimerization as outlined below.

Primary photochemical reaction:

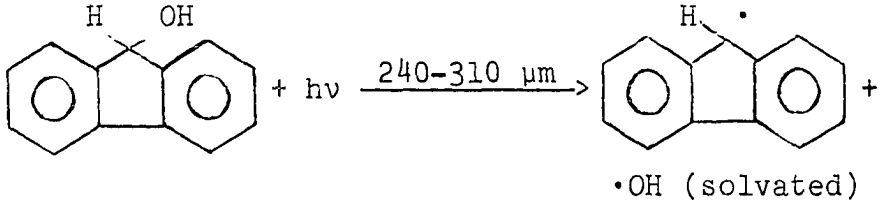

(IV.3)

Homogeneous chemical reactions:

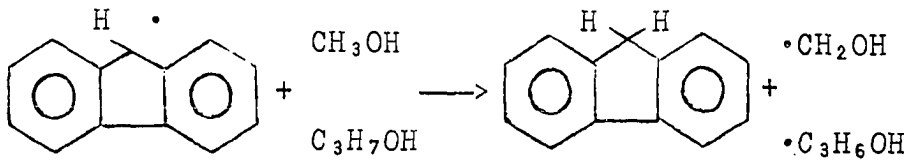

(IV.4)

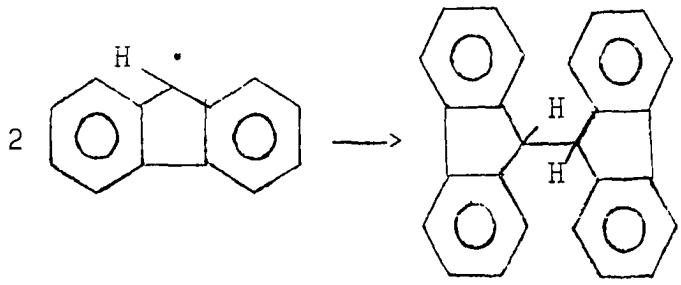

(IV.5)

The dependence of the area of Peak 3 on the wavelength shown in Table IV.3 is approximately shown by the cathodic photocurrent at E_{ring} = -1.40V in Figure IV.9. Note particularly the rapid fall-off at 310 μm. The photoproduct reduced electrochemically at -1.40V is concluded to be the fluorenyl radical. 9-Hydroxyfluorene, fluorene, and 9,9'-bifluorene

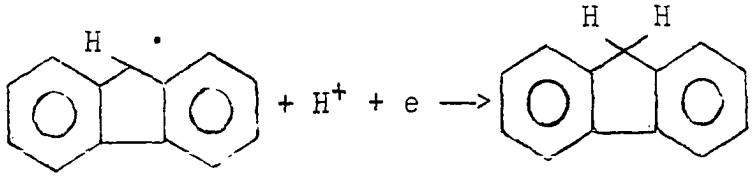

(IV.6)

do not exhibit electroactivity at ring potentials used in this study. 9-Fluorenone is reduced in these media by a two step process described below.

Step 1 ($E_{1/2}$ = -1.13V):

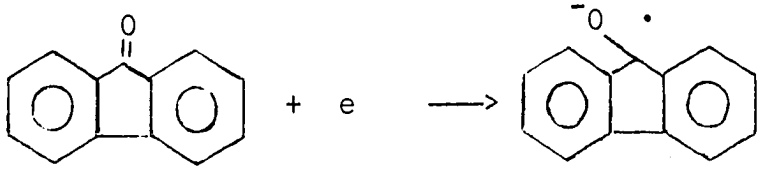

(IV.7)

Step 2 ($E_{1/2}$ = -1.38V):

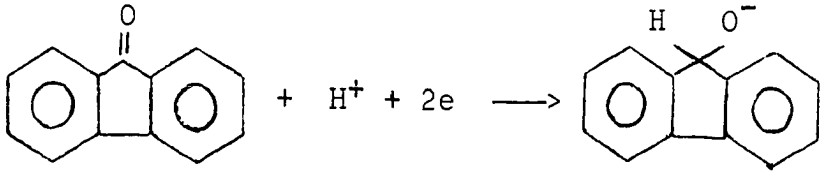

(IV.8)

The absence of a cathodic photocurrent peak at 310 nm in Figure IV.9 is evidence that the production of 9-fluorenone by Reaction IV.2 is slow on the time scale of mass transport at the RPE.

A chromatographic peak was not obtained for 9-fluorenone following photolysis of the isopropanol solution at 290 nm. Isopropanol is a very efficient proton donor in abstraction reactions. Proton abstraction by the oxyfluorenyl radical of 9-hydroxyfluorene and the absence of a peak for 9-fluorenone is evidence of the high efficiency of this reaction. Only a very small anodic current at E_{ring} = -0.80V was obtained in methanol at 310 nm whereas a large quantity of 9-fluorenone was obtained. It is concluded that hydrogen abstraction from methanol by the oxyfluorenyl radical does not occur to an appreciable extent in the time for mass transport from the zone of the optical disk to the ring electrode of the RPE.

d. Mass spectrometry Mass spectra were obtained for the residues remaining from evaporation of the chromatographic fractions following 48-hr. photolysis of 9-hydroxyfluorene in methanol at 290 nm. The photolysis cell and procedure are described in Section IV.C.2.c. The chromatogram had three peaks with retention times identical to those for the 5-hr. photolysis given in Table IV.2. The mass spectra are summarized in Table IV.4 together with spectra for reference compounds and data for isotopic abundance ratios of compounds with specified empirical formulas. The observed intensities are given in arbitrary units. Also given are the intensities relative to the base peak in each m/e grouping.

The intensities of peaks at m/e 182, 183, and 184 for chromatographic Peak 1 are consistent with the conclusion that 9-hydroxyfluorene (M.W. 182) is eluted under Peak 1. Mass peaks at m/e 196, 197, and 198 are evidence of the presence of a second compound. The relative intensities of these peaks are consistent with the abundance ratios for the empirical formula $C_{14}H_{12}O$ (M.W. 196). The identity of this species is proposed to be 9-hydroxymethenylfluorene which can be formed by the reaction of fluorenyl and hydroxymethyl radicals.

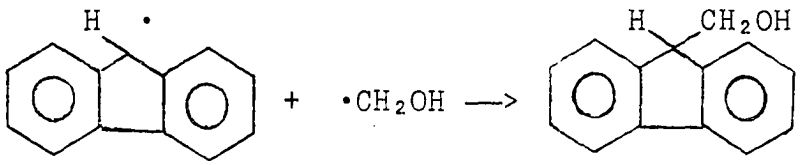

(IV.9)

Table IV.4. Mass spectral data for the chromatographic fractions and other reference compounds

m/e	Fluorene, $C_{13}H_{10}$ (M.W. 166)	9,9'-Bifluorene $C_{26}H_{18}$ (M.W. 330)	9-Fluorenone $C_{13}H_8O$ (M.W. 180)	9-Hydroxyfluorene $C_{13}H_{10}O$ (M.W. 182)	9-Fluorenyl ether $C_{26}H_{18}O$ (M.W. 346)	Irradiated Sample in Isopropanol (no separation)	Peak 1 for methanol (290 nm)	Peak 2 for methanol (290 nm)	Peak 3 for methanol (290 nm)	$C_{13}H_{10}O$ (M.W. 182)[a]	$C_{13}H_{10}$ (M.W. 166)[a]	$C_{13}H_8O$ (M.W. 180)[a]	$C_{14}H_{12}O$ (M.W. 196)[a]	$C_{16}H_{16}O$ (M.W. 224)[a]
165		2.48				5.0	2.0	2.7	6.50					
		100%				24%			65%					
166	10.90	0.50		0.8	1.81	20.4	5.0	1.4	9.98					
	100%	20%			29%	100%			100%		100%			
167	1.38	0.08		0.8	6.34	3.0	1.0	0.2	1.43					
	13%	3%			100%	15%			14%		14.2%			
168	0.15			0.1	1.01	0.2	0.1		0.10					
	1%				16%	1%			1%		0.9%			
180			9.88	0.83	3.79	13.0	2.55	2.93	0.25					
			100%	41%	60%		25%	100%				100.0%		
181			1.54	0.11	6.31	4.5	3.20	1.56						
			16%	5%	100%		31%	53%				14.2%		
182			0.14	2.02	1.49	10.5	10.2	0.22	0.2					
			1%	100%	24%		100%	8%		100%		1.1%		
183				0.33	0.17	1.8	1.68							
				16%	3%		16%			14.2%				
184				0.02		0.2	0.14							
				1%			1%			1.1%				

[a]Data obtained from Appendix A of Reference (137).

Table IV.4. (Continued)

m/e	Fluorene, $C_{13}H_{10}$ (M.W. 166)	9,9'-Bifluorene $C_{26}H_{18}$ (M.W. 330)	9-Fluorenone $C_{13}H_8O$ (M.W. 180)	9-Hydroxyfluorene $C_{13}H_{10}O$ (M.W. 182)	9-Fluorenyl ether $C_{26}H_{18}O$ (M.W. 346)	Irradiated Sample in Isopropanol (no separation)	Peak 1 for methanol (290 nm)	Peak 2 for methanol (290 nm)	Peak 3 for methanol (290 nm)	$C_{13}H_{10}O$ (M.W. 182)[a]	$C_{13}H_{10}$ (M.W. 166)[a]	$C_{13}H_8O$ (M.W. 180)[a]	$C_{14}H_{12}O$ (M.W. 196)[a]	$C_{16}H_{16}O$ (M.W. 224)[a]
346					0.99									
330		0.20 4% 4.61 100%					1.0 1.5		0.45 5% 8.48 100%					
329														
226						2.85 100% 0.55 19% 0.03 1%								100.0% 17.6% 1.6%
225														
224														
198						0.1	<1%	0.18 2%	0.02 1%				1.3%	
197						0.6	0.08 15%	1.82 16%	0.25 15%				15.11%	
196						3.5	0.52 100%	11.0 100%	1.63 100%				100.0%	

Chromatographic retention data is presented above to support the tentative designation of Peak 2 as resulting from 9-fluorenone (M.W. 180). An intense mass spectral peak was obtained at m/e 180 in the corresponding residue. However, the abundance ratios for m/e 181 and 182 are not those expected for pure 9-fluorenone. The coloring of the residue from Peak 2 was cited above as evidence of the presence of a second compound. The conclusion that the oxyradical is formed when 9-hydroxyfluorene is irradiated at 310 nm is not based entirely upon the formation of 9-fluorenone as a photoproduct. The large photocurrent obtained at 310 nm in Figure IV.8 indicates that a species is formed that is an excellent hydrogen abstractor; this is a characteristic of oxyradicals. The highly efficient hydrogen abstraction by the oxyradical results in a small quantum yield for the production of 9-fluorenone (see Section IV.C.3.e). The conclusion that no 9-hydroxyfluorenyl radical is produced is based upon the failure to observe the characteristic p-18 mass spectral peak of the fluorenone pinacol. The second compound is identified as 9-hydroxymethenylfluorene on the basis of the mass spectral pattern at m/e 196, 197, 198.

The mass spectrum for the residue from chromatographic Peak 3 contains peaks at m/e 329 and 330 with relative intensities consistent for the identification of 9,9'-bifluorene (M.W. 330). Mass peaks at m/e 196, 197, and 198

are also observed and again concluded to result from 9-hydroxymethenylfluorene. Mass peaks at m/e 166, 167, and 168 have relative intensities consistent for the identification of fluorene (M.W. 166).

The compound 9-hydroxymethenylfluorene produced by coupling of hydroxymethyl and fluorenyl radicals (Equation IV.9) was present in the residue of each chromatographic fraction with the most intense mass peaks in fraction 2 which probably corresponds to the maximum of a very broad chromatographic band. Photolysis of 9-hydroxyfluorene in isopropanol is expected, therefore, to lead to production of 9-(2-hydroxy-2-propyl)fluorene (M.W. 224). A 48-hr. photolysis was performed in isopropanol at 290 nm and the residue of photoproducts was analyzed by mass spectrometry. The results are included in Table IV.4. Mass spectral peaks were obtained at m/e 224, 225, and 226 with intensity ratios in agreement with expected isotopic abundance ratios for 9-(2-hydroxy-2-propyl)fluorene. Mass spectral peaks were also obtained confirming the presence of 9-hydroxyfluorene, fluorenone, fluorene, and 9,9'-bifluorene. There was no evidence in methanol or isopropanol solutions of coupling between solvent radicals and 9-oxyfluorenyl radicals to form the ether.

High resolution mass spectrometry was used for analysis of the residue following photolysis of 9-hydroxyfluorene in isopropanol at 240 nm. The results are

summarized in Table IV.5. A large mass peak was obtained for fluorene. Two unidentified compounds having formula $C_{13}H_8O_2$ and $C_{14}H_{12}O$ with M.W. 196 were detected for an ionizing energy of 70 eV. These compounds were not detected for an energy of 6 eV and their presence in the mass spectrometer is concluded to result from ion-beam chemistry and not the photolysis reaction. A small amount of 9-(2-hydroxy-2-propyl)fluorene was also detected as expected for the isopropanol solution.

Table IV.5. High-resolution mass spectrometry

m/e	Formula	Identity	Intensity (70 eV)	Intensity (6 eV)
165.070±0.001	$C_{13}H_9$	fluorenyl radical	7.5	0.4
166.078±0.001	$C_{13}H_{10}$	fluorene	8.0	6.5
196.053±0.001	$C_{13}H_8O_2$	?	0.4	n.d.
196.088±0.002	$C_{14}H_{12}O$	?	0.1	n.d.
224.098±0.002	$C_{16}H_{16}O$	9-(2-hydroxy-2-propyl)fluorene	0.5	0.4
330.141±0.003	$C_{26}H_{18}$	9,9'-bifluorene	0.5	0.4

Cathodic photocurrents shown in Figure IV.9 for E_{ring} = -1.40V were concluded to result from reduction of the fluorenyl radical produced by a primary photochemical reaction (Equation IV.3). The fluorenyl radical is produced over the wavelength range 200-310 nm with the peak rate of production occurring at 290 nm. Anodic photocurrents for

isopropanol solutions shown in Figure IV.8 for E_{ring} = -0.80V were concluded to result from oxidation at the ring electrode of the solvent radical produced by hydrogen abstraction (Equation IV.4). The abstracting photoproduct in the wavelength range 200-290 nm is the fluorenyl radical. The sudden increase in anodic current for wavelengths above 300 nm with the peak at 310 nm is concluded to be due to hydrogen abstraction by 9-oxyfluorenyl radical produced in that wavelength region. The increase in anodic current in the region 260-300 nm corresponds very closely with the increase in production of fluorenyl radical in that same wavelength region. On the basis of mass spectral data, the fluorenyl radical is the only primary photoproduct produced in the wavelength range 200-260 nm. The reason for the anodic photocurrent peak at 240 nm (Figure IV.9) is explained if the photochemical production of fluorenyl radical in this region results from a $S_0 \rightarrow S_2$ electronic transition whereas the photochemical reaction in the range 260-300 nm results from a $S_0 \rightarrow S_1$ electronic transition. The excess electronic energy in the fluorenyl radical produced from the S_2 excited state results in a "hotter" hydrogen abstracting character and faster abstraction in comparison with the rate of convective mass transfer at the RPE. No attempt was made to estimate the rate constants for the various abstraction reactions.

e. Quantum yield for photoproducts The area under a chromatographic peak obtained by a spectrophotometric detector for injection of V_x ml of a solution containing an absorbing species at concentration C_x (moles/liter) is given by Equation IV.10. In Equation IV.10, ε is the molar

$$A_x = \varepsilon\, b\, V_x C_x / v_f \qquad \text{(IV.10)}$$

absorptivity (M^{-1} cm^{-1}), b is cell path length (cm), and v_f is the volume flow rate of the eluent (ml/min). The product εb can be easily evaluated from the chromatographic area for an injection of V_s ml of a standard solution of concentration C_s. Substituting for εb yields Equation IV.11. The

$$A_x = A_s(V_x C_x / V_s C_s) \qquad \text{(IV.11)}$$

concentration C_x is that of a photoproduct from photolysis for T_{sec} by a light beam of intensity (quanta/sec) of a solution having total volume V_{tot}. C_x is a function of the quantum yield Φ for the photochemical reaction. In Equation IV.12, N is Avogadro's number (6.02×10^{23} molecules/mole)

$$\Phi = C_x N V_{tot} / I_0 T \qquad \text{(IV.12)}$$

and V_{tot} is in liters. Solving Equation IV.11 for C_x and substituting into Equation IV.12 yields Equation IV.13.

$$\Phi = \left(\frac{A_x}{A_s}\right)\left(\frac{V_s}{V_x}\right)\left(\frac{N\, V_{tot}\, C_s}{I_0\, T}\right) \qquad \text{(IV.13)}$$

Two determinations of Φ for 9-fluorenone at 290 nm for a 5-hr photolysis yielded the values 0.018 and 0.021 molecule/quanta.

The individual values of quantum yield for fluorene and 9,9'-bifluorene could not be determined because chromatographic peaks for these species were not resolved and appeared as Peak 3 (see Figure IV.14). The quantum yield for the combined production of the two species can be determined using the equations above provided the product εb for each are nearly the same. The values of εb were determined by injection of standards to be within 4%. Two determinations of Φ for the combined production of fluorene and bifluorene at 290 nm for a 5-hr photolysis yielded the values 0.101 and 0.088 molecule/quanta.

V. THE ELECTROCHEMICAL BEHAVIOR OF BENZOPHENONE AND BENZIL

A. Introduction

Before the rotating photoelectrode was used to determine the rate constants for the various homogeneous kinetics processes undergone by photolytically generated intermediates, it was decided to conduct a thorough study of the electrochemical behavior of benzophenone and benzil using a mercury-coated, platinum, rotating, ring-disk electrode (MPRRDE).

Kinetic and mechanistic studies in electrochemistry and analysis are frequently conducted with a hanging mercury drop electrode or a dropping mercury electrode. The experimental basis for these studies is the measurement of differences between the observed electrical current under kinetic control and the current predicted assuming mass transport limitation; the difference is a function of the controlling rate constant. It is frequently desirable, therefore, to maximize the rate of mass transport by rapid agitation of the solution especially to permit accurate determination of rate constants for fast reactions. While a mercury electrode has the frequently desired characteristics of high surface activity in many electrochemical reactions and a large overpotential for hydrogen evolution in aqueous media, its liquid state prevents use in rapidly stirred solutions. Mercury-plated

solid electrodes, on the other hand, represent a convenient and useful marriage of the surface properties of mercury electrodes and a solid geometry.

The rotating ring-disk electrode was introduced by Frumkin and Nekrasov (67) as a means of detecting intermediates of the electrode reactions.

In the reaction at the disk

$$A \pm ne \rightarrow B \qquad (V.1)$$

an intermediate B is produced and can be detected by applying a sufficient potential at the ring such that all of B reaching the ring is oxidized or reduced back to A. If B is a stable species, then the ratio of the ring current (I_r) to the disk current (I_d) is a function only of the geometry of the electrode; and this ratio is commonly called the theoretical collection efficiency (N).

If species B undergoes some reaction to form an electroinactive species C while traveling from the disk to the ring, then the observed (or kinetic) collection efficiency N_k will be lower than N due to the decrease in I_r. In this case, the collection efficiency is a function, not only of electrode geometry, but also of the rate constant of the reaction, the rotation speed and other solution parameters.

Prater and Bard have developed and applied a digital simulation technique to first- and second-order EC mechanisms (122-124).

In the pseudo-first order case

$$A \mp ne \rightleftharpoons B \qquad (V.2)$$

$$B \xrightarrow{k_1} C \qquad (V.3)$$

or the pseudo-second order case

$$A \pm ne \rightleftharpoons B \qquad (V.4)$$

$$B + X \xrightarrow{k_2} C \qquad (V.5)$$

or

$$2B \longrightarrow C \qquad (V.6)$$

where C is electroinactive. The concentrations of A and B are simulated at the ring and disk electrodes for changes due to axial and radial convection, axial diffusion and homogenous kinetics. From the concentrations of A and B, the ring and disk currents are then calculated; and finally, the collection efficiency $N_{\underline{k}}$ is outputed. By inputing a series of rate constants, a series of $N_{\underline{k}}$'s are obtained. Then a plot of $N_{\underline{k}}$ versus rate constant yields a working curve from which the experimental rate constant can be obtained. A complete description of the program can be found in references 122 and 123.

B. Benzophenone

1. Experimental

a. Electronic circuitry The four-electrode potentiostat was described in Reference (76).

b. Chemicals and reagents All chemicals and reagents used in this study are described in Section IV.A.2.a.

c. Mercury coating procedure The mercury coating procedure used to coat the PRRDE is described in Section III.B.3.

2. Results and discussion

The mechanism and kinetics for the electrochemical reduction of benzophenone in alkaline, aqueous-alcohol solution have been thoroughly studied and are described in Section II.C.

The kinetics of decay of the ketyl radical and radical anion in 50% isopropanol-50% water solutions was studied using flash photolysis and photoelectric spectrophotometry by Beckett and Porter (15). They pointed out that the rate of formation of dimers by the following three processes:

$$2\emptyset_2\dot{C}OH \xrightarrow{k_7} \text{dimer} \qquad (V.7)$$

$$\emptyset_2\dot{C}OH + \emptyset_2\dot{C}O^- \xrightarrow{k_8} \text{dimer} \qquad (V.8)$$

$$2\emptyset_2\dot{C}O^- \xrightarrow{k_9} \text{dimer} \qquad (V.9)$$

is given by Equation V.10,

$$2d(\text{dimer})/dt = k_7(\emptyset_2\dot{C}OH)^2 + k_8(\emptyset_2\dot{C}OH)(\emptyset_2\dot{C}O^-) + k_9(\emptyset_2\dot{C}O^-)^2 \qquad (V.10)$$

Since

$$K = (H^+)(\emptyset_2\dot{C}O^-)/(\emptyset_2\dot{C}OH) \qquad (V.11)$$

and

$$2d(\text{dimer})/dt = -d\{(\emptyset_2\dot{C}OH) + (\emptyset_2\dot{C}O^-)\}/dt \qquad (V.12)$$

then

$$-d(\emptyset_2\dot{C}O^-)/dt = K'_{obs}(\emptyset_2\dot{C}O^-)^2 \qquad (V.13)$$

where

$$K'_{obs} = k_7(H^+)^2/K((H^+) + K) + k_8(H^+)/((H^+) + K) + k_9K/((H^+) + K) \qquad (V.14)$$

In Equation V.14 K'_{obs} is the observed bimolecular rate constant for decay of the radical anion and is defined by Equation V.13. Beckett and Porter investigated the decay of the radical ion in the pH region 10-13 using it's absorption at 6300Å. Their plot of $\log_{10}(K'_{obs})$ <u>versus</u> pH is linear with a slope of -1 showing that Reactions V.7 and V.9 are unimportant under their conditions. Furthermore,

$$K'_{obs} = K_8((H^+)/K). \qquad (V.15)$$

The intercept at pH = 0 is 18.25 and, since pK = 9.2, $K_8 = 1.1 \times 10^9\ M^{-1}\ sec^{-1}$.

The kinetics of the decay of the free radical anion were studied in 50% isopropanol-50% water, 50% ethanol-50% water and 50% methanol-50% water. Figure V.1 contains typical I-E curves for the benzophenone obtained with a MPRRDE. The first wave is well defined, but the second wave is almost completely masked by hydrogen evolution. The ring current is noted to decrease during the cathodic scan for $E_{\underline{d}} < -1.7V$. This is due to the reduction of the ketyl radical ion at the disk electrode. Table V.1 contains values of pK'_{obs} obtaining from curves similar to those in Figure V.1.

Figure V.1. I_d *vs.* E_d and I_r *vs.* E_d
50% $EtOH/H_2O$ (v/v),
10^{-3} *M* benzophenone,
0.1 *M* NaOH

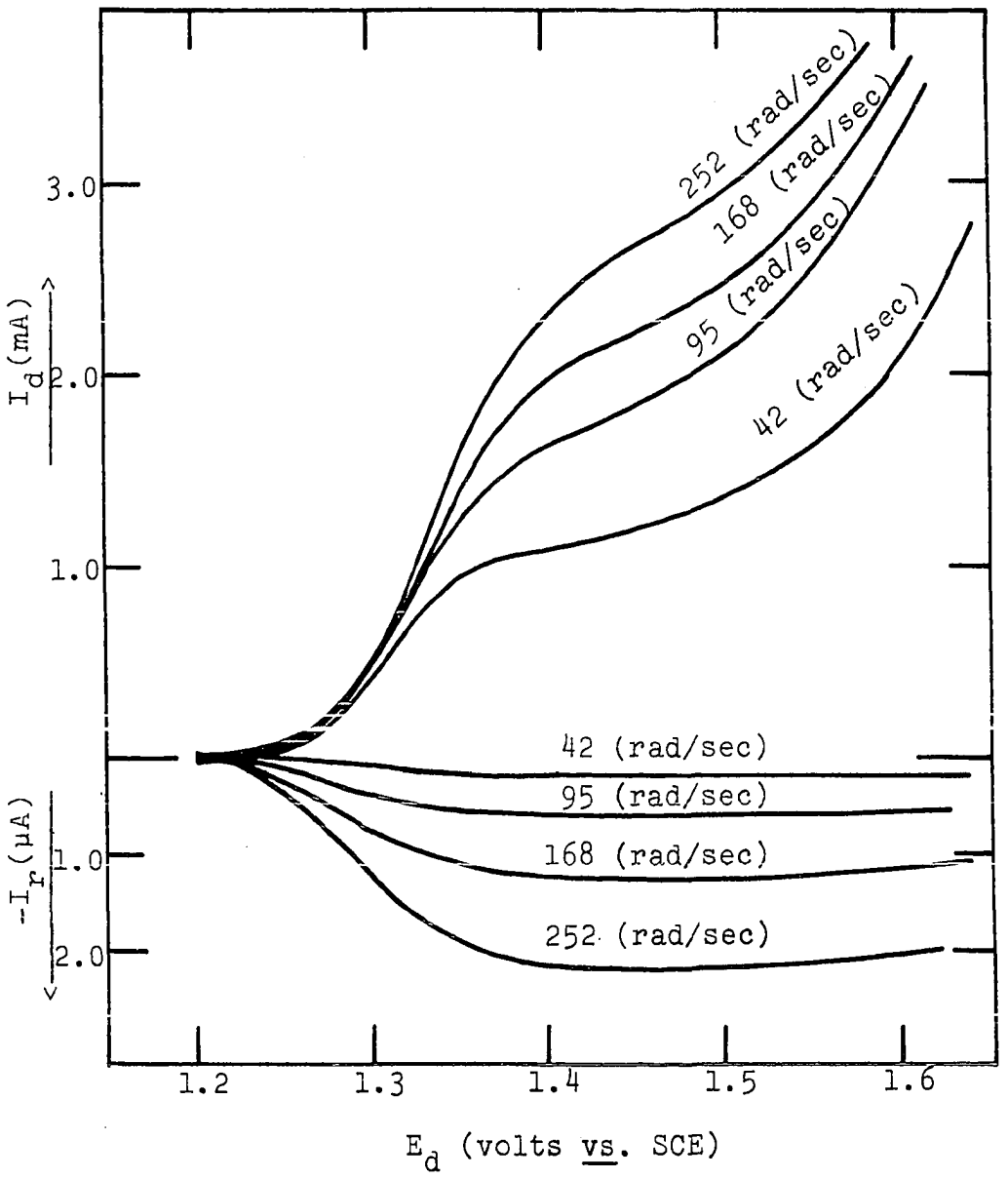
252 (rad/sec)
168 (rad/sec)
95 (rad/sec)
42 (rad/sec)
3.0
2.0
1.0
I_d (mA)
42 (rad/sec)
95 (rad/sec)
168 (rad/sec)
252 (rad/sec)
1.0
2.0
$-I_r$ (μA)
1.2
1.3
1.4
1.5
1.6
E_d (volts vs. SCE)

Table V.1. The observed rate of pinacolization as a function of pH

ω_b = 168 rad/sec

$C_{Benzophenone}$ = 1.0 m$\underline{M}$

Temp. = 25.0°C

Isopropanol		Ethanol		Methanol	
pH	pK'_{obs}	pH	pK'_{obs}	pH	pK'_{obs}
12.45	6.50	12.30	6.52	11.90	6.78
12.62	6.26	12.40	6.35	11.67	6.99
13.10	5.84	12.85	5.90	12.80	6.05
13.40	5.52	13.20	5.53	12.40	6.34

Plots of pH versus pK'_{obs} are linear with slopes of -1 and intercepts at pH = 0 of 18.62, 18.75 and 18.87 for the methanol, ethanol and isopropanol, respectively. The corresponding values of K_s are $K_{s_{MeOH}}$ = 2.6 x 10^9, $K_{s_{EtOH}}$ = 3.5 x 10^9, and $K_{s_{i\text{-}PrOH}}$ = 4.6 x 10^9 M^{-1} sec^{-1}.

C. Benzil

1. Introduction

A review of the literature describing the electrochemical behavior of benzil in alcohol-water solutions is given in Section II.D. A rotating mercury-coated, ring-disk electrode was used to study the electrochemical reduction of benzil in strongly alkaline media. The usefulness of rotating ring-disk

electrodes has been demonstrated for studies of electrochemical reactions of organic molecules involving reactive intermediates (3, 68, 104, 105). Galus and Adams (68) used a ring-disk electrode constructed with electrodes of carbon paste to study the electrochemical oxidation of N,N-dimethylaniline. Nekrasov and Korsun (104, 105) used an amalgamated ring-disk electrode to study the intermediates produced by the reduction of benzophenone and benzaldehyde.

Prater and Bard (122-124) described methods using digital simulation whereby the rate of a homogeneous reaction involving the product of an electrochemical reaction at the disk electrode can be determined from the value of the experimental collection efficiency determined under the kinetic situation, N_k, by the use of a complex function calculated by digital computation. We applied their programs for the case of a first-order decay of the stilbendiolate intermediate produced in this study. For more information on the application of those simulation techniques, the reader should consult the original literature (122, 123).

Albery and Bruckenstein (3) solved the equation of convective-diffusion for the RRDE for the case of the reaction at the ring electrode of a species produced electrochemically at the disk which decomposes homogeneously by a

at the disk which decomposes homogeneously by a first-order process to an electroinactive species. The relationship between N_o, $N_{\underline{k}}$, and the rate constant, k, is given by Equation V.16. In Equation V.16, ν is the kinematic

$$\frac{N_o}{N_{\underline{k}}} = 1 + 1.28(\frac{\nu}{D})^{1/3}\frac{k}{\omega} \qquad (V.16)$$

viscosity of the solution, ω is the angular velocity of electrode rotation and D is the diffusion coefficient of the unstable intermediate. The derivation required certain approximations, and the authors caution that it is valid only when the value of $(k/D\omega)^{1/2}(D/0.51)^{1/3}\nu^{1/6} \leq 0.5$. Equation V.16 was used to evaluate k when it could be accurately applied.

It was concluded on the basis of experimental results given here that both cis- and trans-stilbendiolate are produced by electrochemical reduction of benzil in 1:1 (v/v) methanol-0.1 M NaOH. Both isomers are oxidized at a mercury electrode by processes having virtually identical values of $E_{1/2}$. The values of the rate constants for the ketolization of cis- and trans-stilbendiolate in this media were determined using data obtained with a MPRRDE and the results of a digital simulation of the convective-diffusional processes at the rotating electrode, coupled with the particular electrochemical and chemical reactions for this system.

2. Experimental

Baker Technical Grade benzoin was recrystallized three times from water-ethanol solution and stored in a vacuum desiccator with Anhydrone as the desiccant. The benzil used is described in Section IV.B.2.a. Baker Analyzed Reagent methanol and sodium hydroxide were used without further purification. A stock solution of $Al(OH)_4^-$ was prepared by dissolving Baker U.S.P. Al in NaOH. All water was doubly distilled after deionization with the second distillation being from alkaline permanganate. All solutions were de-areated prior to use by dispersing Air Products high purity nitrogen (99.999%) through them. A nitrogen atmosphere was maintained over the solutions during use. All potentials were measured and are reported in V *versus* SCE.

The ring and disk electrode of the platinum ring-disk electrode were coated with mercury at the start of each experimental day by the procedure described in Section III. B.3.

3. Results and discussion

a. *Determination of collection efficiency* Typical experimental values of N_o for the platinum, rotating ring-disk electrode (RRDE) and the MPRRE are given in Table V.2. The value of N_o for the RRDE is essentially independent of rotational velocity as predicted by theory (3). The average

Table V.2. Experimental values of collection efficiency

Rotational Velocity (rad/sec)	N_o for RPRDE	N_o for MPRRDE
42	0.172	0.171
94	0.172	0.164
168	0.171	0.154
262	0.170	0.152

value of 0.171 is slightly less than the value of 0.189 calculated on the basis of the pertinent radii of the ring and disk electrodes. The decrease of N_o for the MPRDE with increasing ω is thought to result because of deformation of the films of mercury at the surfaces of the ring and disk electrodes due to centrifugal force. On several occasions when the mercury films were prepared by dipping the RPRDE in a pool of mercury, the excess mercury at the electrode surfaces was intentionally not removed by wiping with a lint-free tissue. Values of N_o measured under those circumstances were considerably less than 0.171 at ω = 42 rad/sec and decreased by much more than the 12% shown in Table V.2 when ω was increased to 262 rad/sec. After wiping off excess mercury, the values of N_o obtained were approximately the same as those given in Table V.2. Because of the obvious dependence of N_o for the MPRRDE on the condition of the mercury films, values of N_o were determined at the beginning

and end of each experimental day. If the values at a single rotational velocity changed by more than 5%, the data for that day was discarded.

b. I-E curves for benzil Current-potential (I-E) curves for the reduction of benzil at the disk electrode and the oxidation of stilbendiolate at the ring electrode of the MPRRDE are shown in Figure V.2 for three values of rotational velocity. The rate of scan for E_d was sufficiently slow so that the curves show no contribution from charging of the double layer. A second cathodic wave on the $I_d - E_d$ curve was obtained at $E_d < -1.5V$ due to the reduction of benzoin produced near the disk by the ketolization of stilbendiolate. Benzoin is not electrochemically oxidized or reduced at potentials included in Figure V.2. The values of $-N_o \cdot I_{d,\ell}$ for each rotational velocity are given. These are the values of I_r predicted if the stilbendiolate undergoes no homogeneous reaction to give an electroinactive product. The $I_r - E_d$ curves have a characteristic maxima in the region $E_d = -0.9V$ with the anodic values of I_r at $E_d = -0.9V$ being much greater than at $E_d = -1.3V$. All values of I_r are $> -N_o \cdot I_{d,\ell}$. It is obvious from a brief inspection of the curves in Figure V.2 that the ratio $I_r/-N_o \cdot I_{d,\ell}$ increases as the value of the rotational velocity is increased which is characteristic of the collection of an intermediate reacting by a homogeneous chemical process to produce an electroinactive species.

Figure V.2. $I_{\underline{d}}$ - $E_{\underline{d}}$ and $I_{\underline{r}}$ - $E_{\underline{d}}$ curves for benzil in alkaline media. 1.00×10^{-3} M benzil, 1:1 (v/v) methanol-0.1 M NaOH, $E_{\underline{r}}$ = -0.40 V, scan rate = 1.0 V/min

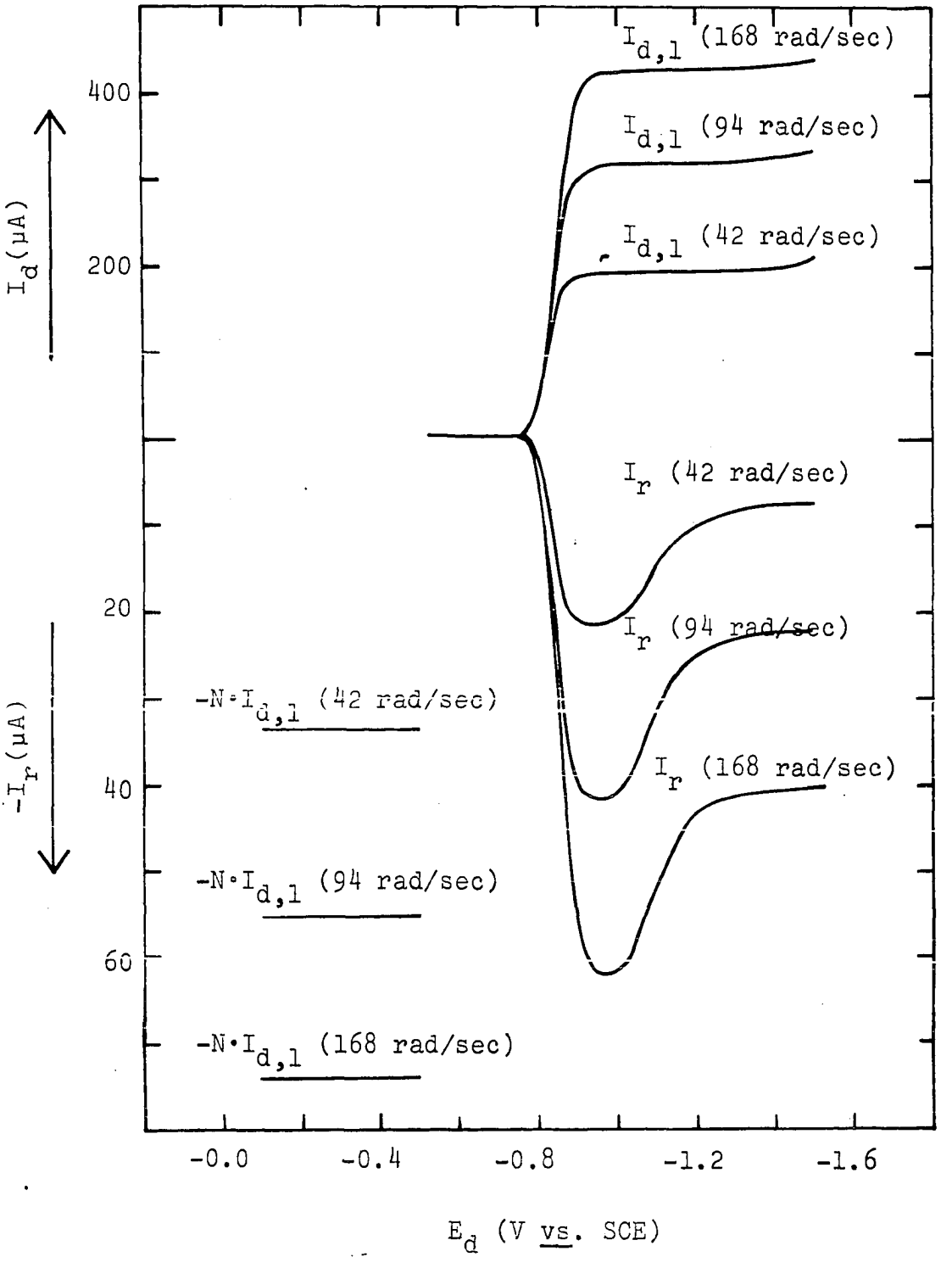
$I_{d,l}$ (168 rad/sec)
$I_{d,l}$ (94 rad/sec)
$I_{d,l}$ (42 rad/sec)
I_r (42 rad/sec)
I_r (94 rad/sec)
I_r (168 rad/sec)
$-N \cdot I_{d,l}$ (42 rad/sec)
$-N \cdot I_{d,l}$ (94 rad/sec)
$-N \cdot I_{d,l}$ (168 rad/sec)
400
200
20
40
60
I_d (μA)
$-I_r$ (μA)
-0.0
-0.4
-0.8
-1.2
-1.6
E_d (V vs. SCE)

These results are consistent with the conclusion that cis- and trans-stilbendiolate are produced at the disk electrode by the reduction of benzil and that the relative amount produced is dependent on E_d. Previous studies in acidic and neutral media (39,138) showed that the rate of ketolization of cis-stilbendiolate is less than that of trans-stilbendiolate. On that basis, we conclude that the cis-isomer is the species primarily produced at E_d = -0.9V and the trans-isomer is produced at E_d = -1.3V.

Cyclic voltammetry at the disk electrode of the stationary MCRDE in an unstirred solution yielded a I_d - E_d curve with a single anodic peak as reported by Stapelfeldt and Perone for a hanging mercury-drop electrode (139). I_r - E_r curves were recorded for the RMCRDE for E_d = -0.9V and -1.3V. Each curve had a single anodic wave and the values of $E_{1/2}$ for the two anodic waves were virtually identical. We conclude that the $E_{1/2}$ for oxidation of cis- and trans-stilbendiolate are identical in this media in agreement with the observation of Stapelfeldt and Perone (139).

c. Current-potential curves with Al(III) present

Aluminum(III) is known to form very stable chelates with many multidentate ligands. I_r - E_d and I_d - E_d curves were obtained for a solution of benzil containing a large excess of Al(III) on the presumption that the Al(III) would

selectively chelate with the cis-stilbendiolate and stabilize it against ketolization. Since the two oxygen atoms of trans-stilbendiolate can not simultaneously occupy coordination sites around Al(III), it was hoped that the presence of Al(III) would have negligible effect on the ketolization of that isomer. The I-E curves obtained for the absence and presence of Al(III) are shown in Figure V.3. The various designations of values of I_r in Figure V.3 are used for calculations described in a later section. The I_d - E_d curve was unaffected by the presence of Al(III). The value of I_r at E_d = -1.3V was unaffected by addition of Al(III), and we conclude that in this region of the potential axis only trans-stilbendiolate is produced at the disk electrode and this isomer does not react with Al(III). The value of I_r at E_d = -0.9V was significantly greater with Al(III) present and our presumption that chelation occurs between Al(III) and cis-stilbendiolate was verified. Because the values of $-I_r$ at E_d = -0.9V determined in the presence of 0.06 M Al(III) was $< -N_o \cdot I_{d,\ell}$, we conclude that a mixture of cis- and trans-stilbendiolate is produced at that potential.

Values of I_r for E_r = -0.4V were measured at E_d = -0.9V and are plotted in Figure V.4 as a function of the concentration of Al(III) for three values of rotational velocity. The value of I_r for all values of rotational

Figure V.3. I_d - E_d and I_r - E_d curves for benzil in the presence and absence of Al(III). 1.00×10^{-3} M benzil, 0 M and 0.06 M Al(III), 1:1 (v/v) methanol-0.1 M NaOH, E_r = -0.40 V, rotational velocity = 42 rad/sec, scan rate = 1.0 V/min

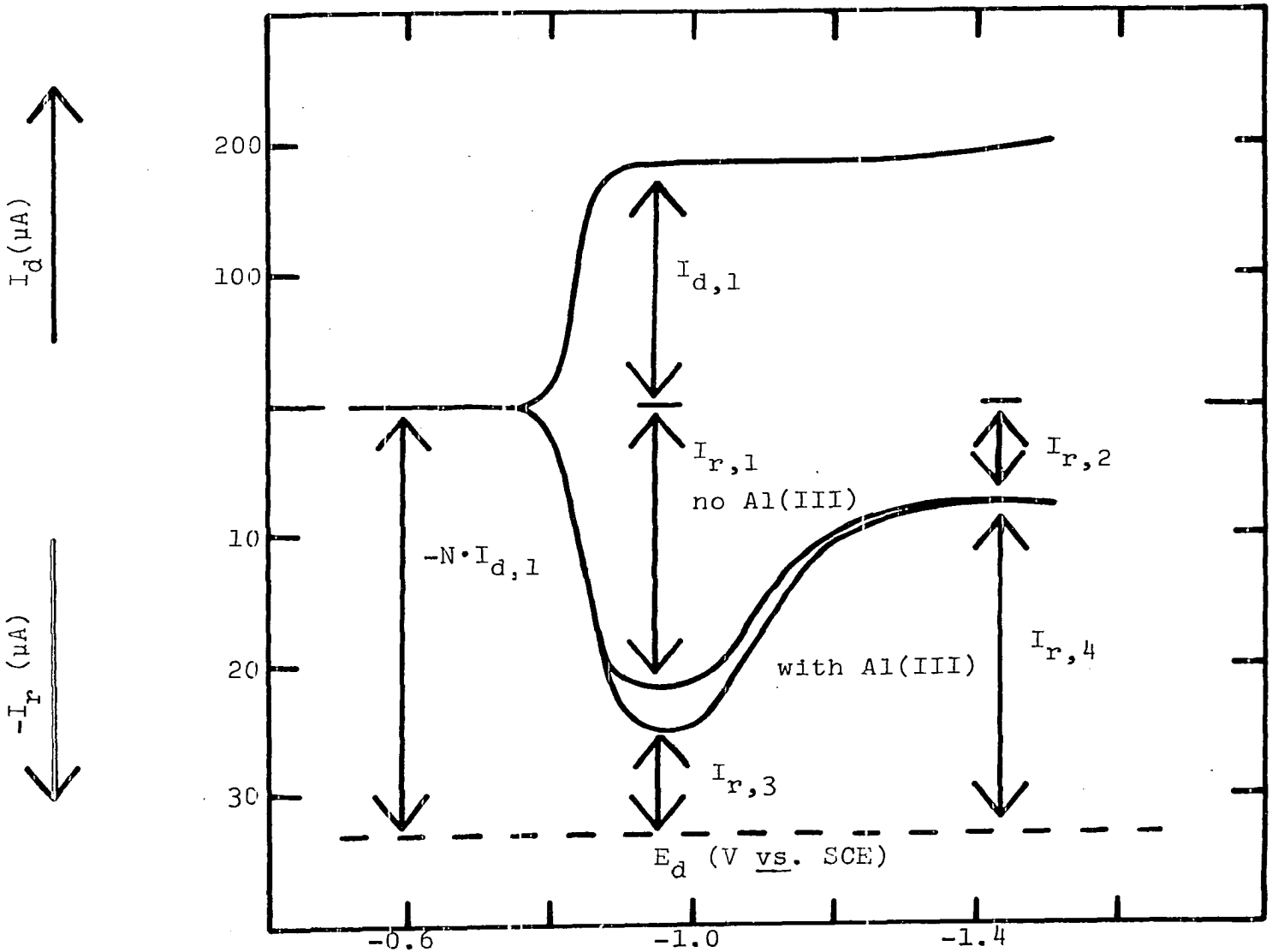
I_d (μA)
$-I_r$ (μA)
200
100
10
20
30
$I_{d,1}$
$I_{r,1}$
no Al(III)
$-N \cdot I_{d,1}$
$I_{r,2}$
with Al(III)
$I_{r,4}$
$I_{r,3}$
E_d (V vs. SCE)
-0.6
-1.0
-1.4

Figure V.4. I_r for E_d = -0.9 V for benzil as a function of [Al(III)].

1.00×10^{-3} M benzil, 1:1 (v/v) methanol - 0.1 M NaOH, E_r = -0.4 V

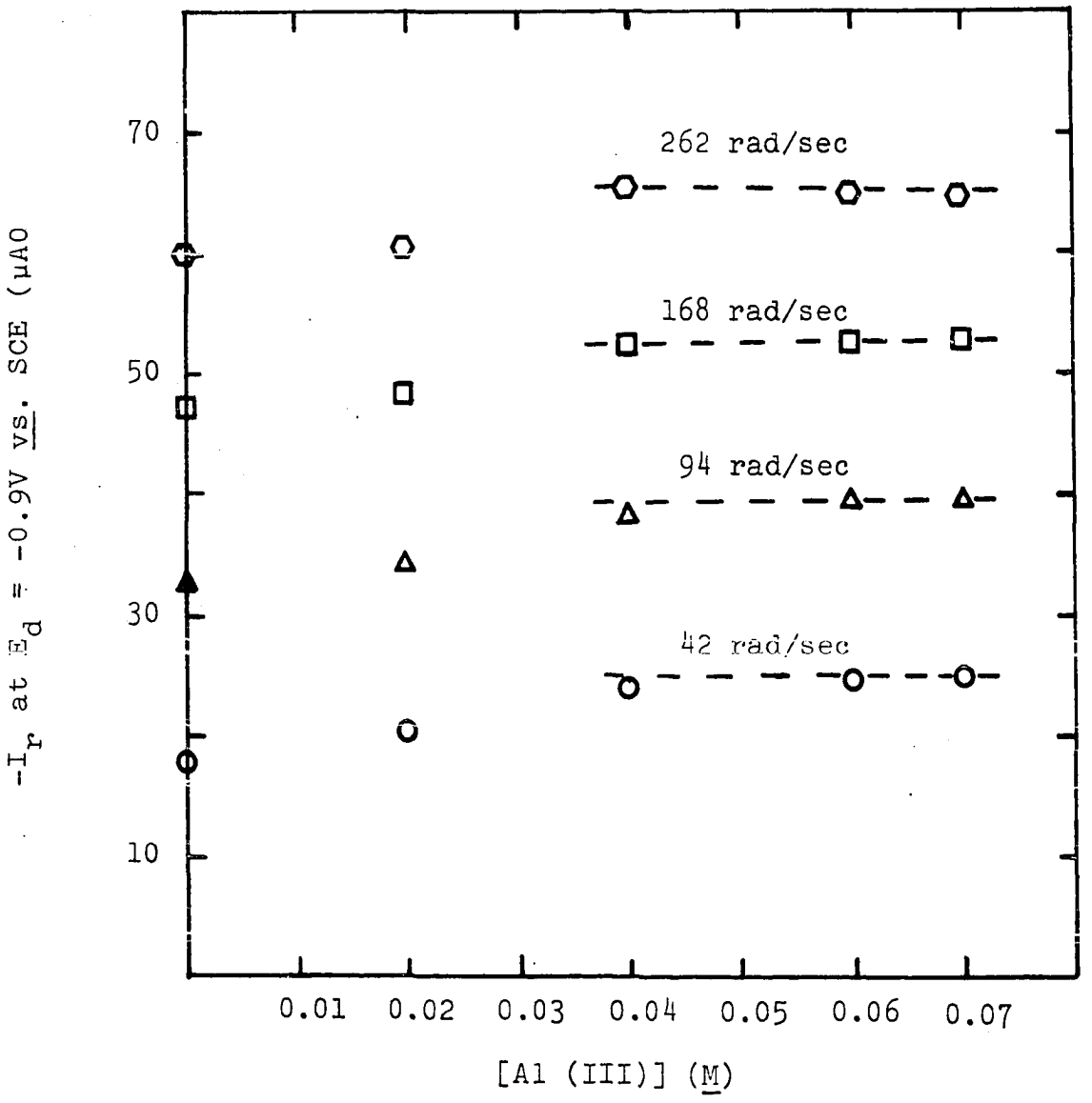
70
50
30
10
262 rad/sec
168 rad/sec
94 rad/sec
42 rad/sec
0.01
0.02
0.03
0.04
0.05
0.06
0.07
[Al (III)] (M)
$-I_r$ at E_d = -0.9V vs. SCE (μA0

velocity was constant for [Al(III)] $\geq$ 0.06 M, and we conclude that this concentration is sufficient to cause quantitative chelation of the cis-stilbendiolate produced at the disk electrode. Furthermore, because the value of I_r loses dependency on [Al(III)] at the same values of concentration for all rotational velocities, it is concluded that the rate of formation of the chelate is fast relative to the rate of convective-diffusional mass transport. Assuming a value of 50 for the ratio of chelated to unchelated cis-stilbendiolate when [Al(III)] = 0.06 M, which corresponds to a quantitative reaction, an approximate value for the equilibrium constant for the formation of the chelate is 8×10^2.

It is necessary, in order to determine the rate of ketolization of cis-stilbendiolate from the I-E curves, to know the fraction of $I_{d,\ell}$ at E_d = -0.9V which results in the production of the cis-isomer. It is shown in a latter section that this can be done using the I-E curves, of Figure V.3. The argument presumes, however, that the ratio of the concentrations of the isomers produced at E_d = -0.9V is not affected by the addition of Al(III) to the solution. Chodkowska and Grabowski (39) studied the effect of different cations on the ratio of the concentrations of isomers of stilbendiol produced at a stationary mercury electrode in acidic and neutral solutions. They observed that for an electrode potential at which the two

isomers are produced simultaneously, the relative amount of the cis-isomer increased when the charge-to-size ratio of the cation of the supporting electrolyte was decreased. They explained the phenomenon in terms of an acceleration of a homogeneous trans → cis transformation caused by polarization of trans-stilbendiol in the high electric field of the double layer. They did not discuss the contradictory evidence, however, that at more negative electrode potentials, at which the field is certainly greater, only trans-stilbendiol is produced.

Our conclusion that the addition of Al(III) does not alter the relative amounts of the cis- and trans-isomers is based on theoretical and experimental evidence which is as follows: (i) at the high pH of our supporting electrolyte, Al(III) exists in solution as $Al(OH)_4^-$ (31) and, since the potential of the electrode is negative of the value of the ECM, $Al(OH)_4^-$ is not primarily adsorbed in the compact double layer. The counter-ion in the double layer is OH^- because of its large charge-to-size ratio. Hence, the gradient of the electric potential is not changed appreciably by addition of $Al(OH)_4^-$. (ii) If $Al(OH)_4^-$ increases the relative amount of the cis-isomer produced at the disk electrode either by unexpected changes in the double layer or in some way by promoting a transformation of trans → cis, an increase would be expected in the range of values of E_d

over which the cis-stilbendiolate is detected. Such was not the case. The $E_{1/2}$ for the reduction of benzil at the disk electrode was not affected by addition of $Al(OH)_4^-$, and the value of E_d on the cathodic scan at which the production of the cis-isomer terminated was identical for the presence and absence of $Al(OH)_4^-$.

d. Determination of rate constants The use of Equation V.16, or the results of the digital simulation to calculate the rate constant for this first-order kinetic situation, requires an evaluation of N_k for the trans- and cis-stilbendiolates. These values were calculated, using I-E curves such as those shown in Figure V.3.

For E_d = -1.3V (only trans-stilbendiolate produced at disk electrode):

$$N_{k,trans} = -I_{r,2}/I_{d,\ell} \qquad (V.17)$$

For E_d = -0.9V (both cis- and trans-stilbendiolate produced at the disk electrode):

$$I_{r,trans} = I_{r,3}\,(I_{r,2}/I_{r,4}) \qquad (V.18)$$

$$I_{d,trans} = -I_{r,trans}/N_{k,trans} \qquad (V.19)$$

$$= \frac{-I_{r,3}\,(I_{r,2}/I_{r,4})}{N_{k,trans}}$$

$$I_{r,cis} = I_{r,1} - I_{r,trans} \qquad (V.20)$$

$$= I_{r,1} - I_{r,3}\,(I_{r,2}/I_{r,4})$$

$$I_{\underline{d},\underline{cis}} = I_{\underline{d},\underline{\ell}} - I_{\underline{d},\underline{trans}}$$

$$= I_{\underline{d},\underline{\ell}} + \frac{I_{\underline{r},3}\,(I_{\underline{r},2}/I_{\underline{r},4})}{N_{\underline{k},\underline{trans}}} \qquad (V.21)$$

$$N_{\underline{k},\underline{cis}} = -I_{\underline{r},\underline{cis}}/I_{\underline{d},\underline{cis}}$$

$$= -\left[\frac{I_{\underline{r},1} - I_{\underline{r},3}\,(I_{\underline{r},2}/I_{\underline{r},4})}{I_{\underline{d},\underline{\ell}} + \dfrac{I_{\underline{r},3}\,(I_{\underline{r},2}/I_{\underline{r},4})}{N_{\underline{k},\underline{trans}}}}\right]$$

$$= \frac{(I_{\underline{r},3} \cdot I_{\underline{r},2} - I_{\underline{r},1} \cdot I_{\underline{r},4})}{I_{\underline{d},\underline{\ell}}\,(I_{\underline{r},3} - I_{\underline{r},4})} \qquad (V.22)$$

Values of $k_{\underline{cis}}$ and $k_{\underline{trans}}$ were determined as a function of rotational velocity, and the results are tabulated in Table V.3.

Values of $k_{\underline{cis}}$ were calculated only for low rotational velocities because at high velocities the difference $N_o - N_{\underline{k},\underline{cis}}$ was approximately equal to the uncertainty in the calculation of $N_{\underline{k},\underline{cis}}$. Equations V.17-V.22 were developed with the assumption that the cis-stilbendiolate does not undergo ketolization when chelated by Al(III). If this assumption is not valid, one would observe change of the values of $k_{\underline{cis}}$ in Table V.3 as rotational velocity is varied. We conclude that the assumption is valid on the time scale of this experiment.

Table V.3. Rates of ketolization for cis- and trans-stilbendiolate

[NaOH] = 0.10 M
ν = 9.47 x 10^{-3} cm^2/sec
D = 3.8 x 10^{-6} cm^2/sec

Experiment	[Benzil]	(rad/sec)	k_{cis} (sec^{-1})	k_{trans} (sec^{-1})
1	1.0 x 10^{-3} M	42	0.4	3.7
		94	0.4	5.0
		168	---	5.0
		262	---	5.6
2	1.00 x 10^{-3} M	42	0.6	3.5
		94	0.4	4.5
		168	---	5.1
		262	---	5.3
3	1.00 x 10^{-3} M	42	0.5	3.8
		94	---	4.5
		168	---	5.0
		262	---	5.6
4	1.00 x 10^{-3} M	42	0.7	3.7
		94	0.6	4.9
		168	---	5.3
		262	---	6.0
5	0.75 x 10^{-3} M	42	0.8	3.6
		94	0.8	4.7
		168	---	5.3
		262	---	6.0
6	0.50 x 10^{-3} M	42	0.5	3.4
		94	0.6	4.1
		168	---	4.5
		262	---	5.0
	mean ± std. dev.		0.6±0.2	4.7±0.8

The increase of the value of $k_{\underline{trans}}$ with increasing rotational velocity is thought to be an artifact of the use of the mercury-coated electrode rather than the consequence of an incorrect assumption for the reaction mechanism. The value of N_o determined experimentally for the MPRRDE was observed to decrease significantly as rotational velocity increased (see Table V.2). That variation was concluded to result from the deformation of the liquid mercury film caused by centrifugal force at high rotational velocity. The differential equations used for all derivations pertaining to rotating ring-disk electrodes are solved assuming co-planarity of the electrodes. Likewise, the digital simulation of Prater and Bard does not account for the decreasing nature of N_o. The experimental decrease of collection efficiency has the effect of decreasing $-I_{\underline{r},\underline{k}}$, and the result on the simulation is a larger calculated value of the rate constant. Since values of N_o for the MPRRDE at ω = 42 rad/sec were identical to those for the RPRDE, values of $k_{\underline{trans}}$ and $k_{\underline{cis}}$ calculated for ω = 42 rad/sec are concluded to be more correct than those calculated at higher rotational velocities.

Equation V.16 was applicable only for calculating $k_{\underline{trans}}$ when ω = 262 rad/sec. The restriction in the use of Equation V.16 was presented above. Using N_o = 0.152 from Table V.2,

$k_{\underline{trans}}$ was calculated for Experiment 3, as an example, to be 4.4 sec^{-1} which is in fair agreement with the result of the digital simulation.

Stapelfeldt and Perone (139) determined the rate of the homogeneous rearrangement of stilbendiolate in strongly alkaline media to be 2 sec^{-1}. They were unable to distinguish the cis- and trans-isomers, so their rate constant was intermediate the correct values for the two species. Hence, their results and ours are in agreement.

Stilbendiolate and benzoin, produced by the electrochemical and chemical reactions may react with benzil in the solution adjacent the ring and disk electrodes to produce a free-radical anion as described by Equations II.15 and II.16 in Section II.D. The free-radical anion is oxidized at the ring electrode at the same values of electrical potential for the oxidation of stilbendiolate. Since $k_{\underline{cis}}$ and $k_{\underline{trans}}$ were calculated by a simulation program ignoring Equations II.15 and II.16, the possible effect of those reactions must be examined. A solution containing 0.01 M benzil, 0.01 M benzoin, and 0.1 M NaOH was prepared and the electrical current for the oxidation of the free-radical anion was determined using the disk of the MPRRDE as a function of the rotational velocity. The plot of I_{ℓ} vs. $\omega^{1/2}$ was linear for 11 rad/sec $\leq \omega \leq$ 105 rad/sec. Since the concentration of the free-radical anion at the surface of the disk electrode

in this experiment was zero, the equilibrium of Reaction II.15 was perturbed and the forward chemical reaction would be expected to occur so as to restore the equilibrium concentration of free-radical anion. This mechanism has been discussed by Prater and Bard (123) and Haberland and Landsberg (72). A linear plot of I_ℓ vs. $\omega^{1/2}$ is obtained only if the rate of the forward chemical reaction is negligible in comparison to the rate of convective-diffusional transport at the rotating electrode. Using as a value of D for the free-radical anion, the value determined for benzil, the equilibrium concentration of the free-radical was calculated to be 8×10^{-5} M. The value of equilibrium constant for Reaction II.15 was calculated to be 6×10^{-5}. A value of 4×10^{-3} was reported by Berg (18). The equilibrium constant calculated from the plot of I_ℓ vs. $\omega^{1/2}$ for a solution containing 0.005 M benzil, 0.005 M benzoin, and 0.1 M NaOH was also 6×10^{-5}.

The effect of added Al(III) on the equilibrium of Reaction II.15 was determined using ESR measurements. The spectrum for the free-radical anion in the solutions used in the previous experiment was unaffected when Al(III) was added. Apparently there is no interaction between $Al(OH)_4^-$ and the free-radical anion.

Values of k_{trans} were calculated and are given in Table V.3 for concentrations of benzil equal to 1.00×10^{-3}

M, 0.75×10^{-3} M, and 0.50×10^{-3} M. No trend in k_{cis} or k_{trans} was observed with changes of the benzil concentration and it is concluded that the forward rates of Reaction II.15 and II.16 are negligible in comparison with the rate of convective-diffusional mass transport for this study.

VI. KINETIC MEASUREMENTS USING THE PHOTOELECTRODE

A. Introduction

The rotating ring-disk electrode has been demonstrated to be very useful for kinetic studies of homogeneous reactions involving products of electrochemical reactions (4). Rates of reaction can be determined for which the reaction half-life is approximately of the order of the time for species generated at the disk electrode to be transported by convective-diffusional processes to the ring electrode. The hydrodynamic profiles at the surface of the rotating photoelectrode and ring-disk electrode are identical and it is expected that the RPE will prove to be very useful for kinetic studies of species generated photochemically in the vicinity of the optically transparent disk.

The photocurrent in the ring electrode is expected to be a function of the following parameters:

1. intensity of the light beam,
2. molar absorptivity and concentration of the absorbing species,
3. quantum efficiency of the primary photolytic process,
4. mechanism and rate of chemical reactions involving products of the photolytic process,
5. angular velocity of electrode rotation.

Lubbers and coworkers developed a computer program for the digital simulation of the various processes at the RPE. The program is described in Reference (93) together with the results obtained in this research for its application to the photodimerization of benzophenone in alkaline alcohol-water solutions.

The mechanism for the photochemical reduction of benzophenone in aqueous-alcohol media is presented in Section II.B. The experimental results for a study of the dependence of the photocurrent upon the electrode rotation velocity, ring-potential, and wavelength of the excitation light beam are presented in Section IV.A.3.

B. Experimental

1. Electronic circuitry

The three-electrode potentiostat mentioned in Section III.A was used in conjunction with the rotating photoelectrode (RPE) and is described in Reference (147).

2. Chemicals and reagents

All chemicals and reagents used in this investigation are described in Section IV.A.2.a.

3. The quantum yield, wavelength of radiation, molar absorptivity, and light intensity

The quantum yield, Ø, for the overall photolytic process in our media is 1.0 (38). All further photolytic studies

were performed with 270 nm radiation.

The value of molar absorptivity for benzophenone, ε_A, was determined at 270 nm to be 2.3×10^4 $\underline{M}^{-1}$ cm^{-1}. The intensity of the light beam transmitted by the quartz disk of the RPE was determined to be 6.0×10^{14} quanta/sec at 270 nm.

C. Results and Discussion

1. Simulation of $\underline{I}_{h\nu}$ vs. XK

Simulated values of photocurrent, $\underline{I}_{h\nu}$, as a function of the rate of dimerization, XK, are shown in Figure VI.1 for a bulk concentration of benzophenone, CBULKA, equal to 0.010 $\underline{M}$. Initial simulations were made by Lubbers and co-workers (93) calculating the effects of convection, diffusion, photolysis, and chemical reaction of the fractional concentration of benzophenone, FA, and the fractional concentration of the ketyl radical FB, for all volume elements in the irradiated zone of the quartz disk. Closer examination of these processes for benzophenone led to the conclusion that to a first approximation the rate of photolysis is negligible in comparison to the rate of mass transport at all values of rotational velocity used in this research. Hence, FA = 1.0 for all volume elements. The program was revised and the simulations repeated under this assumption and the results were identical to those

Figure VI.1. $I_{h\nu}$ *vs.* XK.

XII = 6.0×10^{14} quanta-sec, CBULKA = 0.010 M, values of ω: O - 41.9 rad/sec, Δ - 94.3 rad/sec, □ - 167.7 rad/sec, and ⬡ - 261.8 rad/sec

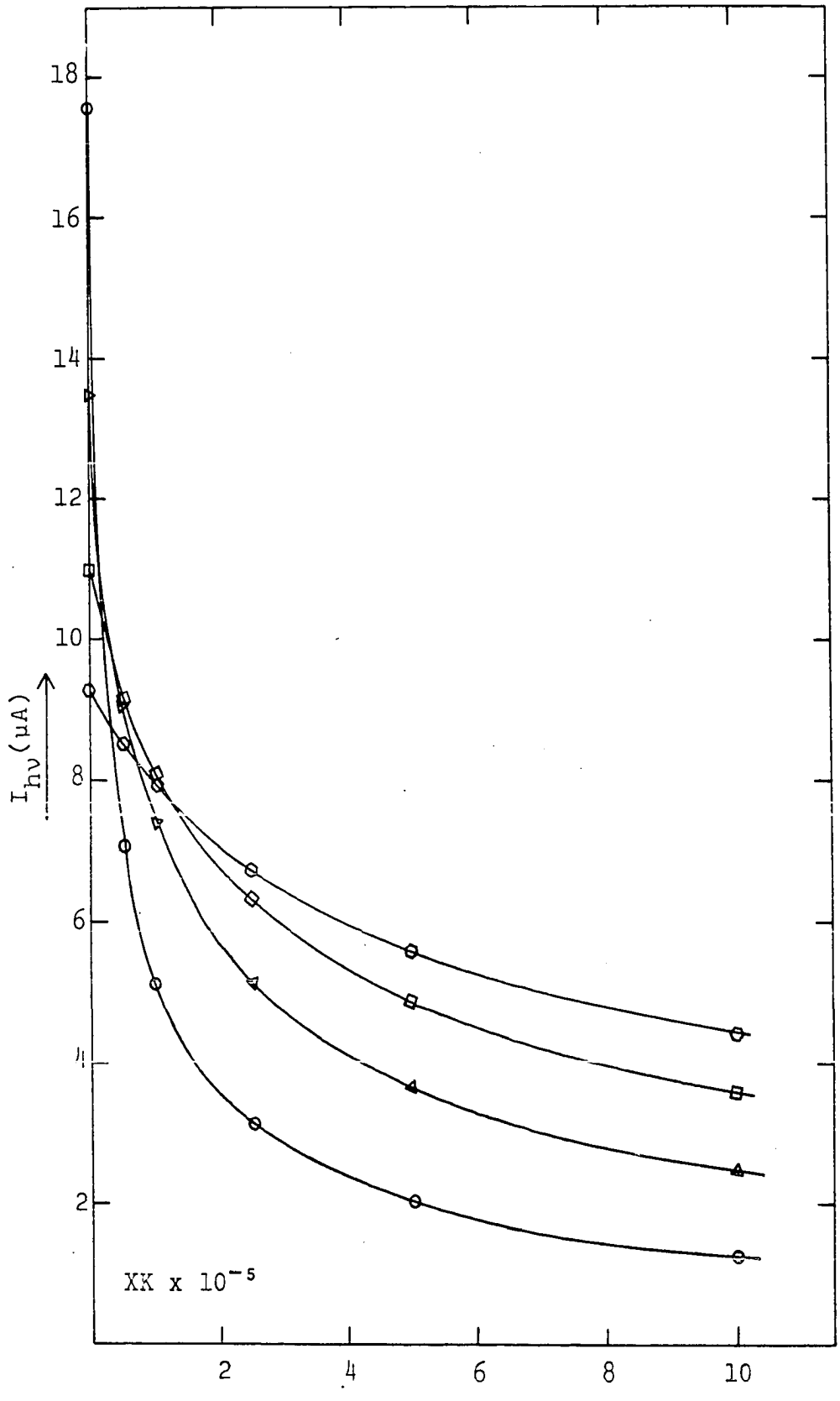
18
16
14
12
10
8
6
4
2
$I_{h\nu}$ (μA)
XK x 10^{-5}
2
4
6
8
10

in Figure VI.1 confirming the validity of the assumption. The assumption was retained for all further simulations.

As expected for XK >> 0.0, $\underline{I}_{h\nu}$ increases as the rotational velocity, ω, is increased since the rate of radial transport increases with ω allowing less time for the chemical reaction of the intermediates. Unexpected is the prediction that for XK = 0.0, $\underline{I}_{h\nu}$ is largest for the lowest value of ω. This dependence probably results because near the surface of the electrode the rate of radial transport increases more rapidly than the rate of axial transport as ω is increased (91). Hence, species generated photolytically at a finite distance from the surface of the quartz disk are transported to the ring electrode at low ω but are swept clear of the ring surface at high ω. This dependence of $\underline{I}_{h\nu}$ on ω at XK = 0.0 has not yet been tested experimentally.

Values of XK for the benzophenone system were calculated from experimental data using observed values of $\underline{I}_{h\nu}$ and the smooth curves fitting the simulated data in Figure VI.1. Results are given in Table VI.1 for 0.10 M NaOH and in Table VI.2 for 1.0 M NaOH. Results of repeated determinations for 0.10 M NaOH were scattered comparable to data in Table VI.1. The higher precision of XK values in Table VI.2 as compared with Table VI.1 results partly from the greater sensitivity of $\underline{I}_{h\nu}$ to change in XK in that region of the simulation. The values of the observed rate constant are in good agreement with literature values.

Table VI.1. Experimental determination of XK for 0.10 M NaOH

CBULKA = 0.010 M

XII[a] = 6.0×10^{14} quanta/sec

ω (rad/sec)	$I_{h\nu}$ (μA)	XK (M^{-1} sec^{-1})
41.9	2.2	4.6×10^5
94.3	4.5	3.5×10^5
168	5.4	3.9×10^5
262	6.6	2.7×10^5
	Avg.	3.7×10^5
	Std. Dev.	0.8×10^5

[a]XII = The intensity of the photolysis light beam at the surface of the quartz disk.

Table VI.2. Experimental determination of XK for 1.0 M NaOH

CBULKA = 0.010 M

XII = 6.0×10^{14} quanta/sec

ω (rad/sec)	$I_{h\nu}$ (μA)	XK (M^{-1} sec^{-1})
41.9	4.4	1.3×10^5
94.3	6.9	1.2×10^5
168	7.7	1.2×10^5
262	7.7	1.2×10^5
	Avg.	1.2×10^5
	Std. Dev.	$<0.1 \times 10^5$

The values of $I_{h\nu}$ observed for the two largest values of ω in 1.0 M NaOH (Table VI.2) are identical and correspond to

the point of intersection of simulated curves for those values of ω in Figure VI.1. This is supporting evidence for the correctness of the program and the predicted inversion of ω-dependence as a function of decreasing XK. Thorough consideration of the results shown in Figure VI.1 leads to the conclusion that for any finite value of XK, a recording of $\underline{I}_{h\nu}$ *vs.* ω will be characterized by a maximum. An increased value of XK will result in a shift of the maximum toward a higher value of ω. Figure VI.2 contains a plot of $\underline{I}_{h\nu}$ *vs.* ω for 1.0 M NaOH. The maximum exists at ω = 200 rad/sec. No digital simulation of the data in Figure VI.2 was performed. The broadness of the maximum probably prevents accurate diagnostic application of this phenomenon for evaluating XK.

2. Simulation of $\underline{I}_{h\nu}$ *vs.* XII

Simulated values of $\underline{I}_{h\nu}$ as a function of the intensity of the photolysis light beam, XII, for XK - 0.0, 1.2×10^5, and 3.7×10^5 $\underline{M}^{-1}$ sec^{-1} are shown plotted in Figure VI.3 for ω = 41.9 rad/sec and in Figure VI.4 for ω = 94.3 rad/sec. Experimental results are also plotted and the agreement between experimental and simulated data is good. The observation is interesting that at XK = 0.0 $\underline{M}^{-1}$ sec^{-1}, $\underline{I}_{h\nu}$ is simulated to be a linear function of XII. No experimental confirmation of this correspondence has as yet been made.

Figure VI.2. $I_{h\nu}$ *vs.* rotational velocity
XII = 6.0×10^{14} quanta/sec,
CBULKA = 0.010 *M*, [NaOH] = 1.0 *M*

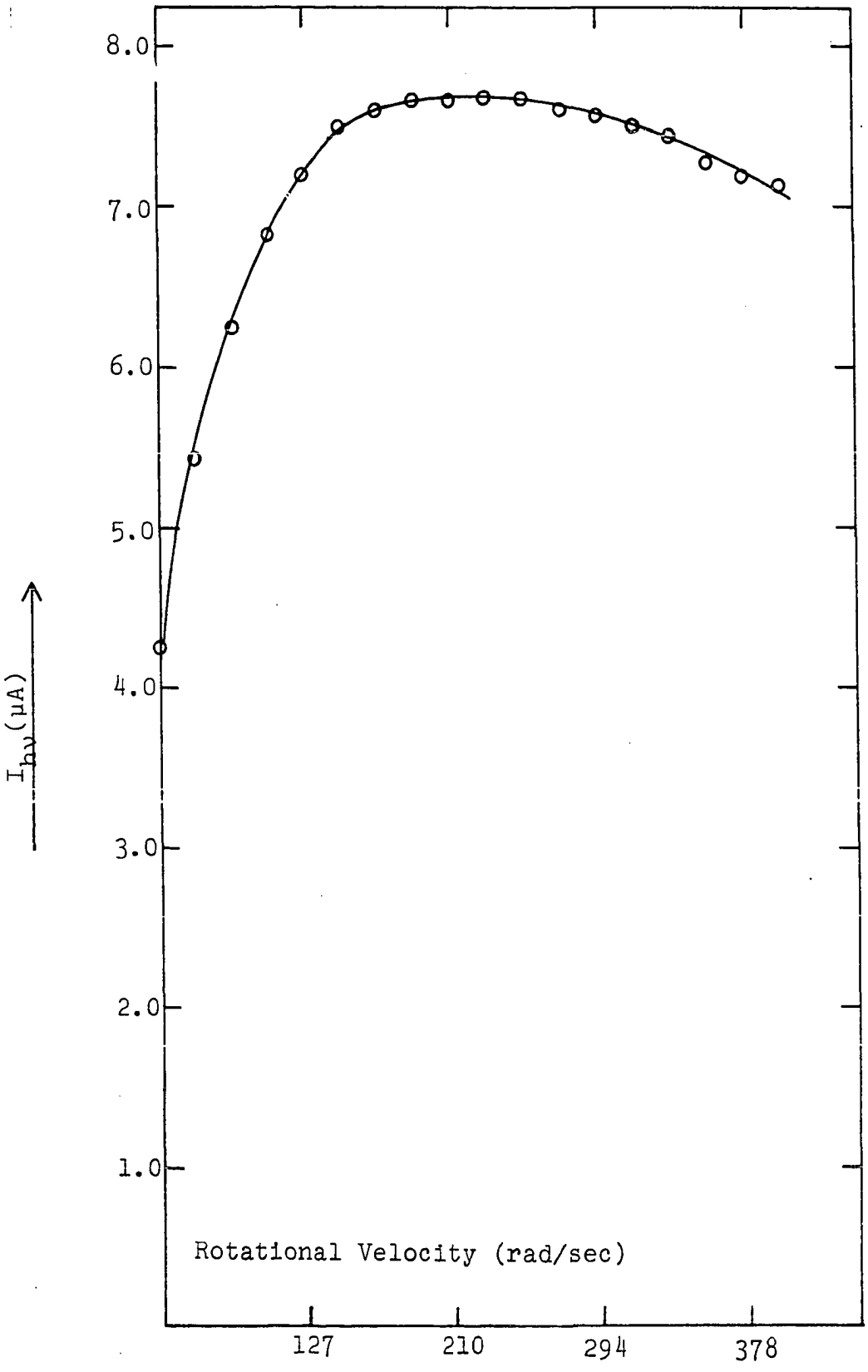
8.0
7.0
6.0
5.0
4.0
3.0
2.0
1.0
$I_{h\nu}$ (μA)
Rotational Velocity (rad/sec)
127
210
294
378

Figure VI.3. $I_{h\nu}$ *vs.* XII

CBULKA = 0.010 M, ω = 41.9 rad/sec;

values of XK: —•—•— 0.0 M^{-1} sec^{-1},

— — — 1.2 x 10^5 M^{-1} sec^{-1}, and

——— 3.7 x 10^5 M^{-1} sec^{-1};

O - simulated and Ẍ - experimental

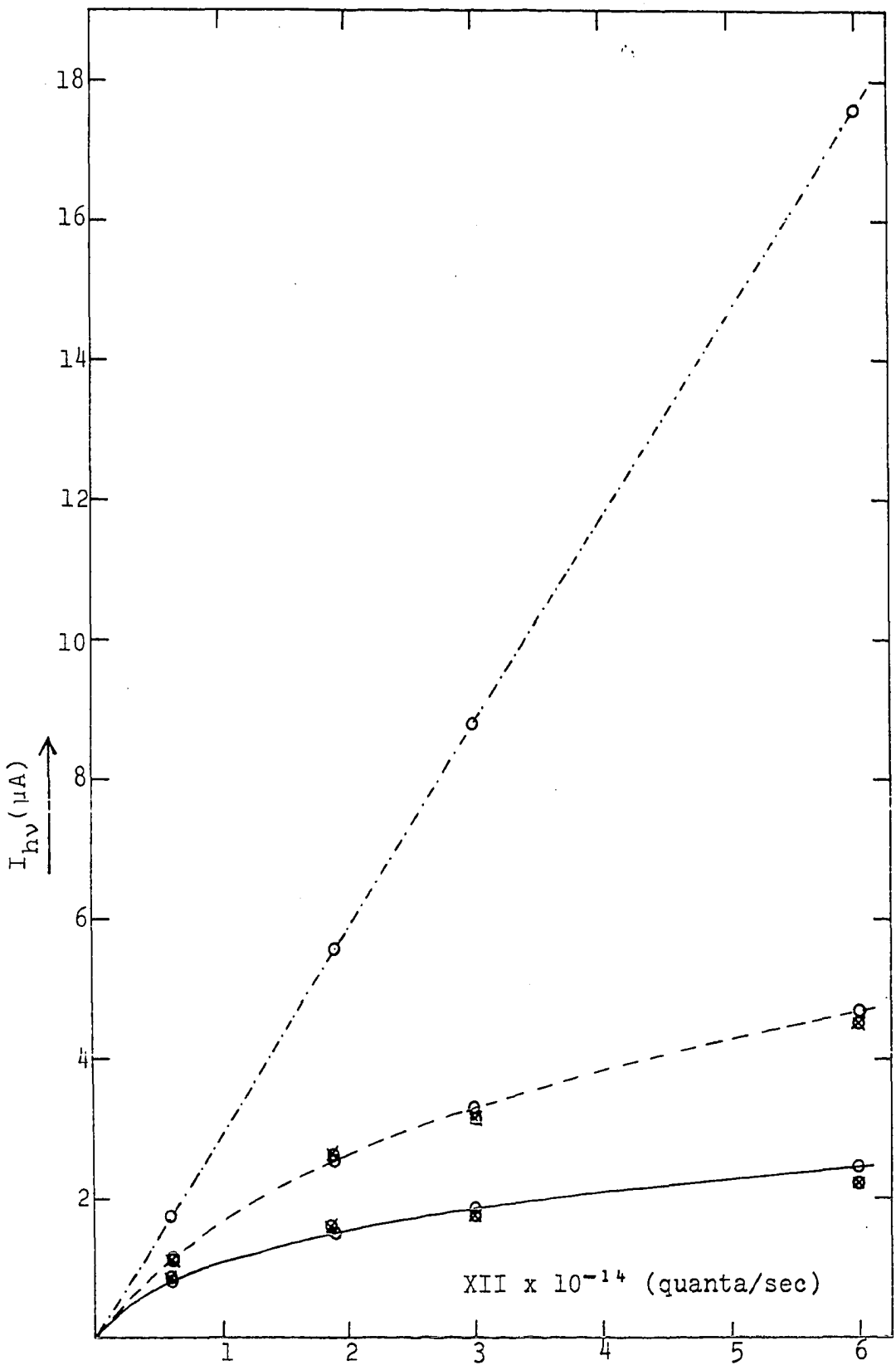
18
16
14
12
10
8
6
4
2
$I_{h\nu}$ (μA)
1
2
3
4
5
6
XII x 10^{-14} (quanta/sec)

Figure VI.4. $I_{h\nu}$ *vs.* XII

CBULKA = 0.010 M, ω = 94.3 rad/sec;

values of XK: —•—•— 0.0 M^{-1} sec^{-1},

– – – 1.2 x 10^5 M^{-1} sec^{-1}, and

——— 3.7 x 10^5 M^{-1} sec^{-1};

Δ – simulated and ± – experimental

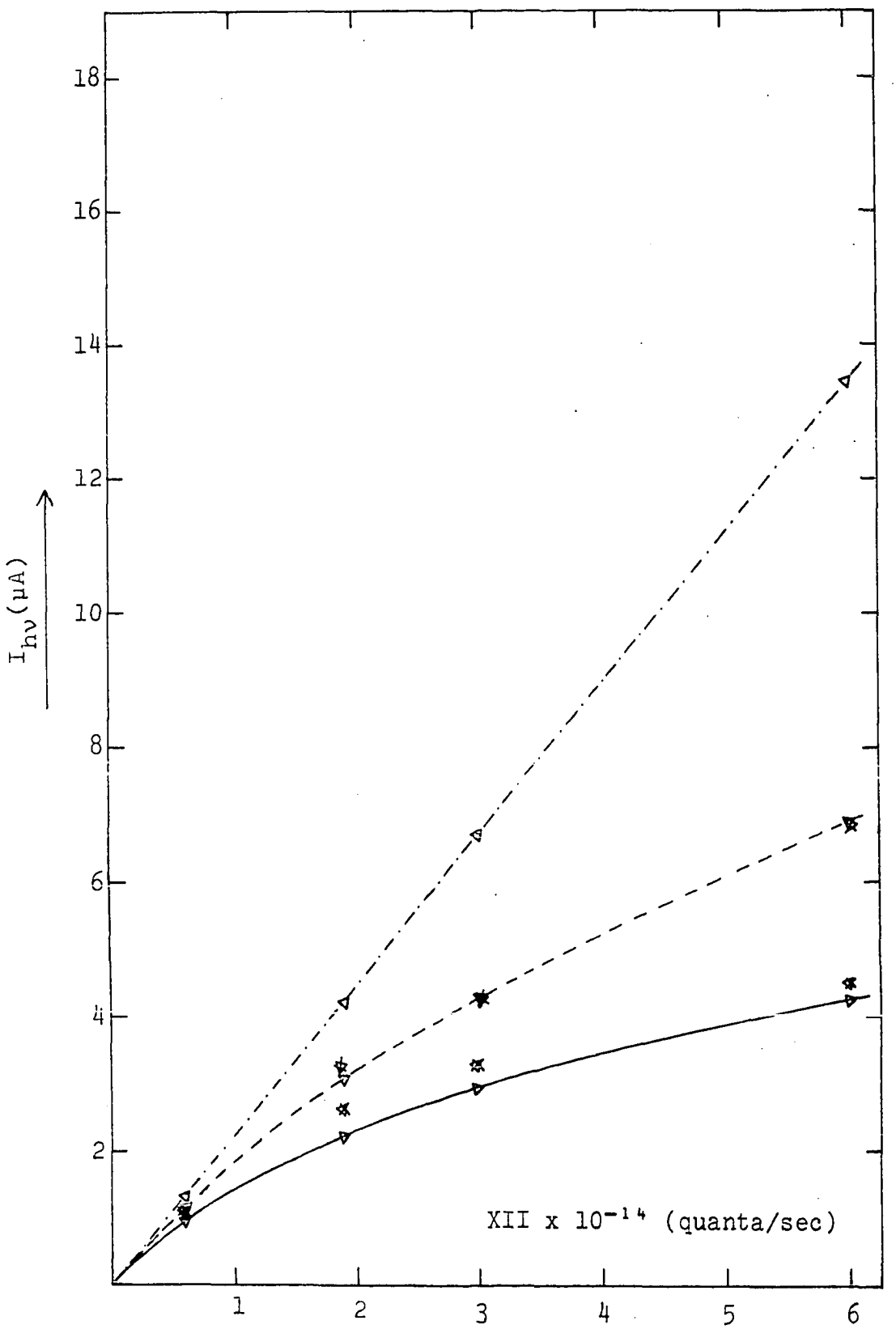
18
16
14
12
10
8
6
4
2
$I_{h\nu}$ (μA)
1
2
3
4
5
6
XII x 10^{-14} (quanta/sec)

3. Simulation of $I_{h\nu}$ vs. CBULKA

Simulated values of $I_{h\nu}$ are shown plotted in Figure VI.5 for XK = 0.0 and 3.7 x 10^5 M^{-1} sec^{-1}. Also shown are values obtained experimentally. The agreement between experimental and simulated data is good.

4. Light intensity profile

Uniformity of light intensity was assumed across the surface of the quartz disk for development of the digital program. The assumption permitted simplification of the calculations of mass transport and photochemical reaction in the zone of the quartz disk. Two intensity profiles taken on perpendicular diameters across the surface of the quartz disk are shown in Figure VI.6. These profiles demonstrate that the assumption of uniform intensity is not strictly valid. The effect of the incorrect assumption is that experimental values of XK are too large, particularly at low values of ω. This follows since rate of photochemical generation of electroactive intermediate near the outer edge of the zone of the quartz disk is actually less than the rate simulated. At low values of ω, the main source of a chemically reactive electroactive intermediate reaching the surface of the ring electrode is the outer edge of the zone of the quartz disk. Lack of funds prevented digital simulation based on measured intensity profile and the

Figure VI.5. $I_{h\nu}$ *vs.* CBULKA

XII = 6.0×10^{14} quanta/sec;

values of XK: – – – 0.0 $\underline{M}^{-1}$ sec^{-1} and

——— 3.7×10^{5} $\underline{M}^{-1}$ sec^{-1}; values of

ω: O - 41.9 rad/sec, Δ - 94.3 rad/sec,

and □ - 167.7 rad/sec; x - experimental

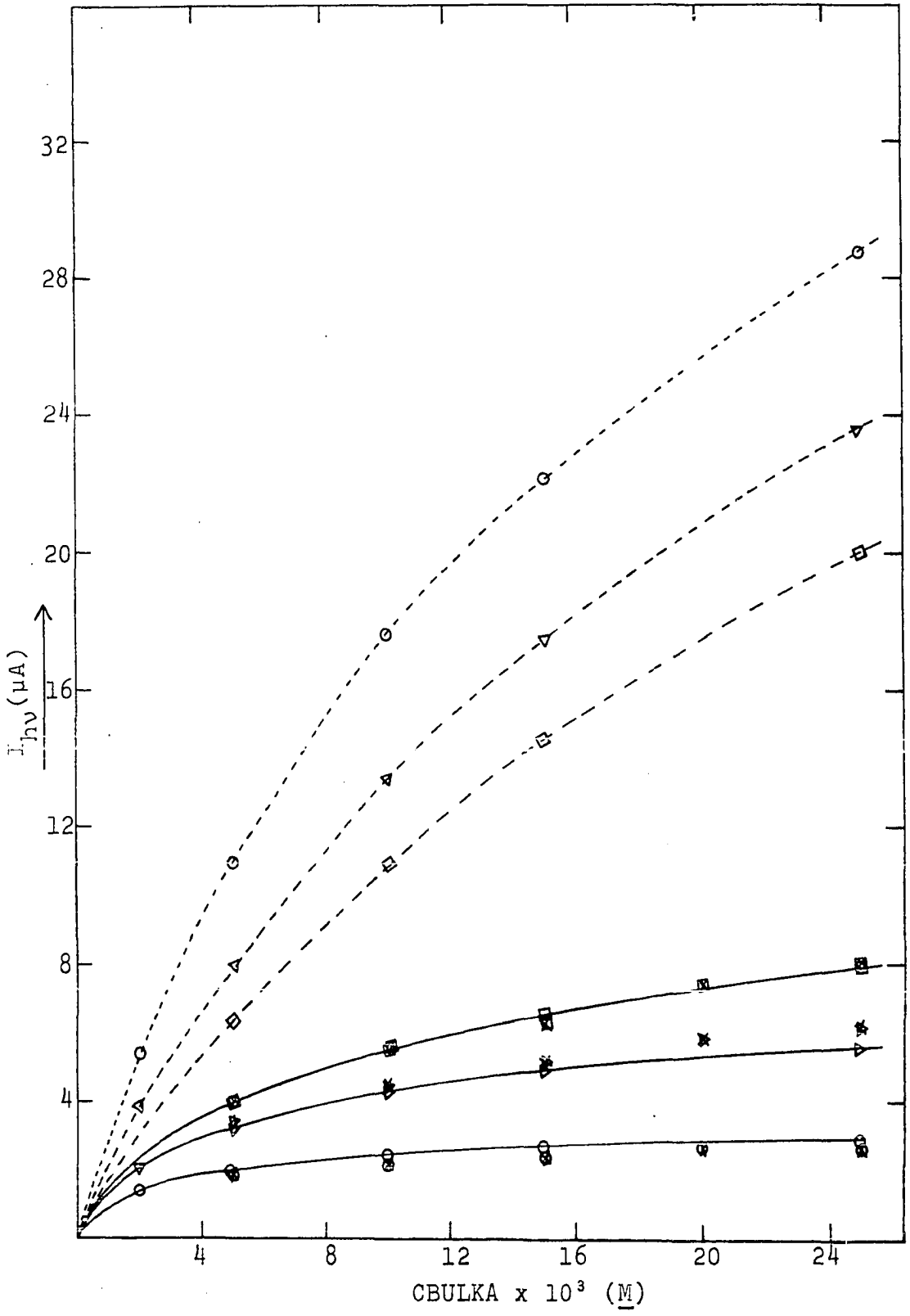
32
28
24
20
16
12
8
4
$I_{h\nu}$ (μA)
4
8
12
16
20
24
CBULKA x 10^3 (M)

Figure VI.6. Light intensity profiles. Measured along perpendicular diameters

Profiles of Light Intensity
at Quartz Disk Taken
at Right Angles

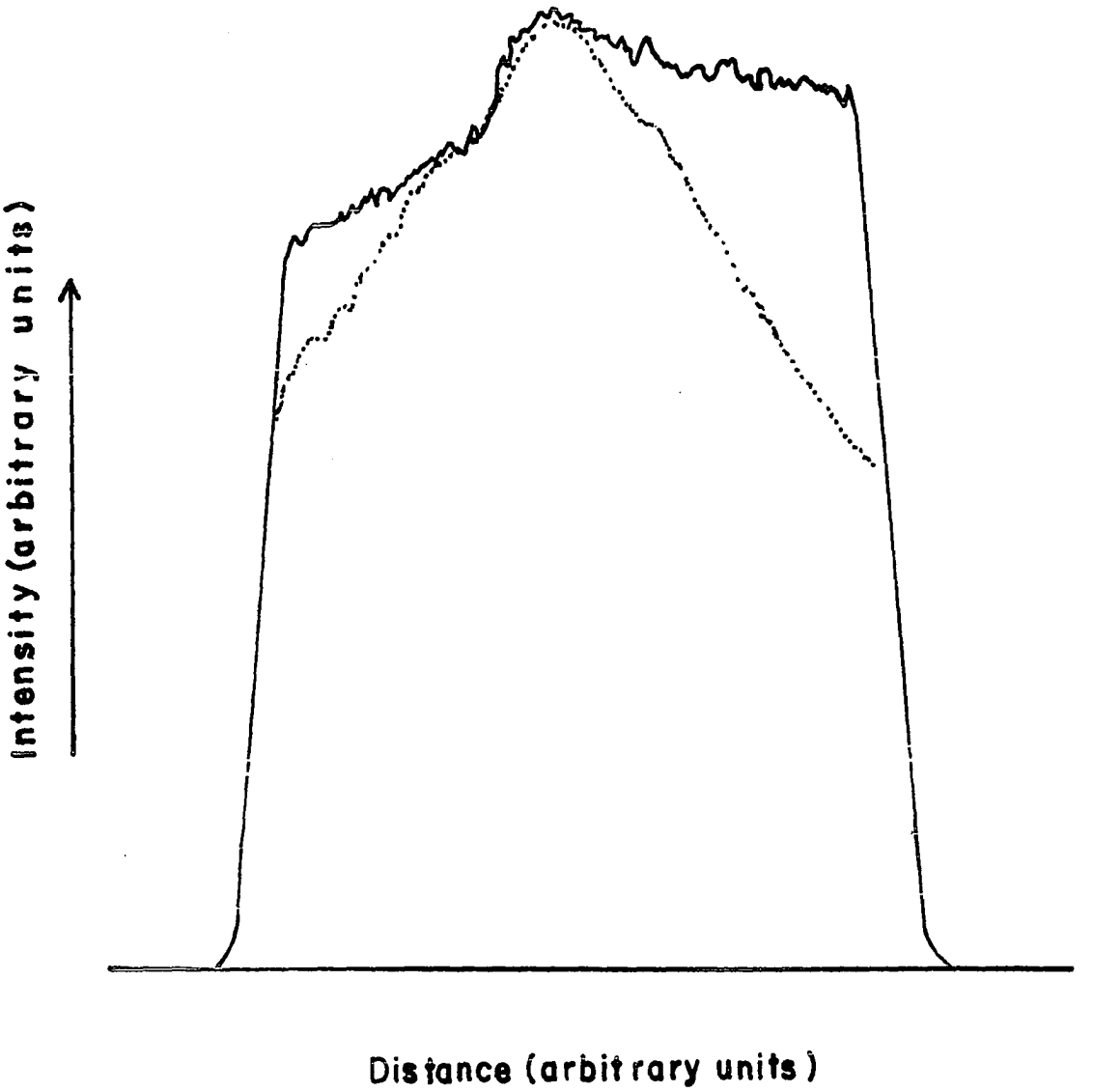

magnitude of error produced by the assumption has not been evaluated at this time.

5. Interference of the methyl-hydroxymethyl radical

One methyl-hydroxymethyl radical is formed for every benzophenone molecule that is photoreduced. It has been shown in Section IV.C. that the methyl-hydroxymethyl radical would be oxidized at the potentials used for the oxidation of the ketyl radical. No correction for this additional anodic current was made by the computer simulation.

VII. SUMMARY

A rotating photoelectrode was used to study photochemical processes in liquid media. The photocurrent was shown to be a function of the homogeneous kinetics of the photochemically generated intermediates as well as the wavelength and intensity of the light beam, reactant concentration, nature of the solvent, pH, rotational velocity and electrochemical potential of the detector. The rate constant for the photo-pinacolization of benzophenone was determined by means of a digital simulation.

The results of this study were compared with results obtained by workers using an independent method.

The electrochemical behavior of benzil and benzophenone was investigated with the rotating, mercury-coated, ring-disk electrode. The products of the electrochemical reduction of benzil were concluded to be the cis- and trans-stilbendiolates. The rate constants for the subsequent ketolization of the cis- and trans-stilbendiolates were determined to be 0.6 ± 0.2 sec^{-1} and 4.7 ± 0.8 sec^{-1}, respectively.

The photochemical behavior of 9-hydroxyfluorene was investigated with the aid of the rotating photoelectrode. This investigation tested the applicability of the RPE as a research tool for mechanistic studies of photochemical

reactions. It was determined that the photolysis of 9-hydroxyfluorene in alkaline and neutral media yields the fluorenyl and 9-oxyfluorenyl radicals.

VIII. SUGGESTIONS FOR FUTURE RESEARCH

The photochemical reduction of benzophenone by alcohols such as methanol, ethanol, and isopropanol results in the formation of the alpha radical of these alcohols. These alcohol radicals are electrochemically oxidized over the entire useful potential range on mercury electrodes. A photoelectrochemical study has not been found that had corrected the observed photocurrents for the oxidation of these alcohol radicals. A determination of the rate constant for the decay of these radical alcohols is needed so that the formation, decay, convective-diffusional mass transport of the radical alcohols to the electrode surface, and the following oxidation can be incorporated into the digital simulation. The currents obtained for the oxidation of the radical alcohols could then be subtracted from the observed photocurrents to obtain the photocurrent for the electrochemical oxidation of the primary photochemical product.

Both ultraviolet and electrochemical detection systems have proven to be valuable tools in the study of photochemical processes. The combined use of these detector systems into one instrument should be useful to the photochemical researcher. In order to combine both detection systems, a tubular flow through cell could be divided into three sections. The first section would be constructed of quartz and serve as the photolysis region. The second

section would be a tubular electrode of a material such as platinum, gold, or glassy carbon and used as the electrochemical detector. The third section would be constructed of quartz and serve for ultraviolet detection of photoproducts.

An estimate of the magnitude of the photocurrent obtained can be calculated using Equation VIII.1.

$$\frac{\underline{M}_A(\Delta X)(e_A)(I_o)(\Phi)(F)}{A} = I_{h\nu} \qquad \text{(VIII.1)}$$

where:

M_A = molar concentration of bulk species A

ΔX = thickness of the tube

e_A = molar absorptivity of species A

I_o = incident light intensity

Φ = primary quantum yield for the production of electrochemically active species

F = the Faraday

A = Avogadros number

$I_{h\nu}$ = photocurrent

Using the following values

$M_A \simeq 10^{-3}$ $\underline{M}$

$\Delta X \simeq 0.1$ cm

$e \simeq 10^3$ ℓ mole^{-1} cm^{-1}

$I_o \simeq 10^{15}$ quanta sec^{-1}

$\Phi \simeq 1$ molecule quanta^{-1}

$F \simeq 9.6 \times 10^{4}$ coulombs $mole^{-1}$

$A \simeq 6 \times 10^{23}$ molecules $mole^{-1}$

the photocurrent was calculated to fall in the μA range, which is easily measured electrochemically.

IX. BIBLIOGRAPHY

1. G. E. Adams, J. H. Baxendale, and J. W. Boag, Proc. Roy. Soc. (London) Ser. A 277, 549 (1964).

2. S. Aktipis, Diss. Abstr. Int. B, 27, 1407 (1966).

3. W. J. Albery and S. Bruckenstein, Trans. Faraday Soc. 62, 1946 (1966).

4. W. J. Albery and M. L. Hitchman, in Ring-Disk Electrodes, (Clarendon Press, Oxford, 1971), p. 17.

5. M. Ashworth, Collection Czechoslov. Chem. Communs. 13, 229 (1948).

6. P. W. Atkins, K. A. McLauchlan, and A. F. Simpson, Mol. Spectrosc. Proc. Conf. 4th, 177 (1968).

7. P. W. Atkins, I. C. Buchanan, R. C. Guard, K. A. McLavchlan, and A. F. Simpson, J. Chem. Soc. D9, 513 (1970).

8. E. G. Austen, P. H. Given, D. J. E. Ingram, and M. E. Peover, Nature 182, 1784 (1958).

9. H. L. J. Backstrom and R. J. V. Niklasson, Acta Chem. Scand. 20, 2617 (1966).

10. H. L. J. Backstrom and R. J. V. Niklasson, Acta Chem. Scand. 22, 2589 (1968).

11. H. L. J. Backstrom, K. L. Appelgren, and R. J. V. Niklasson, Acta. Chem. Scand. 19, 1555 (1965).

12. G. C. Baker, A. W. Gardner, and G. Bottura, J. Electroanal. Chem. Interfacial Electrochem. 45, 21 (1973).

13. R. H. Baker and H. Adkins, J. Amer. Chem. Soc. 62, 3304 (1940).

14. J. H. Baxendale, E. M. Fielden, and J. P. Keene, Science 148, 637 (1965).

15. A. Beckett and G. Porter, Trans. Faraday Soc. 59, 2038 (1963).

16. A. Beckett, A. D. Osborne, and G. Porter, Trans. Faraday Soc. 60, 873 (1964).

17. H. Berg, Coll. Czechoslov. Chem. Communs. 25, 3404 (1960).

18. H. Berg, Naturwissenschaften 48, 100 (1961).

19. H. Berg, Naturwissenschaften 49, 11 (1962).

20. H. Berg, Rev. Polarog. 11, 29 (1963).

21. H. Berg, Abhanal. Deut. Akad. Wiss. Berlin 1, 128 (1964).

22. H. Berg, Z. Anal. Chem. 216, 165 (1966).

23. H. Berg, Electrochim. Acta 13, 1249 (1968).

24. H. Berg and P. Reissman, J. Electroanal. Chem. Interfacial Electrochem. 24, 429 (1970).

25. H. Berg and H. Schweiss, Monatsber. Deu. Akad. Wiss. Berlin 2, 513 (1960).

26. H. Berg and H. Schweiss, Naturwissenschaften 47, 546 (1960).

27. H. Berg and H. Schweiss, Nature 191, 1270 (1961).

28. H. Berg and H. Schweiss, Electrochim. Acta 9, 425 (1964).

29. H. Berg, H. Schweiss, E. Stutter, and K. Weller, J. Electroanal. Chem. 15, 415 (1967).

30. J. R. Birk and S. P. Perone, Anal. Chem. 40, 496 (1968).

31. J. Bjerrum, G. Schwarzenbach, and L. G. Sillen in Stability Constants of Metal-Ion Complexes, with Solubility Products of Inorganic Substances, Part II: Inorganic Ligands, Chem. Soc. (London), Spec. Publ. No. 6 (1957), No. 7 (1958).

32. M. I. Bobrova and N. S. Tikhominova, Zhur. Obschei Khim. 22, 2107 (1952).

33. G. Bomehil, D. J. Schiffrin, and J. T. D'Alessio, J. Electroanal. Chem. Interfacial Electrochem. 25, 107 (1970).

34. E. J. Bowen, Electroanal. Chem. 14, 351 (1967).

35. J. S. Bradshaw, J. Org. Chem. 31, 237 (1966).

35a. L. Brubaker, Ph.D. thesis, Princeton University, 1966 (unpublished).

35b. S. Bruckenstein and F. L. Marsh, Anal. Chem. 38, 1498 (1966).

36. A. V. Buettner and J. Dedinas, J. Phys. Chem. 75, 187 (1971).

37. D. L. Bunburg and T. T. Chuang, Can. J. Chem. 47, 2045 (1969).

38. J. G. Calvert and J. N. Pitts, Jr. in Photochemistry (John Wiley and Sons, Inc., New York, 1967), p. 377.

39. A. V. Chodkowska and Z. R. Grabowski, Electrochim. Acta 9, 789 (1964).

40. W. D. Cochran, Proc. Cambr. Phil. Soc. 30, 365 (1934).

41. S. G. Cohen, U. S. At. Energy Comm. NYO-2499-16, (1965).

42. S. G. Cohen and R. J. Baumgarten, J. Amer. Chem. Soc. 87, 2996 (1965).

43. S. G. Cohen and R. J. Baumgarten, J. Amer. Chem. Soc. 89, 3471 (1967).

44. S. G. Cohen and J. I. Cohen, Israel J. Chem. 6, 757 (1968).

45. S. G. Cohen and J. I. Cohen, Tetrahedron Lett. No. 46, 4823 (1968).

46. S. G. Cohen and W. V. Sherman, J. Amer. Chem. Soc. 85, 1642 (1963).

47. S. G. Cohen and N. Stein, J. Amer. Chem. Soc. 91, 3690 (1969).

48. S. G. Cohen and N. Stein, J. Amer. Chem. Soc. 93, 6542 (1971).

49. S. G. Cohen, D. A. Laufer, and W. V. Sherman, J. Amer. Chem. Soc. 86, 3060 (1964).

50. S. G. Cohen, S. Orman, and D. Laufer, Proc. Chem. Soc., 301 (1961).

51. S. G. Cohen, N. Stein and H. M. Chao, J. Amer. Chem. Soc. 90, 521 (1968).

52. F. W. Cox and H. Adkins, J. Amer. Chem. Soc. 61, 3364 (1939).

53. R. S. Davidson, Chem. Commun. No. 16, 575 (1966).

54. R. S. Davidson and P. F. Lambeth, Chem. Commun. No. 24, 1265 (1967).

55. R. S. Davidson and P. F. Lambeth, Chem. Commun. No. 9, 511 (1968).

56. R. S. Davidson and R. Wilson, J. Chem. Soc. B No. 1, 71 (1970).

57. R. A. Day and J. J. Kirkland, J. Amer. Chem. Soc. 72, 2766 (1950).

58. R. A. Day, S. R. Milliken, and W. D. Shults, J. Amer. Chem. Soc. 74, 2741 (1952).

59. R. A. Day, R. H. Philp, and R. L. Flurry, J. Electrochem. Soc. 108, 181 (1961).

60. J. Dedinas, J. Phys. Chem. 75, 181 (1971).

61. R. L. DeGroot, Mol. Photochem. 3, 1 (1971).

62. R. Delevie and J. C. Kreuser, J. Electroanal. Chem. Interfacial Electrochem. 21, 221 (1969).

63. A. Demortier and A. J. Bard, J. Amer. Chem. Soc. 95, 3495 (1973).

64. S. W. Feldberg in Electroanalytical Chemistry, edited by A. J. Bard (Marcel Dekker, Inc., New York, 1969) Volume 3.

65. N. Filipescu and F. L. Minn, J. Amer. Chem. Soc. 90, 1544 (1968).

66. V. Franzen, Annalen der Chemie, 633, 1 (1960).

67. A. N. Frumkin and L. N. Nekrasov, Doklady Akad. Nauk. SSR. 126, 115 (1959).

68. Z. Galus and R. N. Adams, J. Amer. Chem. Soc. 84, 2061 (1962).

69. H. J. Gardner, Chemistry & Industry, 819 (1951).

70. V. P. Gokhshtein and A. I. Kalinin, Trudy Pokhim. Ikhim. Tekhnol. 3, 219 (1960).

71. J. S. Gomez, P. Salmeron, and J. G. Hurtado, Anales Real. Soc. Espaň. Fisyguim 53B, 597 (1957).

72. D. Haberland and R. Landsberg, Z. Elektrochem. 70, 724 (1966).

73. G. S. Hammond and R. P. Foss, J. Phys. Chem. 68, 3739 (1964).

74. M. Heyrovsky, Croat. Chem. Acta 45, 247 (1973).

75. K. Honda, Kogyo Kagaku Zasshi 72, 63 (1969).

76. D. C. Johnson and S. Bruckenstein, J. Electrochem. Soc. 117, 460 (1970).

77. D. C. Johnson and E. W. Resnick, Anal. Chem. 44, 637 (1972).

78. M. K. Kalinowski, Z. R. Grabowski, and B. Pakula, Trans.Faraday Soc. 62, 918 (1966).

79. Kalvoda and G. Budnikov, Collection Czech. Chem. Commun. 28, 838 (1963).

80. W. Kemula, Z. Grabowski, and M. Kalinowski, Naturwissenschaften 47, 514 (1960).

81. L. M. Kindley, Diss. Abstr. Int. B 31, 3924 (1971).

82. F. Kish and K. S. Bagdasar'yan, Zh. Fiz. Khim. 40, 1339 (1966).

83. Klagel, Berichta 43, 2490 (1910).

84. I. A. Korshunov, A. S. Kirillova, and Z. B. Kuznetsova, Zhur. Fiz. Khim. 24, 551 (1950).

85. G. G. Kryukova, Y. I. Turýan, and M. S. Rusakova, Uch. Zap. Yaroslav. Tekhnol. Inst. 22, 61 (1971).

86. T. Kuwana, Electroanal. Chem. 1, 197 (1966).

87. V. A. Kyz'min, A. K. Chibisov, Teor. Eksp. Khim. 7, 403 (1971).

88. E. J. Land and G. Porter, Trans. Faraday Soc. 59, 2016 (1963).

89. I. H. Leaver and G. C. Ramsey, Tetrahedron 25, 5669 (1969).

90. M. B. Ledger and G. Porter, J. Chem. Soc., Faraday Trans. 7, 68, 539 (1972).

91. V. G. Levich in Physicochemical Hydrodynamics, (Prentice-Hall, Englewood Cliffs, New Jersey, 1962.)

92. I. Levin and P. Delahay, J. Electroanal. Chem. Interfacial Electrochem. 24, 17A (1970).

93. J. R. Lubbers, E. W. Resnick, P. R. Gaines and D. C. Johnson, accepted for publication in Anal. Chem.

94. H. Lund, Acta Chem. Scand. 13, 249 (1959).

95. W. M. Manning, Trans. Wisconsin Acad. Sci. 35, 221 (1943).

96. N. Marinus, D. M. Rayner, and C. A. Vincent, Electrochem. Acta 18, 409 (1973).

97. H. Mauser and V. Bihl, Z. Natur. Forsch. B 22, 1077 (1967).

98. H. Mauser and H. Heitzer, Naturwissenschaften 50, 568 (1963).

99. H. Mauser, B. Nickel, U. Sproesser, and V. Bihl, Z. Naturforsch. B, 22, 903 (1967).

100. L. Molnár, K. Molnárová, and E. Benická, Chem. Svesti 14, 783 (1960).

101. W. M. Moore and M. D. Ketchum, J. Phys. Chem. 86, 214 (1964).

102. W. M. Moore, G. S. Hammond, and R. P. Foss, J. Amer. Chem. Soc. 83, 2789 (1961).

103. D. C. Neckers and D. P. Colenbrander, Tetrahedron Lett. No. 48, 5045 (1968).

104. L. N. Nekrasov and A. D. Korsun, Sov. Electrochem. 4, 477 (1968).

105. L. N. Nekrasov and A. D. Korsun, Sov. Electrochem. 4, 899 (1968).

106. Y. Ogata, K. Takagi, and Y. Fujii, J. Org. Chem. 37, 4026 (1972).

107. M. K. Orloff, J. Chem. Phys. 47, 235 (1967).

108. V. Parlov, Z. Chem. 4, 392 (1964).

109. R. Pasternak, Helv. Chim. Acta 30, 1984 (1947).

110. R. Pasternak, Helv. Chim. Acta 31, 753 (1948).

111. J. J. H. Patterson and S. P. Perone, Anal. Chem. 44, 1978 (1972).

112. D. E. Pearson and M. V. Moso, Tetrahedron Lett. No. 39, 3791 (1967).

113. S. P. Perone and J. R. Birk, Anal. Chem. 38, 1589 (1966).

114. S. P. Perone and J. R. Birk, Anal. Chem. 38, 1593 (1966).

115. S. P. Perone, J. R. Birk, H. E. Drew, and H. E. Stapelfeldt, Amer. Chem. Soc. 11, 186 (1967).

116. M. Pfaw, Compt. Rend. 254, 2017 (1962).

117. R. H. Philip, Jr., R. L. Flurry, and R. A. Day, Jr., J. Electrochem. Soc. 111, 328 (1964).

118. J. N. Pitts, Jr., T. Kuwana, and A. Marchetti, Preprints Papers Intern. Sumpo. Free Radicals, 5th, Uppsala, 51-1-13 (1961).

119. J. N. Pitts, Jr., R. L. Letsinger, R. P. Taylor, J. M. Patterson, G. Recktenwald, and R. B. Martin, J. Amer. Chem. Soc. 81, 1068 (1959).

120. G. Porter and F. Wilkinson, Trans. Faraday Soc. 57, 1686 (1961).

121. G. Porter and F. Wilkinson, Trans. Faraday Soc. 59, 2038 (1963).

122. K. B. Prater and A. J. Bard, J. Electrochem. Soc. 117, 207 (1970).

123. K. B. Prater and A. J. Bard, J. Electrochem. Soc. 117, 335 (1970).

124. K. B. Prater and A. J. Bard, J. Electrochem. Soc. 117, 1517 (1970).

125. P. J. Ricca, Diss. Abstr. Int. B, 27, 442 (1966).

126. A. W. Rose, Diss. Abstr. Int. B, 32, 2612 (1971).

127. G. A. Russell and E. J. Geels, Tetrahedron Lett. No. 20, 1333 (1963).

128. J. Saltiel, H. C. Curtis, and B. Jones, Mol. Photochem. 2, 331 (1970).

129. H. Sata, Eisei Shikenjo Hôkoku 77, 51 (1959).

130. G. O. Schenck, G. Koltzenburg, and E. Roselius, Z. Naturforsch B, 24, 222 (1969).

131. G. O. Schenck, W. Meder, and M. Pape, Proc. Intern. Conf. Peaceful Uses At. Energy 29, 352 (1958).

132. G. O. Schenck, M. Cziesla, K. Eppinger, G. Matthias, and M. Pape, Tetrahedron Lett. No. 3, 193 (1967).

133. D. I. Schuster and T. M. Weil, J. Amer. Chem. Soc. 95, 4091 (1973).

134. H. Schweiss, Z. Chem. 2, 382 (1962).

135. H. Schweiss and H. Berg, Abt. Deut. Akad. Wiss. Berlin Kl. Med. No. 4, 391 (1966).

136. W. V. Sherman and S. G. Cohen, J. Phys. Chem. 70, 178 (1966).

137. R. M. Silverstein and G. C. Bassler in Spectrometric Identification of Organic Compounds (John Wiley and Sons, Inc., New York, 1968), p. 34.

138. H. E. Stapelfeldt and S. P. Perone, Anal. Chem. 40, 815 (1968).

139. H. E. Stapelfeldt and S. P. Perone, Anal. Chem. 41, 623 (1969).

140. H. E. Stapelfeldt and S. P. Perone, Anal. Chem. 41, 628 (1969).

141. C. A. Strevliand and W. D. Cooke, Anal. Chem. 26, 963 (1954).

142. E. Stutter, Soviet Electrochem. 4, 127 (1968).

143. M. Suzuki and P. J. Elving, J. Phys. Chem. 65, 391 (1961).

144. A. C. Testa, J. Phys. Chem. 67, 1341 (1963).

145. D. J. Trecker and J. P. Henry, Anal. Chem. 35, 1882 (1963).

146. H. Tsubomura, N. Yamamato, and S. Tanaka, Chem. Phys. Lett. 1, 309 (1967).

147. W. L. Underkofler and I. Shain, Anal. Chem. 35, 1778 (1963).

148. K. Vmemoto, Bull. Chem. Soc. Jap. 40, 1058 (1967).

149. Y. V. Vodzinskiy and I. A. Korshunov, Ser. Khim. No. 32, 2536 (1958).

150. T. Vonkarmon, Z. Angew. Math. Mech. 1, 223 (1921).

151. K. Weller, J. Electroanal. Chem. 10, 270 (1965).

152. K. Weller, Z. Phys. Chem. 284, 217 (1971).

153. K. Wettig, Elektrokhimiya 3, 264 (1967).

154. K. Yamashita and H. Imai, Bull. Chem. Soc. Jap. 45, 628 (1972).

155. H. Yoshida, T. Warashina, Bull. Chem. Soc. Jap. 44, 2950 (1971).

156. P. Zuman, D. Barnes, and A. Ryvolova-Kejharova, Discussions Faraday Soc. No. 45.

X. ACKNOWLEDGEMENTS

The author wishes to offer special thanks to Dr. Dennis C. Johnson for his helpful criticism, assistance and guidance throughout the course of the research and graduate study.

The author thanks the National Science Foundation for financial support throughout the course of this research.

The author would like to thank Val Peacock and Jude Lubbers for their contributions to his research.

Finally, the author thanks his wife, June, and son, Greg, for their support and encouragement during his graduate study.